TECHNICAL REPORT STANDARD TITLE PAGE

1. Report No.	2. Government Accession No.	3. Recipient's Catalog No.
FHWA/TX-87/324-2		

4. Title and Subtitle	5. Report Date
Composite Action of Precast Panel Bridge Decks in Negative Moment Regions	September 1987
	6. Performing Organization Code

7. Author(s)	8. Performing Organization Report No.
F. E. Bonilla, R. W. James, R. A. Osegueda and J. S. Noel	Research Report 324-2

9. Performing Organization Name and Address	10. Work Unit No.
Texas Transportation Institute The Texas A&M University System College Station, Texas 77843	11. Contract or Grant No. Study No. 2-5-82-324
	13. Type of Report and Period Covered
12. Sponsoring Agency Name and Address Texas State Department of Highways and Public Transportation, Transportation Planning Division P. O. Box 5051 Austin, Texas 78763	Interim - September 1981 September 1987
	14. Sponsoring Agency Code

15. Supplementary Notes

Research performed in cooperation with DOT, FHWA.
Research Study Title: Rapid Bridge Deck Replacement

16. Abstract

A one-third scale composite steel-concrete bridge model with a precast deck was tested under negative moments to investigate the behavior of the structure before and after cracking of the deck.

The model was simply supported and an upward concentrated load was applied at midspan to develop negative moments while the supports were restrained against uplift. The experiment included loading sequences before and after cracking of the concrete deck. The first was used to determine the section properties of the model, and the second to study the loss of composite action due to cracking of the concrete deck.

The results show that the effects of the epoxy-grouted joints between the deck panels on the stiffness of the structure are not significant, and that the behavior of the model under positive moments is different from that under negative moments due to the lower modulus of elasticity of concrete in tension. Cracks in the deck were observed first at the joint locations even though these were not the most highly stressed regions. A loss in composite action was observed in a region of length equal to about 18 deck thicknesses due to the development of a crack.

17. Key Words	18. Distribution Statement
Bridge Decks, Precast Concrete, Epoxy Mortar, Composite Bridges, Continuous Bridges, Static Load Test, and Tensile Cracks.	No restrictions. This document is available to the public through the National Technical Information Service 5285 Port Royal Road. Springfield, Virginia 22161

19. Security Classif. (of this report)	20. Security Classif. (of this page)	21. No. of Pages	22. Price
Unclassified	Unclassified	169	

Form DOT F 1700.7 (8-69)

COMPOSITE ACTION OF PRECAST PANEL BRIDGE DECKS IN NEGATIVE MOMENT REGIONS

by

Francisco E. Bonilla
Research Assistant

Ray W. James
Assistant Research Engineer

Roberto A. Osegueda
Research Assistant

and

James S. Noel
Associate Research Engineer

Research Report Number 324-2

Research Study Number 2-5-82-324
Rapid Bridge Deck Replacement

Sponsored by
Texas State Department of Highways and Public Transportation
in cooperation with
The United States Department of Transportation
Federal Highway Administration

September 1987

Texas Transportation Institute
Texas A&M University
College Station, Texas

METRIC CONVERSION FACTORS

Approximate Conversions to Metric Measures

Symbol	When You Know	Multiply by	To Find	Symbol
LENGTH				
in	inches	*2.5	centimeters	cm
ft	feet	30	centimeters	cm
yd	yards	0.9	meters	m
mi	miles	1.6	kilometers	km
AREA				
in^2	square inches	6.5	square centimeters	cm^2
ft^2	square feet	0.09	square meters	m^2
yd^2	square yards	0.8	square meters	m^2
mi^2	square miles	2.6	square kilometers	km^2
	acres	0.4	hectares	ha
MASS (weight)				
oz	ounces	28	grams	g
lb	pounds	0.45	kilograms	kg
	short tons (2000 lb)	0.9	tonnes	t
VOLUME				
tsp	teaspoons	5	milliliters	ml
Tbsp	tablespoons	15	milliliters	ml
fl oz	fluid ounces	30	milliliters	ml
c	cups	0.24	liters	l
pt	pints	0.47	liters	l
qt	quarts	0.95	liters	l
gal	gallons	3.8	liters	l
ft^3	cubic feet	0.03	cubic meters	m^3
yd^3	cubic yards	0.76	cubic meters	m^3
TEMPERATURE (exact)				
°F	Fahrenheit temperature	5/9 (after subtracting 32)	Celsius temperature	°C

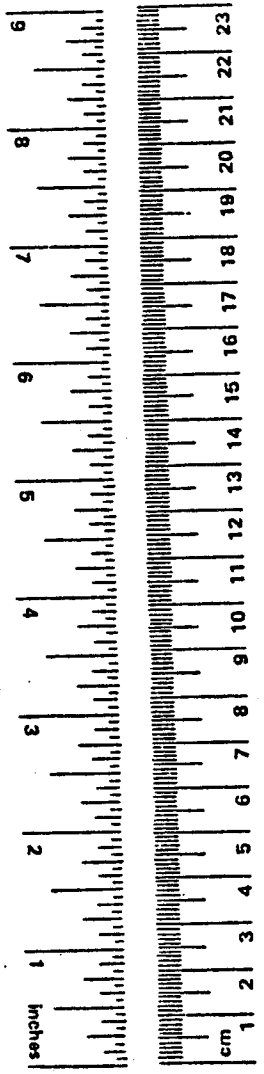

Approximate Conversions from Metric Measures

Symbol	When You Know	Multiply by	To Find	Symbol
LENGTH				
mm	millimeters	0.04	inches	in
cm	centimeters	0.4	inches	in
m	meters	3.3	feet	ft
m	meters	1.1	yards	yd
km	kilometers	0.6	miles	mi
AREA				
cm^2	square centimeters	0.16	square inches	in^2
m^2	square meters	1.2	square yards	yd^2
km^2	square kilometers	0.4	square miles	mi^2
ha	hectares (10,000 m^2)	2.5	acres	
MASS (weight)				
g	grams	0.035	ounces	oz
kg	kilograms	2.2	pounds	lb
t	tonnes (1000 kg)	1.1	short tons	
VOLUME				
ml	milliliters	0.03	fluid ounces	fl oz
l	liters	2.1	pints	pt
l	liters	1.06	quarts	qt
l	liters	0.26	gallons	gal
m^3	cubic meters	35	cubic feet	ft^3
m^3	cubic meters	1.3	cubic yards	yd^3
TEMPERATURE (exact)				
°C	Celsius temperature	9/5 (then add 32)	Fahrenheit temperature	°F

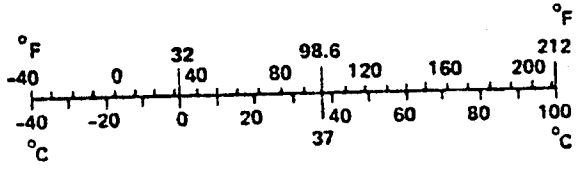

*1 in = 2.54 (exactly). For other exact conversions and more detailed tables, see NBS Misc. Publ. 286, Units of Weights and Measures, Price $2.25, SD Catalog No. C13.10:286.

DISCLAIMER

The contents of this report reflect the views of the authors, who are responsible for the opinions, findings, and conclusions presented herein. The contents do not reflect the official views or policies of the Federal Highway Administration. This report does not constitute a standard, specification, or regulation.

KEY WORDS

Bridge Decks, Precast Concrete, Composite Bridges, Epoxy Mortar, Continuous Bridges, Static Load Test, and Tensile Cracks.

ACKNOWLEDGEMENTS

The authors are grateful to the Texas State Department of Highways and Public Transportation and the Federal Highway Administration for sponsoring this investigation.

ABSTRACT

A one-third scale composite steel-concrete bridge model with a precast deck was tested under negative moments to investigate the behavior of the structure before and after cracking of the deck.

The model was simply supported and an upward concentrated load was applied at midspan to develop negative moments while the supports were restrained against uplift. The experiment included loading sequences before and after cracking of the concrete deck. The first was used to determine the section properties of the model, and the second to study the loss of composite action due to cracking of the concrete deck.

The results show that the effects of the epoxy-grouted joints between the deck panels on the stiffness of the structure are not significant, and that the behavior of the model under positive moments is different from that under negative moments due to the low modulus of elasticity of concrete in tension. Cracks in the deck were observed first at the joint locations even though these were not the most highly stressed regions. A loss in composite action was observed in a region of length equal to about 18 deck thicknesses due to the development of a crack.

TABLE OF CONTENTS

LIST OF TABLES

LIST OF FIGURES

CHAPTER I

INTRODUCTION

Nature of the Problem

The advantages of composite construction over non-composite, or conventional construction, are several (18,4). Probably the most important is the larger live load carrying capacity of the composite structure compared to a similar conventional structure.

Composite behavior in bridges is achieved by interconnecting the slab and the beams by means of a shear transfer mechanism which could be either a bond or mechanical shear connectors. In steel stringer bridges the most common type of shear transfer device is shear studs welded to the top flange of the stringer. Once the shear studs are welded, the concrete slab is cast; however, precast concrete panels may also be used. In the latter, cast holes in the panels accept the shear connectors. After the panels are placed over the stringer, the studs are welded and the holes are filled, usually with a concrete or epoxy mortar, developing rigid or semi-rigid connections between the slab and the stringer.

A rapid method to rehabilitate decks of highly deteriorated structures is to replace the old deck with precast concrete panels. This rehabilitation process is accelerated if epoxy mortar is used to seal the joints between adjacent precast panels, and to fill the pocket connections so that shear forces are transferred from the steel stringer to the deck.

In the negative moment regions of continuous composite concrete-steel bridges tensile forces are induced in the concrete, and development of cracks in the deck is expected. When the deck is made of precast concrete panels, cracks are expected to develop first at the joint locations since these are considered weak areas due to the discontinuities in steel reinforcement. The questions that arise with respect to the use of precast concrete panels in negative moment regions of composite continuous bridges are the following:

1. What influence does the discontinuity in materials at the joints have on the stiffness of the structure and on the cracking pattern of the deck?

2. Can the cracking pattern of the deck be predicted if it is assumed that the development of cracks in the concrete will be limited to the location of the joints?
3. What influence does the cracking of the concrete have on the behavior of the structure?

Background and Significant Work

Construction of composite bridges began during the early 1930's; however, it was not until the early 1960's that the use of composite sections became economical (6). By the late 1950's and early 1960's the elastic behavior of composite beams was well understood (4), and elastic design methods served as the basis for the 1957 AASHO Specifications (14). In 1951 Newmark et al. (11) published a theory in which composite sections were analyzed considering a linear strain distribution over the length of a composite beam but with a strain discontinuity at the beam-slab interface due to deformations of the shear transfer mechanisms. This and other similar theories led to the development of inelastic methods of analysis of composite beams. The ultimate strength design approach found its way into bridge design when AASHO adopted the procedure as an alternate design method in 1971 (1). Most of the recent research conducted on continuous composite steel stringer-concrete beams is primarily oriented to the study of the ultimate strength capacity of such structures.

One of the first important studies on continuous composite steel-concrete bridges with monolithic decks was published by Sherman (13) in 1954. The analysis proposed by Sherman was based on the assumption that concrete could not carry tensile loading; therefore, composite action was only developed in the positive moment regions. A method was presented to calculate the non-composite length of composite continuous bridges, but the method was limited to the analysis of symmetrical two-span and three-span bridges only. Later research on continuous composite beams at Lehigh University (4) showed that a cracked concrete slab in negative moment regions continues to participate in the development of composite action with the longitudinal reinforcement, but the degree of participation decreases as the loading in the structure increases.

Presently, it is a common design practice to assume that concrete does not have any capacity to carry tensile stresses; therefore, unless special arrangements are made it is assumed that concrete in negative moment regions of a continuous bridge is ineffective, and the bending resistance in these regions is reduced to that of the steel stringer acting alone. Construction and design procedures have been developed to deal with the problem of retaining composite action in negative moment regions. The most common procedures are:

1. Prestressing the slab using various methods, so that under all conditions of loading the concrete is always in compression. When tensile stresses are prevented from developing in the concrete deck the section properties of the structure may be calculated using a transformed area of the concrete, thus increasing the carrying capacity of the structure. The two most common prestressing methods are the use of steel tendons and prestress by cambering, in which the steel stringer is deflected while the slab is cast in place.
2. Providing additional reinforcement in the slab in the negative moment regions so that composite action is developed between the steel reinforcement of the deck and the steel stringer.

Prestressing of the concrete deck in continuous composite bridges has not been considered to be economically feasible in the United States, and it is seldom used (4). Neither AASHTO (15) nor AISC (10) codes contain provisions for bridges with prestressed composite steel-concrete decks. However, both AASHTO in section 10.38.4.2 and AISC in section 1.11.2.2 incorporate provisions which allow the inclusion of reinforcement in the deck to compute the effective composite section properties if sufficient shear connectors are provided. These codes also mention that shear connectors are not needed in the negative moment regions if the contribution of the reinforcement in the deck is not considered in the computation of section properties.

The use of precast concrete decks on continuous composite bridges is still not common; few codes through the world contain provisions for this type of composite structure (4). However, precast concrete panels have been used recently in the United States to rehabilitate bridges and upgrade them by developing composite action. Some major public transportation agencies

including the New York Thruway Authority, the Pennsylvania Turnpike Commission, and the Santa Fe Railway are known to have used this method of construction.(16)

Prestressed precast concrete panels were used by the Santa Fe Railway to replace old timber decks in several bridges. The bridges were simple span and composite action was achieved by bonding the deck to the stringers with an epoxy mortar. Stress measurements made before and after development of composite action showed that the stresses were reduced by 50 per cent at the top flanges and by 11 per cent at the bottom flanges (7). Details of the connections are shown in Fig. 1. The New York State Thruway Authority constructed a precast deck bridge on the thruway, where it crosses the Krum Kill Road near Albany. The bridge was a simple span overpass that used welded shear studs as shear transfer devices as is shown in Fig. 2. The Pennsylvania Turnpike Commission replaced the deck of the Clark's Summit bridge in Lackawanna County using precast concrete panels. The structure was a continuous stringer bridge 1627 ft long built in 1956. Details of the shear connector used in this structure are shown in Fig. 3. The replaced precast concrete deck was not designed to act compositely with the stringers, although it is very likely that some composite action may have developed because of the bonding strength of the epoxy mortar (16). No problems in the performance of the structure have been reported.

It may be that other continuous precast concrete-steel bridges designed to be non-composite but acting compositely, like the Clark's Summit bridge, are in use. However, the real behavior of such structures is still not understood. It is the purpose of this investigation to study the development and loss of composite action in the continuous composite precast concrete-steel bridges by testing a model structure subjected to negative moments.

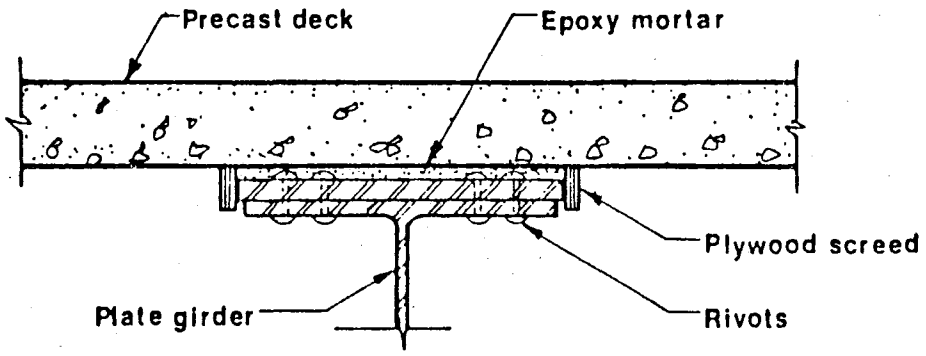

FIG. 1. Connection Detail, Santa Fe Railroad Bridges (9)

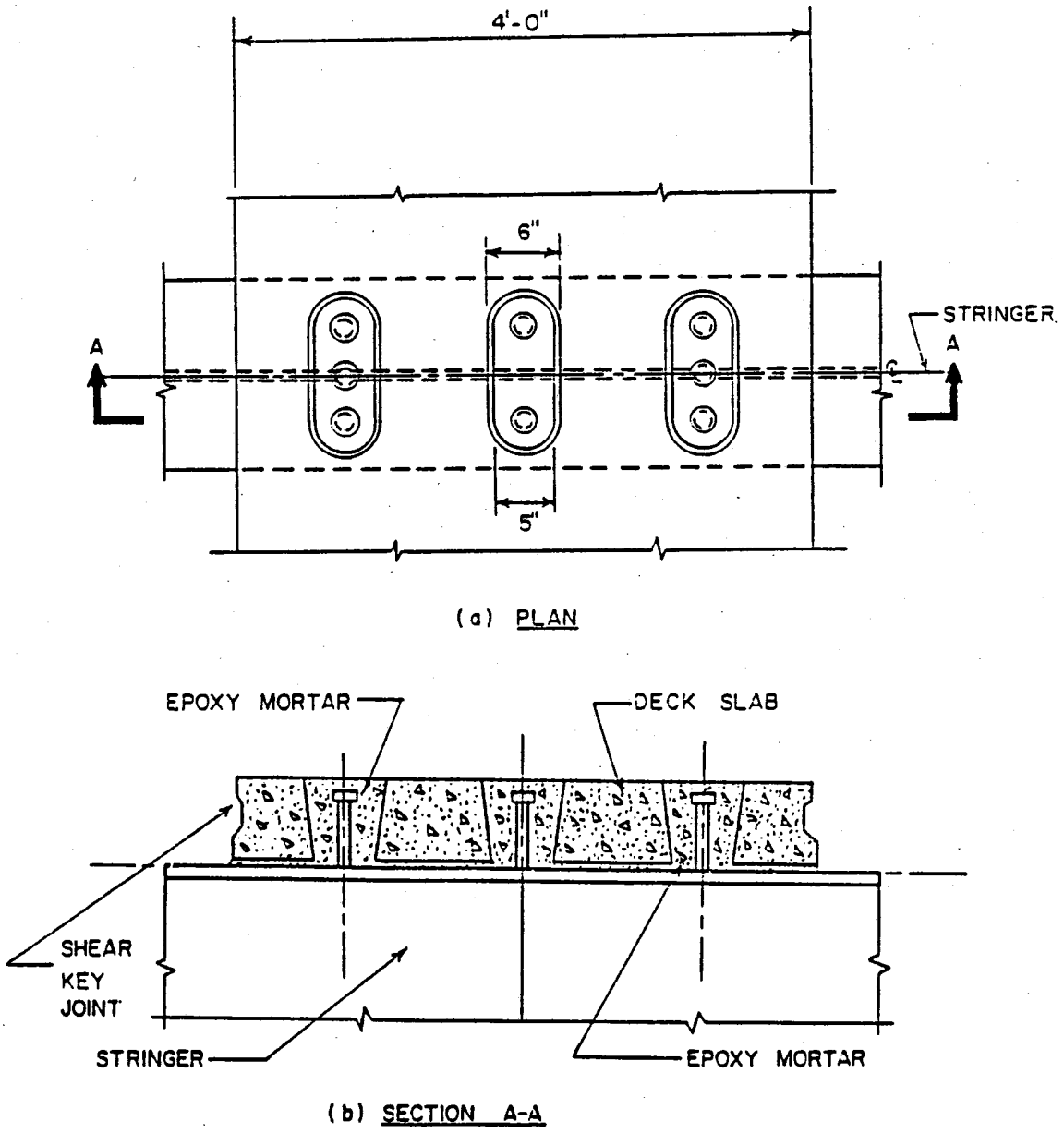

FIG. 2. Welded Stud Connection Details, New York Thruway Overpass (12)

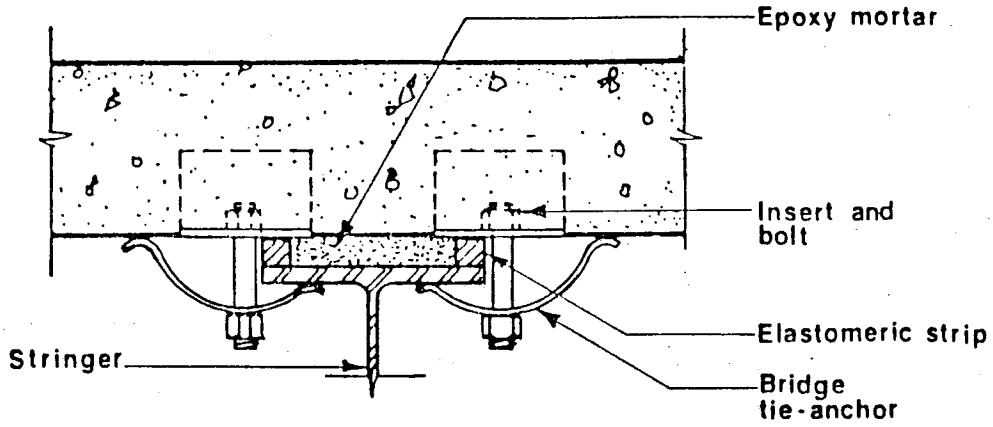

FIG. 3. Connection Detail, Clark's Summit Bridge (9)

Objectives of The Study

The objectives of this study were:

1. To determine the composite section properties of a one-third scale model of a prototype bridge typical of the Texas Highway System.
2. To study the extent of loss of composite action in the model due to cracking of the concrete deck subjected to negative moments.

Scope of the Study

The experimental work of this study was limited to the instrumentation and testing of a one-third scale composite steel-concrete bridge model with a precast deck under negative moments.

During the analytical work, the behavior of the model before cracking of the concrete deck was studied, so that the cracking pattern of the deck could be predicted. Flexural stresses were closely monitored along the length of one steel stringer to observe the effect of cracking of the concrete deck on the behavior of the structure.

CHAPTER II

EXPERIMENTAL WORK

The experimental work in this investigation involves the instrumentation and testing in negative moment regions of a one-third scale bridge model acting compositely.

Description of the Model

The tested structure is a one-third scale model of a prototype non-composite bridge typical of the Texas Highway System. The model was built and tested in positive moment regions (slab in compression) by Osegueda (12). Extensive information about the design procedure of the model and properties of both the model and the prototype are given in Ref. 12.

The structural model is a simple span, 20-ft-long stringer bridge. It consists of two steel stringers spaced 32 in. apart and a concrete deck made of ten precast reinforced concrete panels. Shear transfer mechanisms in the form of studs are welded to the steel beams and embedded in the precast concrete panels to develop composite action. Fig. 4 shows the geometry and dimensions of the model.

The stringers are made of two modified W12X19 A36 steel beams with 3/16-in.-thick cover plates welded to the top and bottom flanges in the center span region. A 3/8-in.-wide strip has been removed from the top and bottom flanges of the steel beams at each end. Details of the stringers are shown in Fig. 5 and Fig. 6.

Shear studs are welded to the steel beams to provide for the necessary connection between the steel beams and the precast concrete panels to develop composite action. Pairs of 1/4-in.-diameter studs, 2-1/2 in. long, spaced at 6 in., and 1-3/4 in. apart with an ultimate shear capacity of 3556 lbf, as calculated by AASHTO recommendations, are used.

The precast concrete panels are 23-5/8 in. long, 64 in. wide, and 2.7 in. thick. Each panel has four tapered pocket holes per stringer for the shear connectors. A groove in the long side of the panels was molded during casting. The grooves of two panels placed side by side form a 3/8-in.-wide

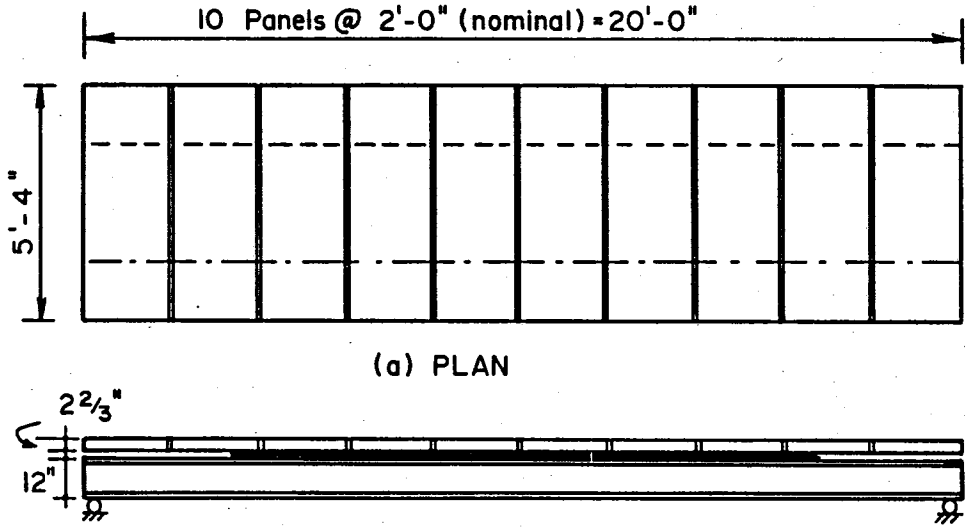

FIG. 4. Layout of Bridge Model (3)

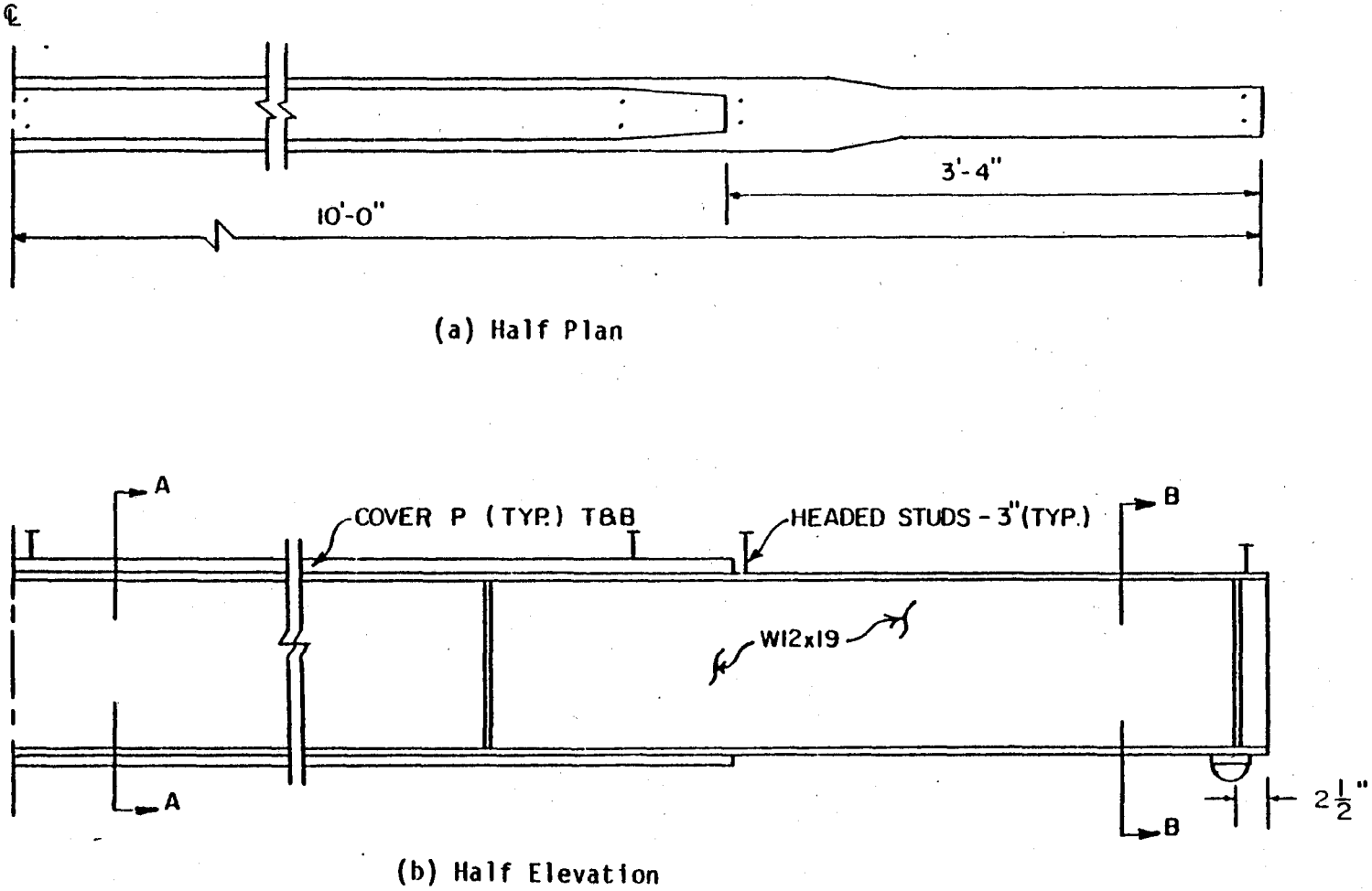

FIG. 5. Details of the Model Stringers (12)

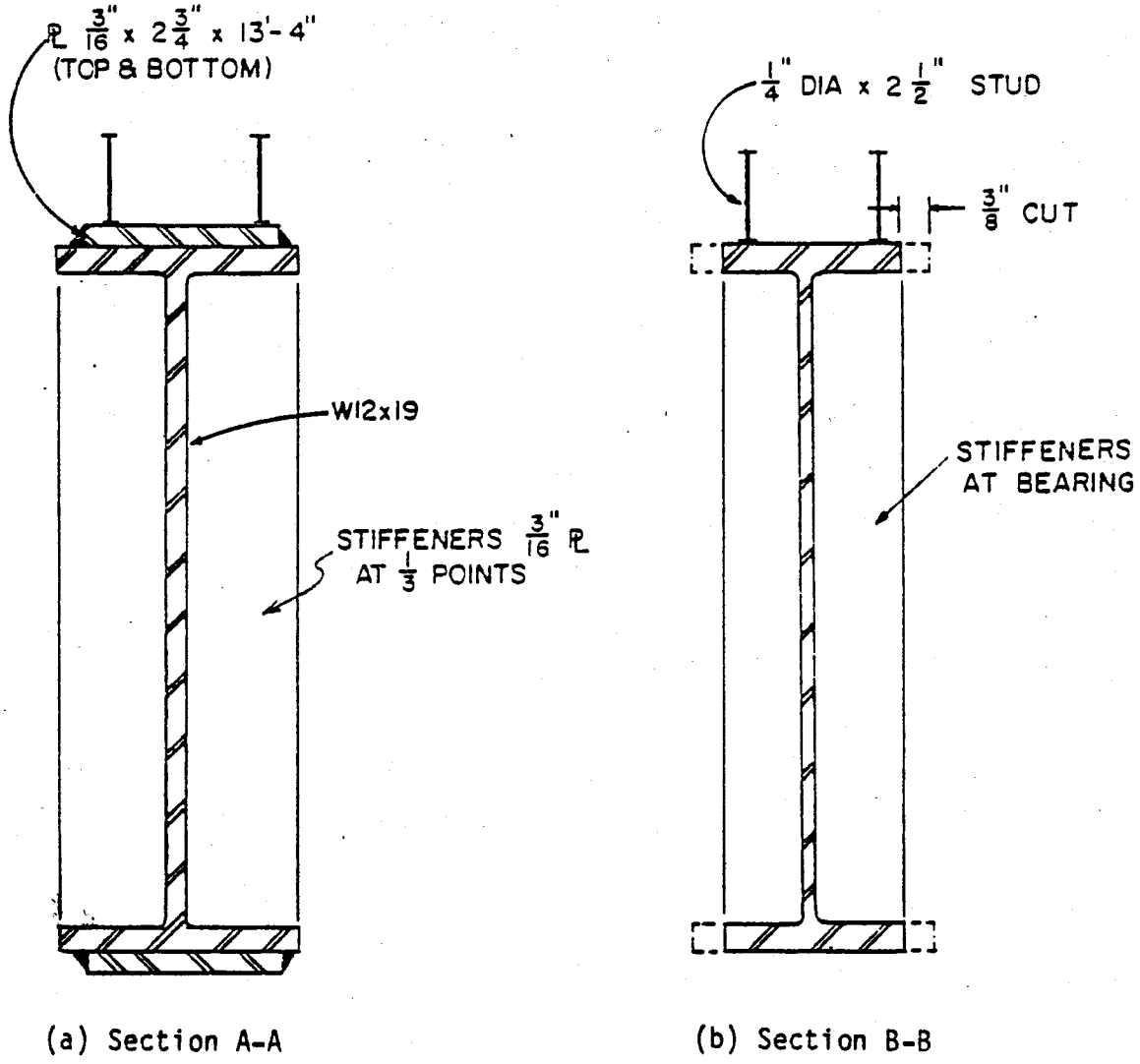

FIG. 6. Cross Section Details of the Model Stringers (12)

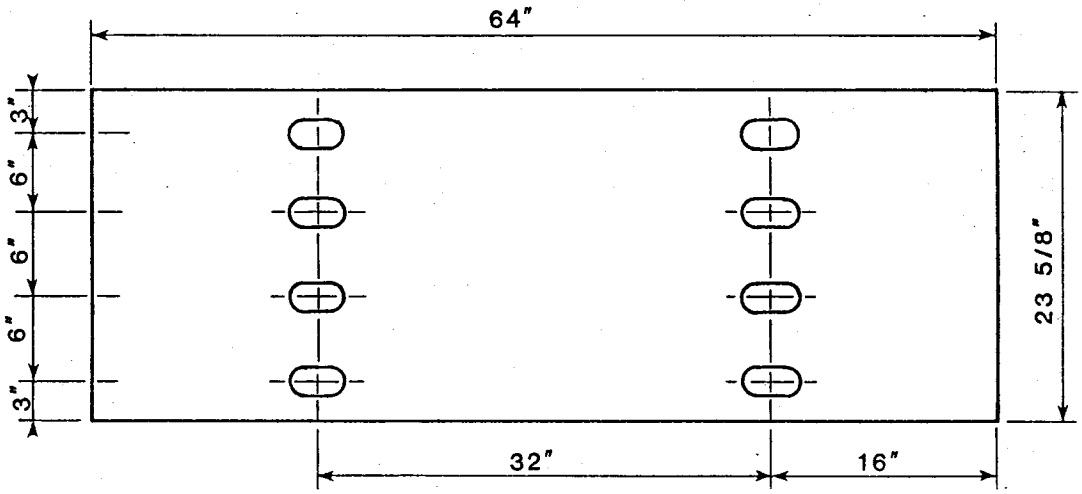

PLAN VIEW

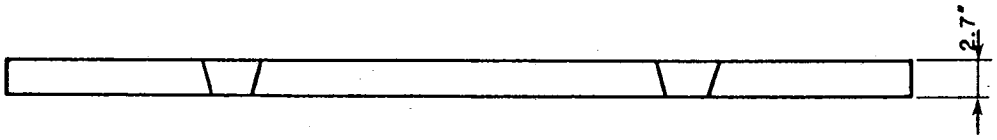

SIDE VIEW

FIG. 7. Precast Concrete Panels

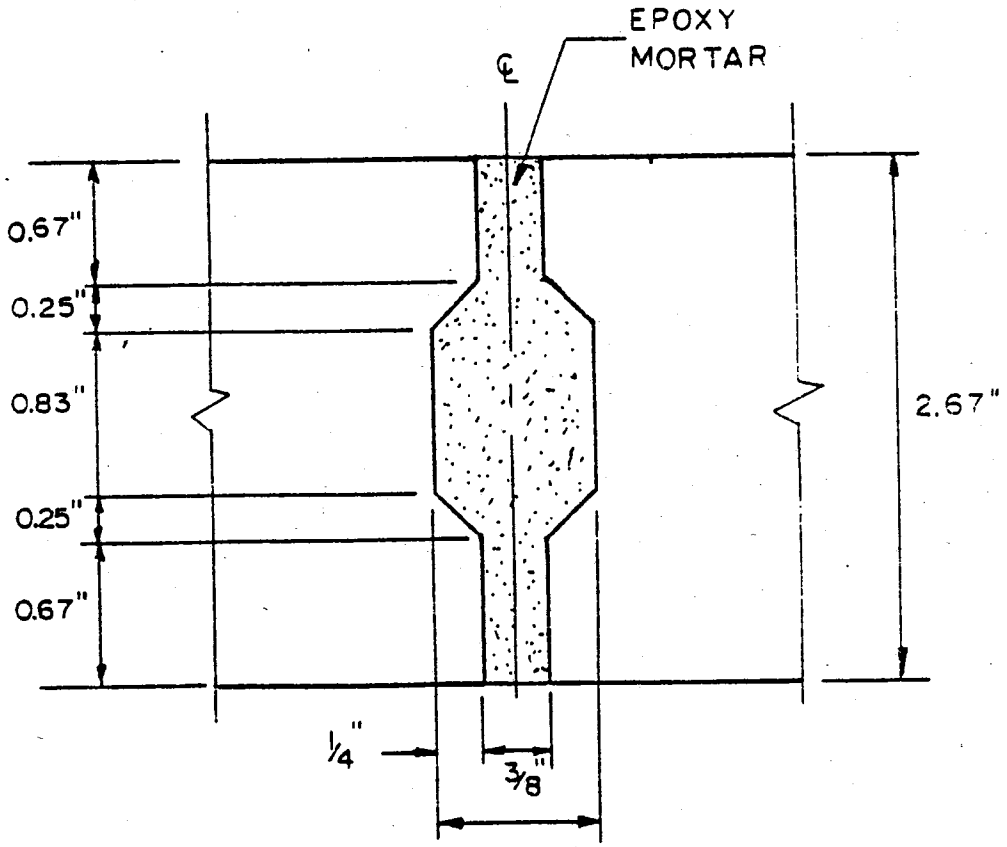

FIG. 8. Details of the Model Shear Key Joints (12)

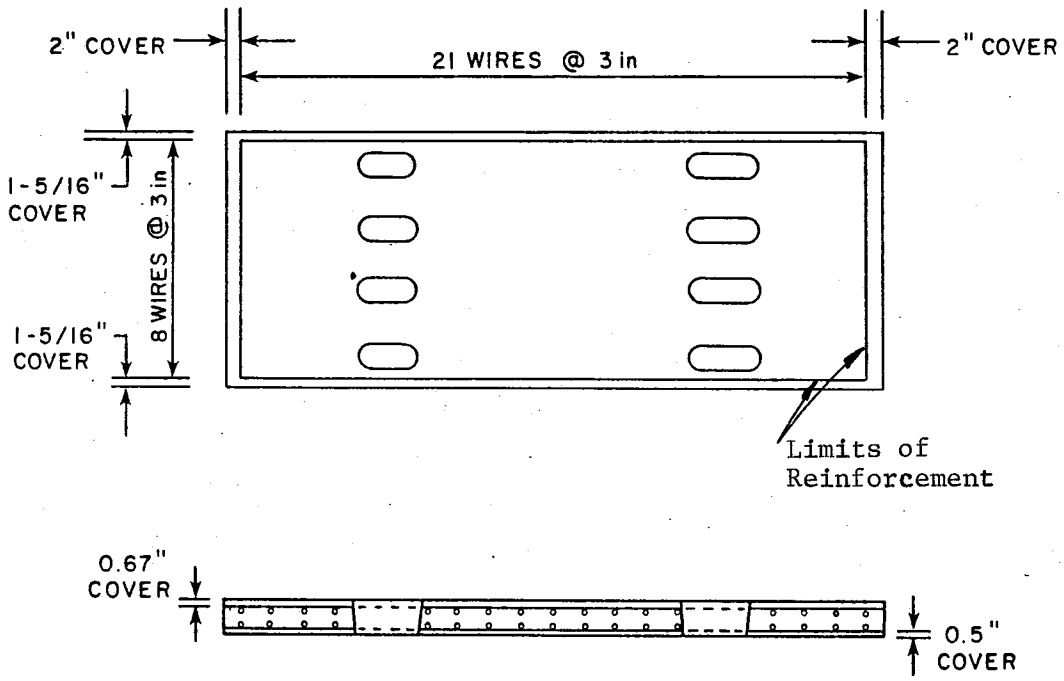

FIG. 9. Details of the Concrete Panel Reinforcement

shear key joint. Details of the precast concrete panels and shear key joints are shown in Fig. 7 and Fig. 8, respectively. The top and bottom reinforcement of the concrete panels consists of welded wire fabric having a yield stress of 60 ksi. A mesh of 3.X3.-D3XD3, 0.195-in. diameter, deformed steel wire spaced 3 in. in both directions, longitudinal and transversal, provided a 0.38 per cent of reinforcement at the top and bottom of the concrete panels in the two directions of reinforcement. The concrete cover distances for the steel wire reinforcement are 0.67 in. at the top, 1/2 in. at the bottom, 1-5/16 in. at the long sides and 2.0 in. at the short sides. The reinforcing steel does not pass through the joints or the pockets. Details of the reinforcing pattern are shown in Fig. 9.

The strength of the concrete in the model was reported to vary significantly between each concrete panel at the time when compressive strength tests were performed. Reported strength on 4-in.-diameter by 8-in.-high cylinders tested thirty to forty days after casting of the concrete varies from 6370 to 7150 psi (12). The actual concrete strength at the time this experiment was performed (about 1 year after the concrete was cast) is not known, but the variations in concrete strength between slabs are expected to be smaller than when first reported.

Longitudinal transfer of shear forces between the steel beams and the concrete slab is provided by the shear studs grouted into the pocket holes of the concrete panels. The shear studs were designed to fail at design positive moment loading. The size selected was 1/4 in. diameter by 2-1/2 in. long. The studs were placed in pairs 1-3/4 in. apart and spaced every 6 in. The pocket geometry was then chosen to fit the studs. A haunch of approximately 1/4 in. resulted from supporting the panels on resilient spacers during grouting. The panels were then placed flushed at the top. An epoxy mortar was used to fill the tapered hole pockets and the shear key joints in the deck of the bridge model. The mortar is made by mixing grade No. 1 aggregates as defined by the Texas Highway Department (see Table 1) with the Texas Highway Department Epoxy Binder B-102 in an aggregate-to-epoxy weight ratio of 3.0. Split tensile tests and compression tests performed 24 hours after the epoxy was mixed show an approximate tensile strength of 1,300 psi and an approximate compressive strength of 8,000 psi.

TABLE 1. Grading Limits for the Texas Highway Department Grade No. 1 Aggregate (12)

Sieve No.	Cumulative Per Cent Retained
No. 4	0 - 5
No. 8	0 - 20
No. 16	15 - 50
No. 30	40 - 75
No. 50	70 - 90
No. 100	90 - 100

Loading System

Negative moments were induced by an upward concentrated load applied at the midspan to each stringer by two identical hydraulic rams resting on the rigid floor system of the testing laboratory. The model was restricted from lifting at the supports by applying a downward force through a pre-tensioned steel bar bolted to a stringer reaction beam.

Reaction Mechanism

The purpose of the reaction mechanism was to prevent any uplift of the model at the supports while the upward external load was applied at midspan. The mechanism consisted of a pair of stringer reaction beams, floor reaction beams, anchor bolts, and stringer bolts.

The floor and stringer reaction beams were fabricated from two 6.8X5 steel channels welded back to back. A gap of approximately 1-1/4 in. was left between the channels to allow room for the reaction bolts. The reaction stringer beams were tack-welded to the interior flanges and webs of the model stringers to prevent any movement of the beams.

A downward force was applied to the model through the reaction mechanism by tightening the nuts at either end of the bolts. The total downward applied force was calculated to be equal to or greater than the sum of the dead load of the model plus the maximum live load. Details of the reaction mechanism are shown in Fig. 10.

For a real bridge the section would be supported, at the center, over a pier, and the ends would be pushed downward at the ends by loading through the deck. In the model, the panels would have a tendency to remain flat and pull away from the model beams; and there would be more uplift forces at the ends than in a real bridge. However, it is also recognized that the level of loading in the model required to cause cracking in the deck would be smaller than the level of loading required to cause an uplift failure at the panel-stringer interface of the end sections because of the high bonding strength of the epoxy mortar present in the panel-stringer gap. Therefore, the reaction mechanism is not expected to affect the test results.

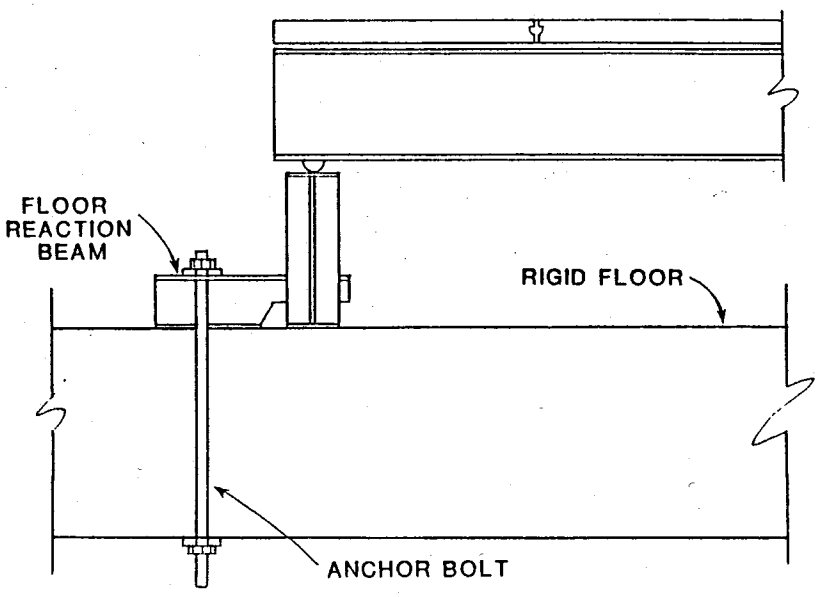

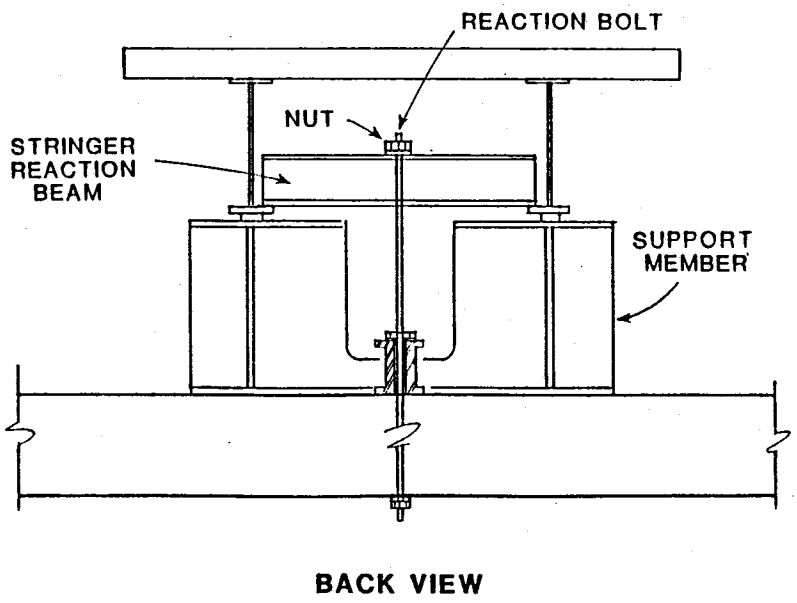

FIG. 10. Details of the End Reaction Mechanism

Instrumentation

The instrumentation of the model was based on the assumption that the longitudinal distribution of flexural strains was symmetric about the midspan and the assumption that the maximum tensile strains occurred at the location of maximum internal moment, as predicted by the basic theory of mechanics of materials.

The data collected during the test included:

1) the static load applied to the model,
2) the normal flexural strain distribution in the steel beams of the model,
3) the vertical deflection of the model stringers, and
4) the width of the cracks in the concrete deck.

The upward load applied to the model was measured using two strain gage load cells, one for each hydraulic ram. The downward load applied at the supports to prevent any lifting of the model was monitored by two longitudinal strain gages bonded diametrically opposite on each pretensioned reaction bolt. Flexural strains in the steel beam were monitored by the use of strain gages bonded to the stringers of the model. Dial indicators and displacement transducers were used to measure the vertical deflection of the stringers and the crack opening displacement in the bridge deck, respectively.

Load Cells

Two 30-kip load cells were used to monitor the static applied load. The load cells were connected directly to a strain indicator. Calibration of the load cells was performed using an INSTRON machine and a 5000 lbf capacity proving ring with 5 lbf resolution.

Strain Gages

Most of the monitored strain gages were located on the west side of one of the beams of the model, stringer 1, since a symmetric behavior about the midspan in the distribution of flexural strains and in the cracking pattern

of the concrete was expected. A total of 30 out of 36 strain gages bonded to the steel beams was located in the west region of stringer 1. The other six gages were bonded to points of symmetry relative to the monitored cross sections to check the expected symmetric behavior. Two strain gages were bonded at the top of the concrete slab longitudinally across the midspan shear key joint.

A total of nine cross sections was monitored in the instrumented one-fourth region of the model. Five of the nine cross sections were located within 24 in. of midspan because cracking of the concrete slab was expectded at this location. Fig. 11 shows the location of the cross sections along stringer 1 where strain gages were installed. Fig. 12 shows the six possible locations of the strain gages along a cross section.

The purpose of the two strain gages bonded to the top of the concrete slab at midspan was to provide a positive indication of transverse cracking at the midspan shear key joint. Strain in the shear key joint at this location was not intended to be monitored by these gages.

Dial Indicators

Two different distributions of dial indicators were used during the experiment. The first distribution was used during the initial part of the experiment, when cracks in the concrete slab were not present. A total of four dial gages was used. Three were located at the quarter points of stringer 1, and the fourth dial gage was located at midspan of stringer 2. The second distribution was used during the final part of the experiment, when the concrete slab was cracked. A total of six dial gages was monitored; five measured the deflection of the steel stringer 1 at locations 45.5 in. and 81.5 in. away from each support and at midspan. The sixth dial indicator was located at midspan of stringer 2. Fig. 13 shows the positions of the dial indicators along the model for both distributions.

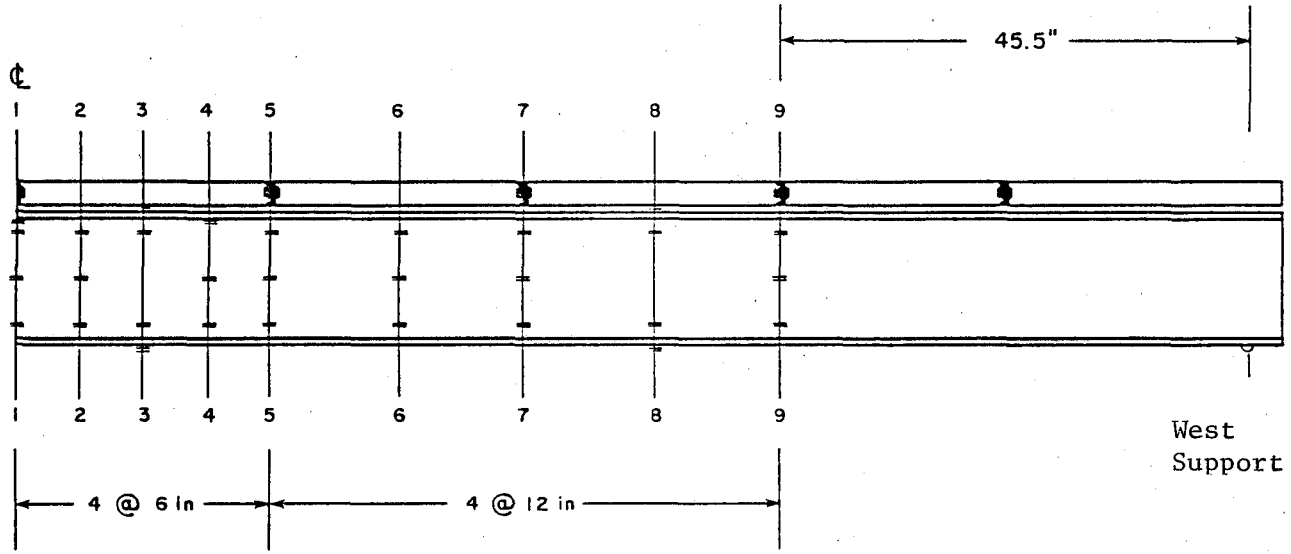

FIG. 11. Location of Monitored Cross Sections in Stringer 1

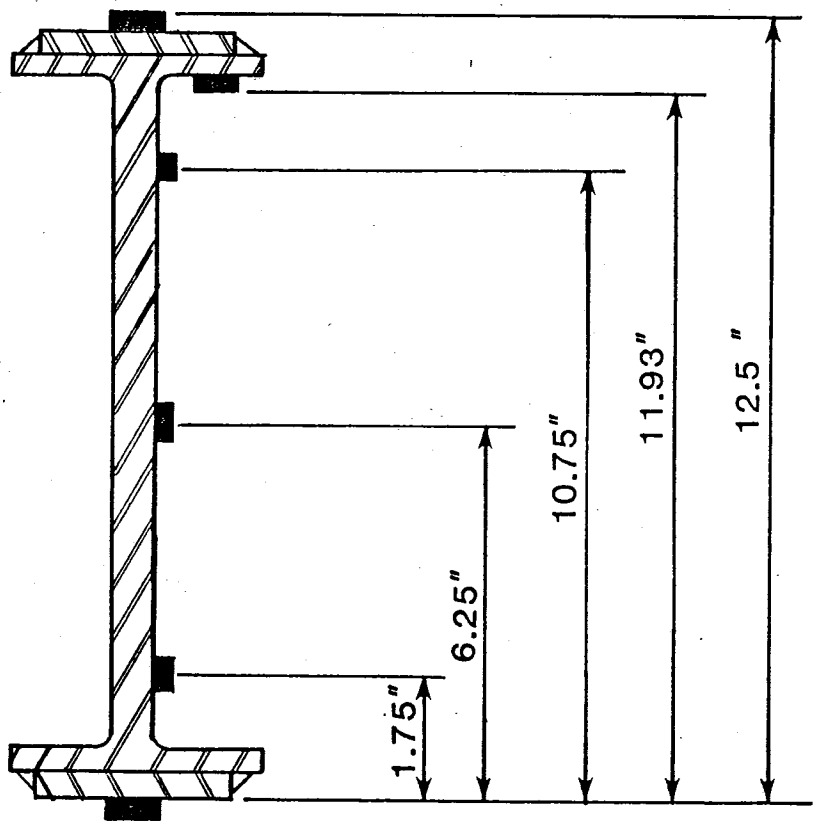

FIG. 12. Various Locations of Strain Gages at the Monitored Cross Sections

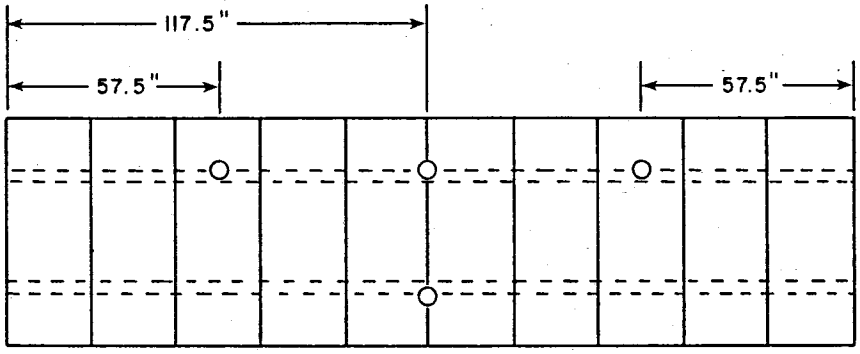

PLAN

West
Support

(a)

○ LOCATION OF DIAL INDICATORS

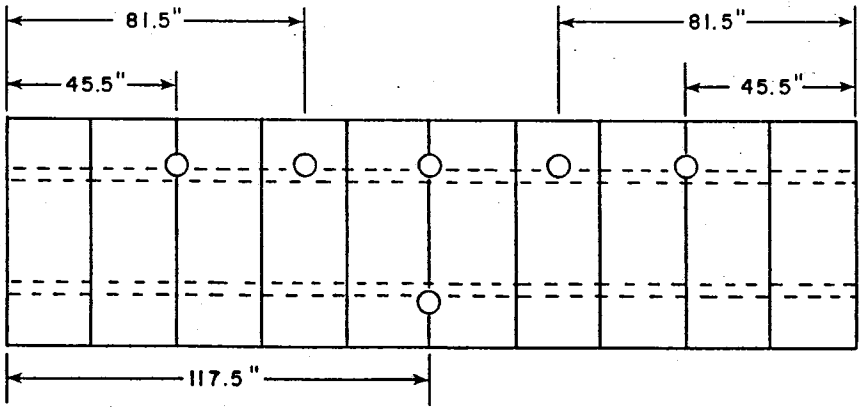

PLAN

West
Support

(b)

FIG. 13. Locations of Dial Indicators (a) For the Uncracked Phase of the Experiment, (b) For the Cracked Phase of the Experiment

Displacement Transducers

Two displacement transducers were installed at the top of the concrete slab across the midspan joint. The purpose of the displacement transducers was to measure the opening displacement of any transverse crack. The displacement transducers had a resolution of 0.001 in.

CHAPTER III

PRESENTATION OF RESULTS

Negative moments in the experiment were generated by the application of an upward concentrated load at the midspan of the model. The load was applied in intervals of either 250 or 500 lbf until the first cracks in the concrete deck developed. The load sequence after the first cracks in the concrete slab were observed was controlled by the increment in the total deflection of the model at the midspan.

The results obtained during the experiment are grouped into two categories:

1. Results before cracking of the concrete deck, and
2. Results after cracking of the concrete deck.

Part 1: Results Before Cracking of the Concrete Deck

This part of the experiment consists of four load-unload sequences. The first load sequence was used to check out the strain gages bonded to the steel beams. A maximum load of 2510 lbf per stringer was applied in intervals of approximately 250 lbf. After the first load sequence some strain gages were removed and replaced. In the second load sequence each stringer was initially loaded to 500 lbf, and the maximum applied load was 2010 lbf. After the maximum load was applied the system was completely unloaded. A small drift in the zero reading of some strain gages was found. All strain readings were re-zeroed and the model was reloaded two hours later to a maximum load of 2765 lbf per stringer. Drift in the zero reading of some strain gages was again found when the system was unloaded. Temperature changes in the laboratory and probably some creeping of the epoxy mortar at the joints were considered the possible causes for the drifts in the strain gages. The last loading sequence started at 2260 lbf per stringer and incremented to a maximum load of 3770 lbf. Up to this loading stage no cracks had been observed in the model.

Flexural Strain Distribution

The flexural strain data measured from the nine monitored cross sections was reduced and compared to the measured data from the four back-up points to check for symmetry in the behavior of the bridge. The measured strain data was multiplied by a correction factor equal to either 2.00/2.11 or 2.00/2.13 depending on the type of strain gages to account for the difference between the gage factor setting of the strain indicator and the gage factor of the strain gages.

Strain data for every cross section at every applied load was plotted, and a best-fit linear strain distribution along the cross section of the steel stringer 1 was determined using curve fitting of the recorded values. Figs. B1 to B18 show the measured strain data and the approximate linear distribution of strains for cross sections 1 to 9, respectively, for the load sequence 2.

Deflections

Deflections were measured at four points in the model; three at the quarter points of the monitored stringer 1 and one at the midspan of stringer 2.

Measured deflections for load sequence 2 are tabulated in Table 2 for the midspan deflection of stringer 1 and 2. The load deflection curve for the values tabulated in Table 2 is shown in Fig. 14.

Displacement Transducers

Data from the displacement transducers on the concrete slab across the midspan joint showed that there was not significant deformation in the shear key joint. Recorded values during the test from the displacement transducers are tabulated in Table 3 for the uncracked load sequence 2.

TABLE 2. Measured Deflection at Midspan in Stringer 1 and Stringer 2 for Uncracked Load Sequence 2

LOAD lbf	MIDSPAN DEFLECTION in.	
	STRINGER 1	STRINGER 2
503	0.011	0.011
754	0.018	0.019
1006	0.025	0.025
1509	0.037	0.037
1760	0.044	0.046
2012	0.051	0.050

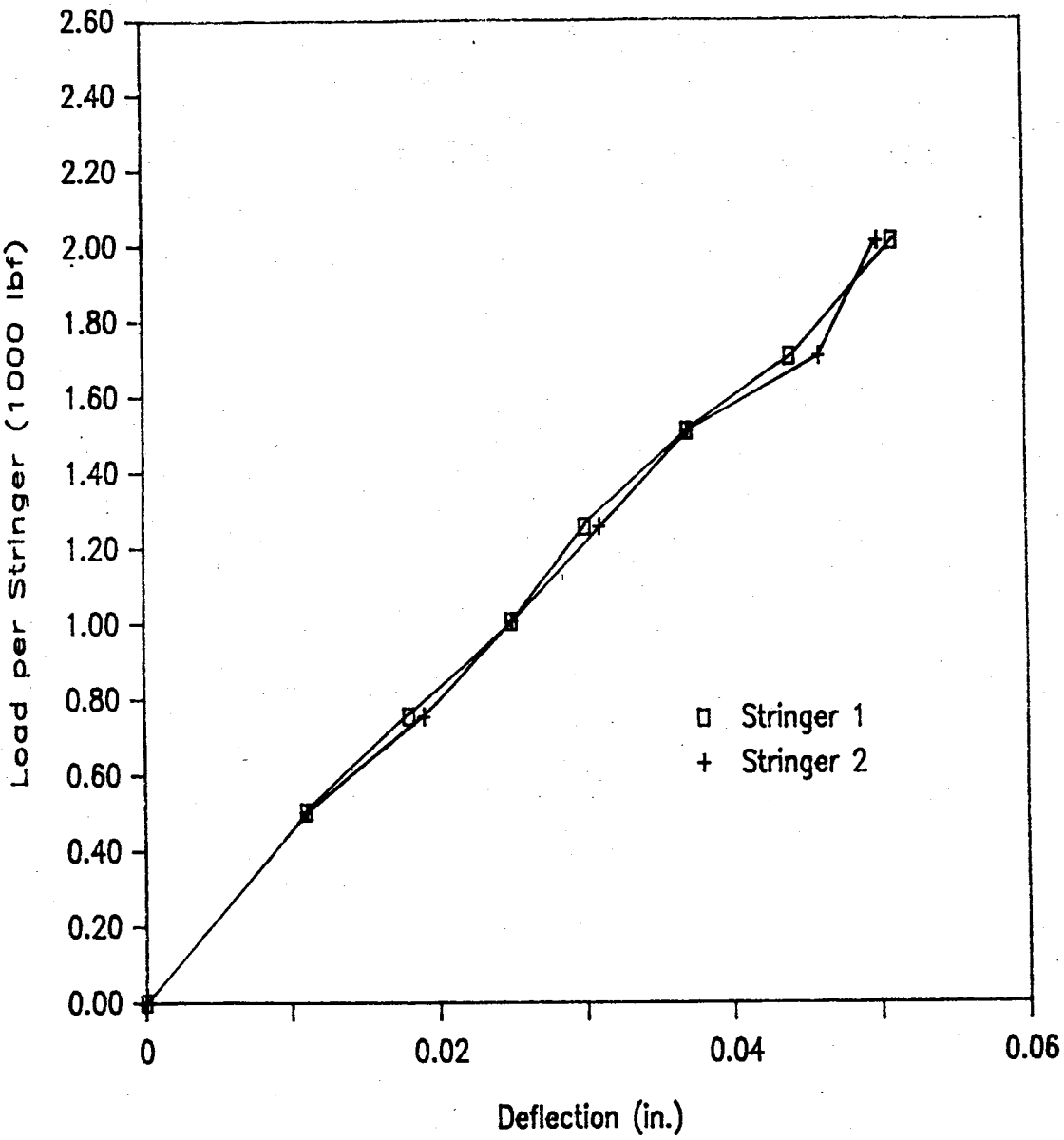

FIG. 14. Measured Midspan Deflection in Stringer 1 and Stringer 2 for the Cracked Load Sequence 2

Part 2: Results After Cracking of the Concrete Deck

The second group of measured data was obtained from two load-unload sequences. In the first load sequence each stringer was initially loaded to 2765 lbf. A maximum load of 4275 lbf was applied in intervals of 250 lbf. The loading was interrupted when the first crack was observed. In the second load sequence the model was completely unloaded and then reloaded until a second crack in the concrete deck was recorded at a force of 4400 lbf per stringer. The applied force after the second crack developed was controlled by the increment in total deflection in the model at midspan of stringer 1. Load was applied until an increment of approximately 0.01 in. was recorded at midspan or until a new crack was observed. The maximum load applied to each stringer was 7240 lbf.

Flexural Strain Distribution

The flexural strain data for the nine monitored cross sections was collected and reduced using the same procedure described before in Part 1. Figs. B19 to B45 show the measured strain data and the approximate linear strain distribution for each cross section at fifteen different loadings during cracked load sequence 2.

Deflections

Deflections were measured at six points in the model. The distribution of the dial indicators is described in Chapter II and shown in Fig. 13. Measured deflections for the cracked load sequence 2 are tabulated in Table 4 and in Table 5. Load deflection curves for values tabulated in Table 4 and Table 5 are shown in Figs. 15 to 17.

TABLE 3. Deformation of Shear Key Joint at Midspan

LOAD lbf	DEFORMATION OF MIDSPAN JOINT in. x 10^{-6}	
	Stringer 1	Stringer 2
503	0	0
750	0	0
1006	0	-68
1257	0	-68
1509	133	-136
1560	-133	-272
2012	0	0

TABLE 4. Measured Deflection at Midspan in Stringer 1 and Stringer 2 for Cracked Load Sequence 2

LOAD lbf	MIDSPAN DEFLECTION in.	
	STRINGER 1	STRINGER 2
1006	0.025	0.022
1509	0.028	0.034
2012	0.051	0.047
2514	0.063	0.060
3068	0.079	0.075
3520	0.093	0.088
4023	0.106	0.101
4425	0.118	0.113
4916	0.135	0.129
5155	0.157	0.144
5368	0.179	0.159
5909	0.201	0.185
6336	0.225	0.210
6613	0.250	0.235
7241	0.284	0.269

TABLE 5. Deflections at 57.5 in. and 81.5 in. from Support in Stringer 1 for Cracked Load Sequence 2

LOAD lbf	DEFLECTION (in.)			
	SECTION 8		SECTION 6	
	EAST	WEST	EAST	WEST
1006	0.014	0.014	0.021	0.021
1509	0.021	0.021	0.032	0.031
2012	0.029	0.027	0.044	0.043
2514	0.037	0.034	0.056	0.055
3068	0.045	0.042	0.068	0.066
3520	0.052	0.048	0.080	0.078
4023	0.059	0.055	0.091	0.089
4425	0.066	0.061	0.102	0.098
4916	0.076	0.071	0.118	0.114
5155	0.087	0.082	---	---
5368	0.099	0.091	0.157	0.152
5909	0.111	0.102	0.177	0.170
6336	0.124	0.112	0.197	0.189
6613	0.138	0.135	0.220	0.210
7241	0.155	0.153	0.247	0.241

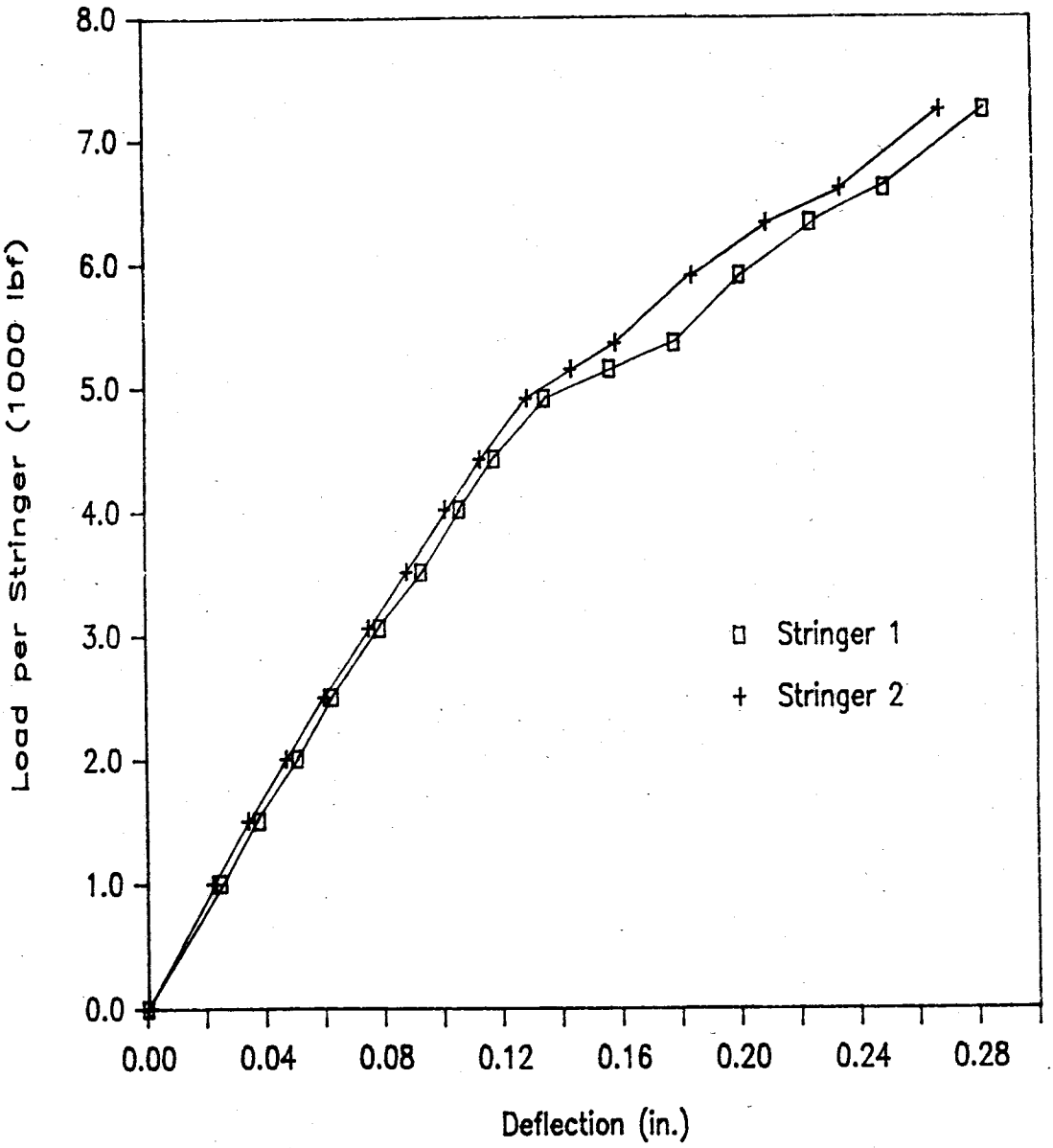

FIG. 15. Measured Midspan Deflection in Stringer 1 and Stringer 2 for the Cracked Load Sequence 2

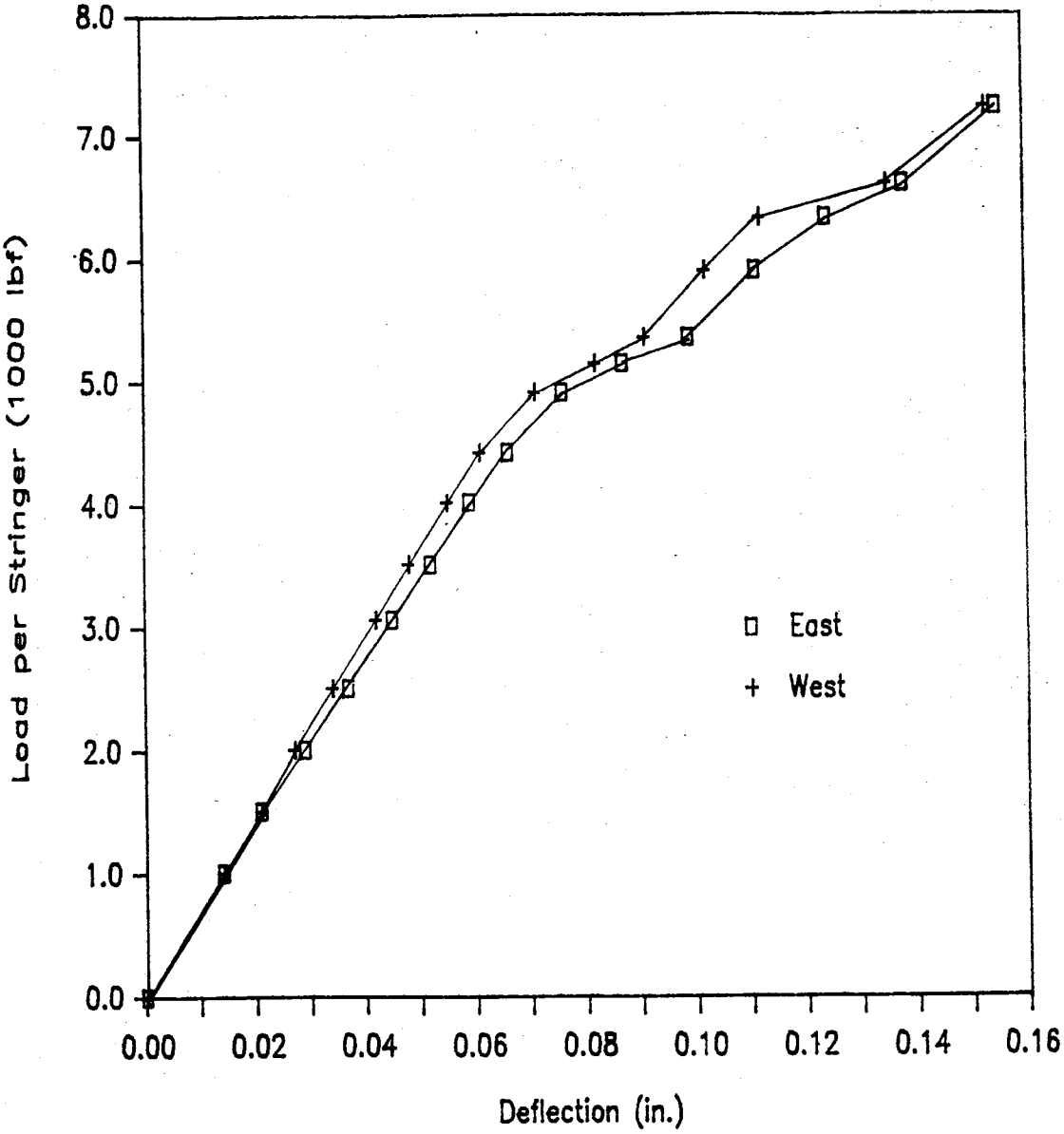

FIG. 16. Measured Deflections in Stringer 1 for Sections 45.5 in. Away from the Supports for the Cracked Load Sequence 2

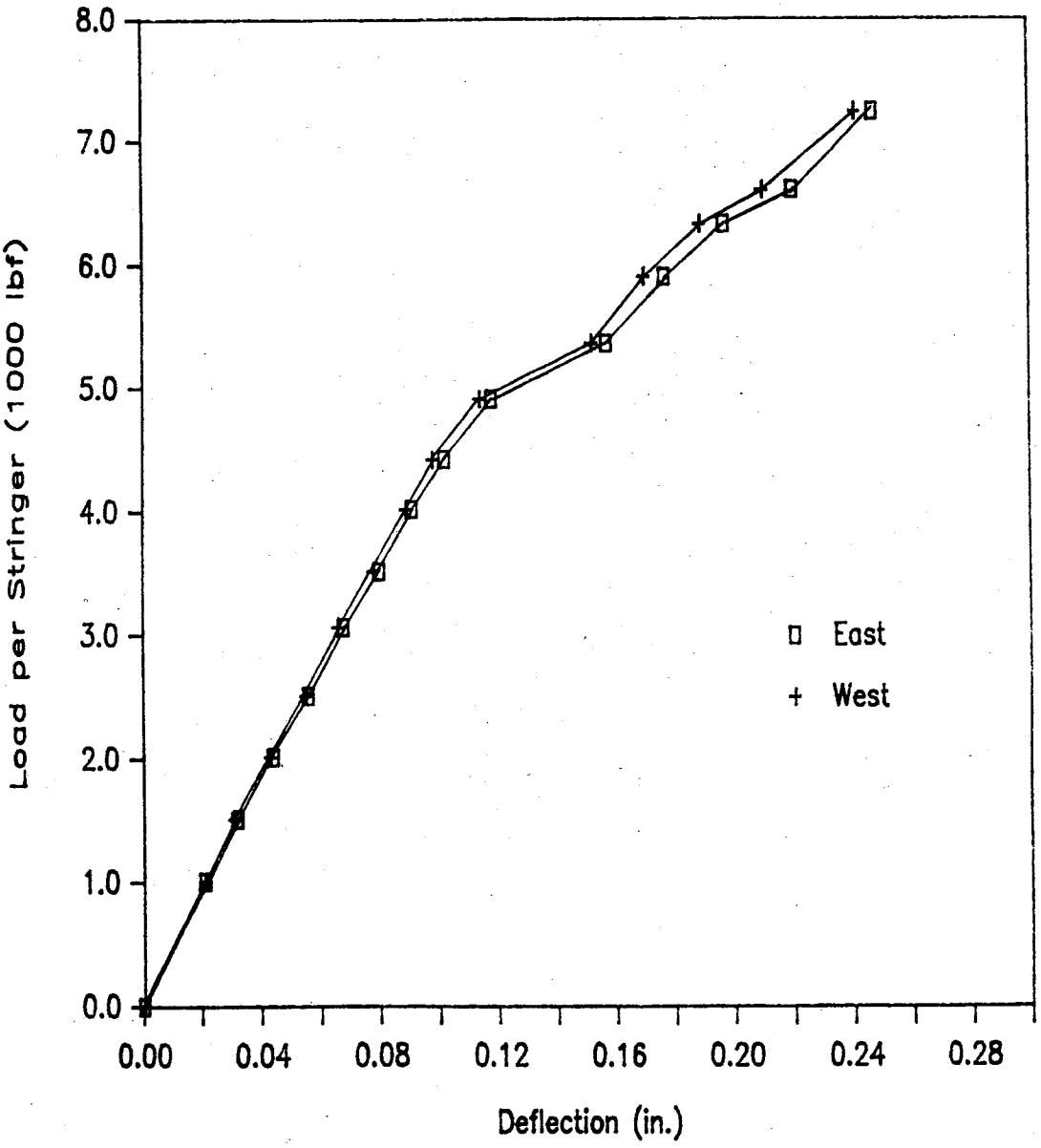

FIG. 17. Measured Deflections in Stringer 1 for Sections 81.5 in. Away from the Supports for the Cracked Load Sequence 2

Cracking Pattern of the Concrete Deck

The cracking pattern of the concrete deck was expected to be symmetric about the midspan. Major structural cracks were expected to develop at sections with highest internal moments. The instrumentation of the model was based on this assumption as discussed above.

The first crack was observed to develop transversely at the third shear key joint from the east support at an applied load of 4275 lbf per stringer. The crack was approximately 3 in. long and developed in the north edge of the concrete deck at the interface between the epoxy mortar and the concrete. This crack was not considered a major structural crack but rather a premature bonding failure between the epoxy-grouted shear key joint and the precast concrete panel.

The first major structural crack developed at the east shear key joint adjacent to the midspan joint at an applied load of 4400 lbf per stringer. As the load was increased a full crack was propagated through the thickness of the slab. The second structural crack was observed to develop at the west shear key joint adjacent to the midspan joint (section 5-5) at an applied load of 4990 lbf per stringer. Even though these cracks appeared at the interface between the concrete panels and the epoxy mortar, a clear failure of the concrete in tension was observed.

The second set of major cracks developed about 12 in. away from the midspan shear key joint (section 3-3 in the west side of stringer 1 and a section symmetric about the midspan in the east side) at a higher applied load compared to the first set. The cracks propagated transversely across the entire width of the bridge deck. The cracking pattern of the concrete deck is shown in Fig. 18. The approximate loads at which cracks developed are also shown. It can be seen from Fig. 18 that the final pattern of cracking was symmetric about the midspan, even though the cracks did not develop in a sequential pattern. It is also important to notice that a structural crack did not develop at the midspan joint as predicted by mechanics of materials.

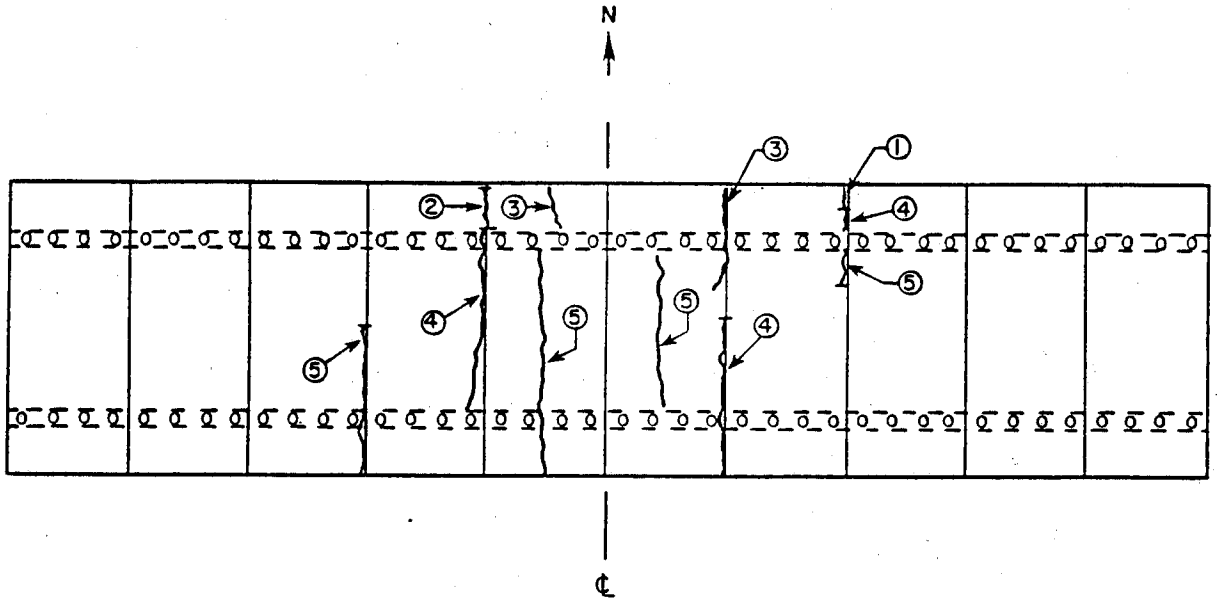

PLAN VIEW

CRACK No.	LOAD (kips)
1	4.275
2	4.400
3	4.900
4	5.155
5	7.240

FIG. 18. Cracking Pattern of the Concrete Deck

CHAPTER IV

DISCUSSION OF RESULTS

In design practice it is usually assumed that concrete does not have any capacity to withstand tensile stresses; however, it is well known that concrete has a tensile strength, even though it is low compared to its compressive strength. Because of the capacity of concrete to carry tensile stresses, concrete-steel stringer composite bridges under negative moment loadings may be expected to behave linearly, i.e. without cracking in the deck, up to a point at which a critical cracking stress is reached. However, the uncertainty of the ultimate tensile strength of concrete makes it difficult to predict with confidence the magnitude of the load at which cracking in the slab of a composite bridge will occur.

The results of this experiment, as presented in Chapter III, are divided into 2 parts, results before and after cracking of the concrete deck. The purposes of the first part of the experiment are to study the model section properties and the influence of the epoxy joints on the linear behavior of the structure. The results of the second part of the experiment are used to study the loss of composite action in the model due to the cracking of the concrete deck and to determine the magnitude of the cracking stress at which significant composite action is lost.

Part 1: Model Before Cracking of the Concrete Deck

Before any analysis of the structure could be performed, the section properties of the model had to be determined. A partial interaction theory was used to study the changes in section properties of the structure in the vicinities of the shear key joints and in the areas of transition between concrete and epoxy in the model deck.

The partial interaction theory used was developed by Newmark (11), and is based on the following assumptions:

a) the discrete shear connections can be modeled by an equivalent uniform continuous linearly elastic medium,

b) initially plane sections remain plane after bending,

c) the sections of concrete and steel are constant over the beam length,

d) there is no vertical separation between the beam and the slab, and

e) the concrete and steel are isotropic elastic materials.

It was also assumed for the analysis that the modulus of elasticity of concrete in tension was equal to the modulus of elasticity in compression. Continuity conditions were used at the interface of the concrete-steel sections and epoxy-steel sections so that assumption (c) was not violated.

For the analysis of composite sections using the partial interaction theory, it is convenient to consider the bending moment acting on a composite beam as the resultant of internal forces acting in the deck and stringer individually. These forces can be represented by a moment in the stringer, M_s, a moment in the deck, M_d, and two equal and opposite axial forces, N_d and N_s, acting in the deck and stringer, respectively. The theory considers a linear distribution of strains in the steel and concrete sections with a discontinuity at the beam-slab interface due to deformations of the shear transfer mechanisms. Fig. 19 shows strain diagrams for a composite section under flexure. In the partial interaction strain diagram a slip strain, ε_{slip}, due to the relative movement between the stringer and the deck is shown as well as the internal forces acting in the section. Continuity of slip strains and curvature across the deck-stringer interface is assumed.

Following the procedure outlined by Knowles (9), the slip strain can be derived as a function of the axial force and the applied moment.

For equilibrium,

$$M(x) = M_s + M_d + N\, d_t \qquad (1)$$

where

$N = N_d = -N_s$ and

d_t = distance from the centroid of the stringer to the centroid of the deck.

For curvature compatibility,

$$\frac{M_d}{E_d I_d} = \frac{M_s}{E_s I_s} \qquad (2)$$

where

E_d = modulus of elasticity of the deck,

E_s = modulus of elasticity of the steel stringer,

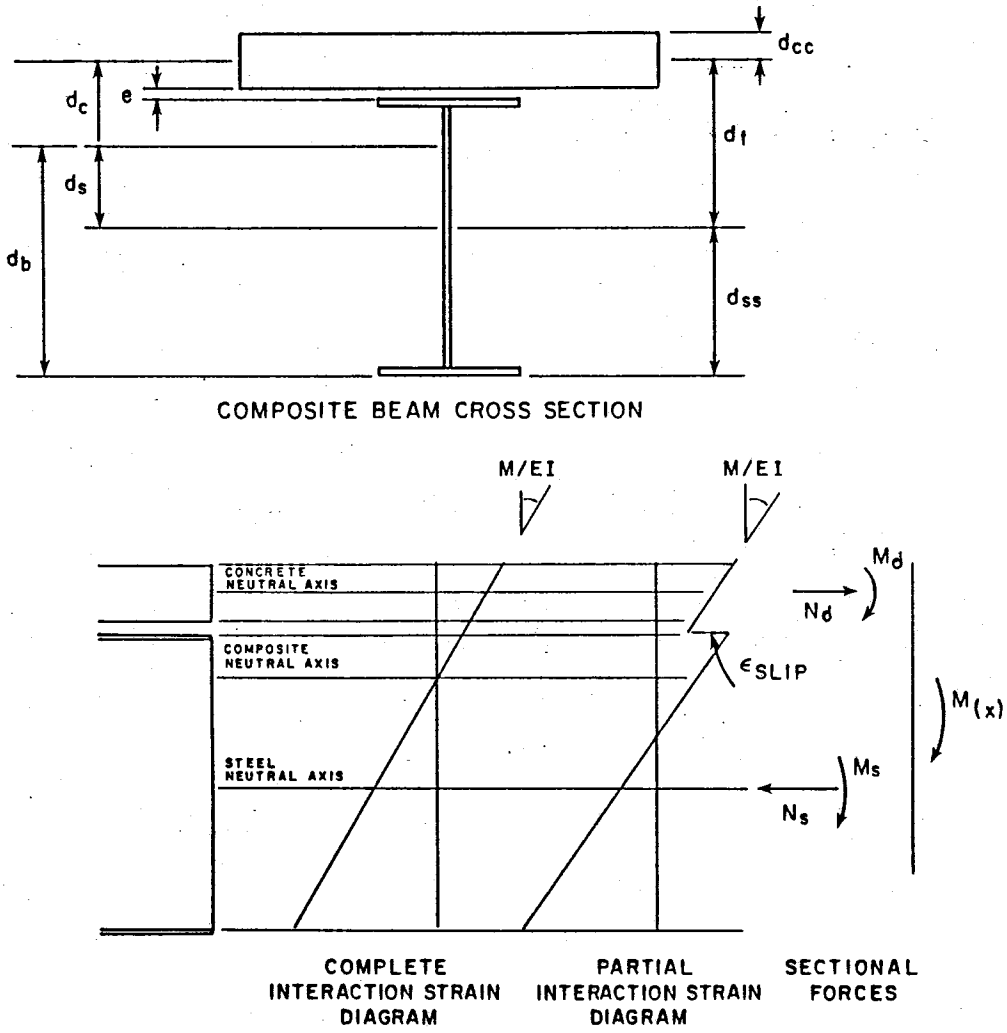

FIG. 19. Distribution of Strains and Internal Forces in a Steel-Concrete Composite Beam (9)

I_d = moment of inertia of the deck, and

I_s = moment of inertia of the steel.

If a portion of composite beam dx long is considered with a slip displacement s, the the slip strain is given by

$$\varepsilon_{slip} = \frac{s}{d_x} \tag{3}$$

If the modulus of the medium (slip caused by unit shear) is denoted μ, the the slip in length dx is

$$s = \mu \, (dN / dx) \tag{4a}$$

$$\varepsilon_{slip} = \mu \frac{d^2N}{dx^2} \tag{4b}$$

Since slip strain ε_{slip} is caused by the difference between the strains in the slab and beam at the interface,

strain in slab at interface =

$$\frac{-N}{A_d E_d} - \frac{M_d}{E_d I_d} \left(d_{cc} + e \right) \tag{5}$$

strain in beam at interface =

$$\frac{N}{A_s E_s} - \frac{M_s}{E_s I_s} \left(d_t - d_{cc} - e \right) \tag{6}$$

Solving for M_d in Eq. 2, substituting in Eq. 5 and subtracting Eq. 6 from Eq. 5, yields

$$N\left(\frac{1}{A_s E_s} + \frac{1}{A_d E_d}\right) - \frac{M_s d_t}{E_s I_s} = \varepsilon_{slip} \tag{7}$$

and from Eq. 1 and Eq. 2,

$$M_s = \frac{M - N d_t}{\left(\frac{E_s I_s}{E_d I_d + E_s I_s}\right)} \tag{8}$$

Writing parameters in terms of the section properties, gives

$$\frac{E_d A_d \quad E_s A_s}{E_d A_d + E_s A_s} = \overline{EA} \tag{9}$$

$$E_d I_d + E_s I_s = \Sigma EI \tag{10}$$

$$\Sigma EI + \overline{EA}\, d_t^2 = \overline{EI} \tag{11}$$

where

A_s = area of steel stringer and

A_d = effective area of the bridge deck.

Substituting Eq. 8 into Eq. 7 and using Eqs. 9, 10, and 11, yields

$$\mu \frac{d^2N}{dx^2} - \frac{N\,\overline{EI}}{\overline{EA}\;\Sigma EI} + \frac{M\,d_t}{\Sigma EI} = 0 \tag{12}$$

or

$$\frac{d^2N}{dx^2} - B^2 N + C = 0 \tag{13}$$

where

$$B^2 = \frac{\overline{EI}}{\mu\;\Sigma EI\;\overline{EA}} \tag{14}$$

and

$$C = \frac{M\,d_t}{\mu\;\Sigma EI} \tag{15}$$

For an interior region of a simply supported beam with a concentrated load applied at midspan as shown in Fig. 20, the interior moments can be written as

$$M(x) = M_A + V\,x \tag{16}$$

where

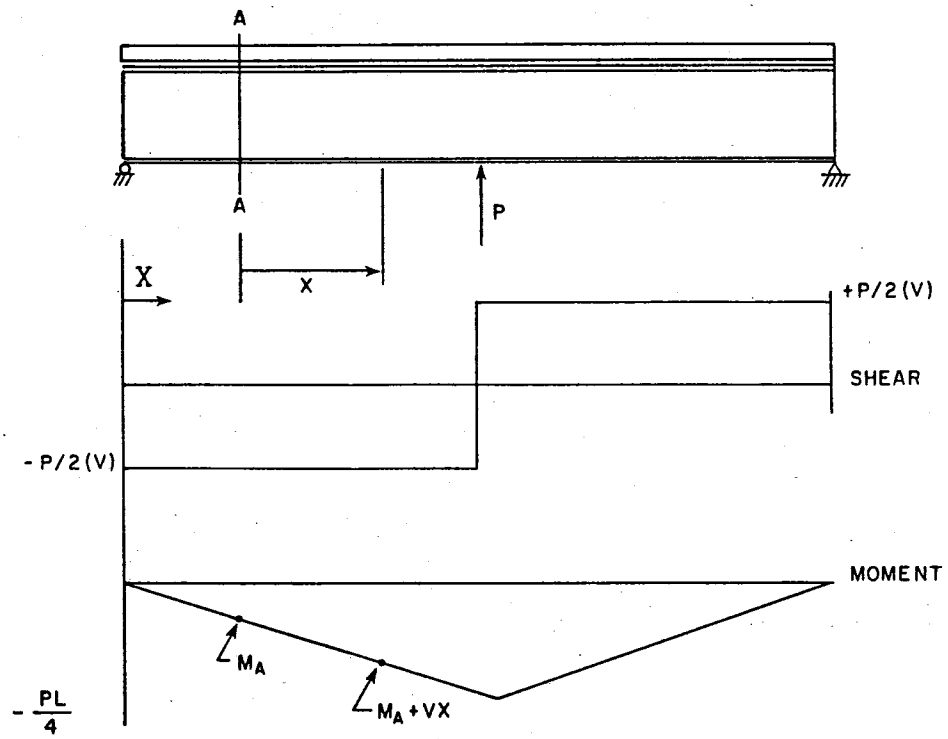

FIG. 20. Shear and Bending Moment Diagram for the Tested Model

$M(x)$= moment at distance x,

M_A = moment at section A, and

V = constant shear

Then, substituting Eq. 16 into Eq. 15, gives

$$\frac{d^2N}{dx^2} - B^2 N + K M_A + K V x = 0 \tag{17}$$

where

$$K = \frac{d_t}{\mu \Sigma EI} \tag{18}$$

The general solution of this second-order differential equation is,

$$N(x) = c_1 e^{Bx} + c_2 e^{-Bx} + \frac{V K x}{B^2} + \frac{M_A}{B^2} \tag{19}$$

where c_1 and c_2 are constants depending on the boundary conditions.

For the beam shown in Fig. 21 having axial forces N_1 and N_2 at sections A and B, respectively, the distribution of axial forces between sections A and B is given by

$$N(x) = \frac{N_1 \sinh B (L - x)}{\sinh B L} + \frac{N_2 \sinh B x}{\sinh B L} + V K \left(x - \frac{L \sinh B x}{\sinh B L} \right)$$

$$+ \frac{M_A K}{B} \left(1 - \frac{\sinh B (L - x) + \sinh B x}{\sinh B L} \right) \tag{20}$$

where L = length of the region analyzed

Using Eq. 4a and Eq. 20 the horizontal distribution of slip displacements, s(x), along the region A-B can be shown to be,

$$s = \mu \frac{dN(x)}{dx}$$

or,

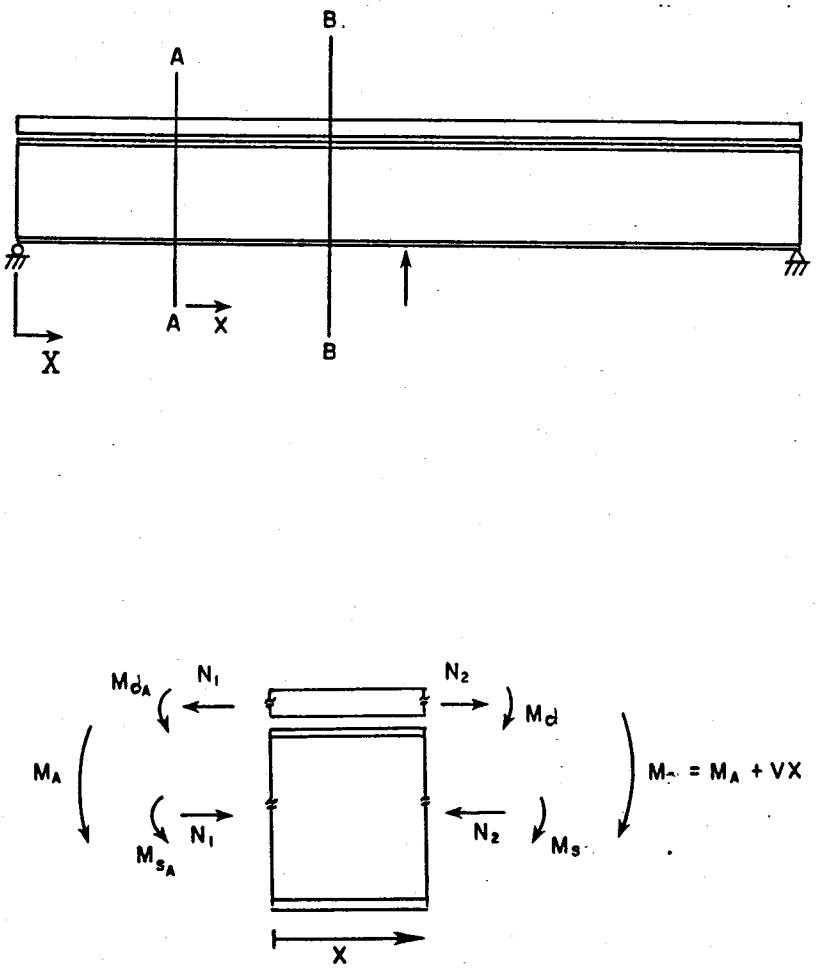

FIG. 21. Internal Forces in a Section of a Composite Beam Under Flexure

$$s = \mu\left[\frac{-N_1 B \cosh B (L - x)}{\sinh B L} + \frac{N_2 B \cosh B x}{\sinh B L} + \frac{V K}{B^2}\left(1 - \frac{L B \cosh B x}{\sinh B L}\right)\right.$$
$$\left. + \frac{M K}{B}\left(\frac{\cosh B (L - x) - \cosh B x}{\sinh B L}\right)\right] \qquad (21)$$

Distribution of Axial Forces

To find the distribution of axial forces over a region having a discontinuity in section properties, i.e., a shear key joint, continuity conditions with respect to the slip displacement have to be applied. Fig. 22 shows a section of the model that includes two precast concrete slabs and a shear key joint. Regions 1 and 3 are concrete-steel sections, and region 2 is an epoxy-steel section. Local coordinates x_1, x_2, x_3 for the three regions are shown, respectively. The slip displacement continuity conditions are,

$$s(x_1 = L_1) = s(x_2 = 0) \qquad (22)$$

$$s(x_2 = L_2) = s(x_3 = 0) \qquad (23)$$

where L_1 and L_2 are the lengths of regions 1 and 2, respectively.

In Fig. 22 the initial boundary conditions, N_1, at regions 1, 2, and 3 are represented by $\overline{N}_1$, $\overline{N}_2$, and $\overline{N}_3$, respectively, and the final boundary conditions, N_2, by $\underline{N}_2$, $\underline{N}_3$, and $\underline{N}_4$. Notice that the final boundary conditions for any region are equal to the initial boundary conditions for its adjacent region. If $\overline{N}_1$ and $\underline{N}_4$ are known, $\underline{N}_2$ and $\overline{N}_3$ can be found using Eq. 22 and Eq. 23. Note that in Eq. 21 the parameters K and B are functions only of the section properties of each region. Subscripts are used to identify the constants at the respective region, i.e., K_1 and B_1 denote the K and B factors in region 1. Since regions 1 and 3 are both steel-concrete sections,

$$B_3 = B_1 \qquad (24)$$

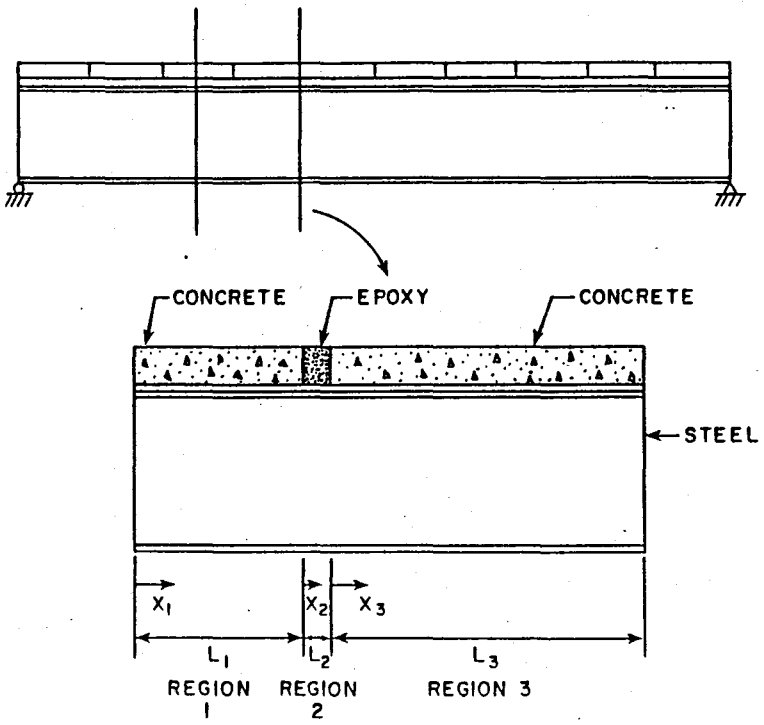

(a)

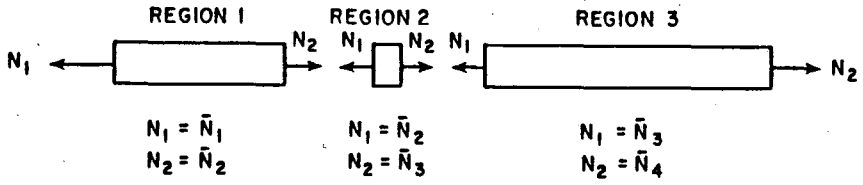

(b)

FIG. 22. (a) Steel-Concrete Regions and Steel-Epoxy Regions in the Model, (b) Internal Axial Forces Acting in the Deck of the Model at the Different Regions

$$K_3 = K_1 \tag{25}$$

Using Eqs. 21-25, the solutions for $\bar{N}_3$ and $\bar{N}_2$ are,

$$\bar{N}_3 = \frac{B_2 S_2}{S_2^2 \overline{BT}_1 \overline{BT}_2 - B_2^2} \left\{ \frac{\bar{N}_1 B_1}{S_1} + \frac{\bar{N}_4 B_1 D}{S_3} - \frac{M_1 K_1}{B_1}\left(\frac{1}{S_1} - T_1\right) \right.$$

$$- \frac{M_2 K_2}{B_2}\left(\frac{1}{S_2} + T_2\right)(1 + D) - \frac{M_3 K_1}{B_1}\left(\frac{1}{S_3} + T_3\right) D - V\left[\frac{K_1}{B_1^2}(1 - D)\right.$$

$$\left. \left. - \frac{K_2}{B_2^2}(1 - D) - \frac{R_1 T_1 K_1}{B_1^2} + \frac{R_2 K_2}{B_2^2} - \frac{R_2 T_2 K_2 D}{B_2^2} + \frac{R_3 K_1 D}{S_3 B_1^2}\right]\right\} \tag{26}$$

and

$$\bar{N}_2 = \frac{1}{\overline{BT}_1}\left[\bar{N}_3 \frac{B_2}{S_2} + \bar{N}_1 \frac{B_1}{S_1} - \frac{M_1 K_1}{B_1}\left(\frac{1}{S_1} + T_1\right) - \frac{M_2 K_2}{B_2}\left(\frac{1}{S_2} + T_2\right)\right.$$

$$\left. - V\left(\frac{K_1}{B_1^2} - \frac{K_2}{B_2^2} - \frac{R_1 T_1 K_1}{B_1^2} + \frac{R_2 K_2}{S_2 B_2^2}\right)\right] \tag{27}$$

where

i = region studied,

S_i = $\sinh (L_i B_i)$,

T_i = $\coth (L_i B_i)$,

R_i = $L_i B_i$,

M_i = initial external moment at region i,

BT_1 = $B_1 T_1 + B_2 T_2$,

BT_2 = $B_2 T_2 + B_3 T_3$, and

D = $S_2 BT_1 / B_2$

For the analysis of the model strain data recorded from the test during the uncracked load sequence 2 was used to determine $\overline{N}_1$ and $\overline{N}_4$. The magnitude of the axial force in the composite section was obtained from the strain diagrams shown in Figs. B13-B15 and Figs. B7-B9 for sections 8 and 5, respectively, for 3 different external load magnitudes. The relationship used to find $\overline{N}_1$ and $\overline{N}_4$ was based on linear behavior of the steel stringer and is the following,

$$N = \varepsilon_b E_s \left(1 - \frac{d_{ss}}{d_b}\right) A_s \qquad (28)$$

where

ε_b = bottom fiber strain of the steel stringer, obtained from extrapolation of the strain data,

d_{ss} = distance from the neutral axis of the steel stringer to the extreme bottom fibers, and

d_b = distance from the neutral axis of the composite section to the extreme bottom fibers, obtained from extrapolation of the strain data.

Once the values for $\overline{N}_1$ and $\overline{N}_4$ were known, $\overline{N}_3$ and $\overline{N}_2$ were obtained using Eq. 26 and Eq. 27, respectively. The value used in these equations for , the flexibility of the shear connection per unit length, was based on experimental data from push-out tests made by Fullmer (5) on full-scale models of composite steel-concrete beams connected by single shear studs and grouted with epoxy mortar similar to that used for the construction of the bridge model. Data from Fullmer's tests was scaled down to one-third for the purpose of analysis of this study. Table 6 is a summary of the properties of the material used, section properties, and the values of the constants K and B for each region.

The axial force distribution for each region was obtained from Eq. 20 using the values of $\overline{N}_2$ and $\overline{N}_3$ previously found and the values of $\overline{N}_1$ and $\overline{N}_4$ obtained from the test data. Figs. 23 to 25 show the distribution of N from section 8 to section 5 for three different external loadings. Axial forces obtained from experimental data for sections 6 and 7 are also plotted for comparison. As the external load increased it was observed that the response deviated from the behavior predicted by the theory. This effect was expected

TABLE 6. Properties and Constant Parameters Used During the Analysis of Distribution of Axial Forces

PROPERTY		MAGNITUDE
Modulus of Elasticity		
concrete steel epoxy	E_c E_s E_e	4,000,000 psi 29,000,000 psi 500,000 psi
Area		
concrete steel epoxy	A_c A_s A_e	86.40 $in.^2$ 6.53 $in.^2$ 86.40 $in.^2$
Moment of Inertia		
concrete steel epoxy	I_c I_s I_e	52.49 $in.^4$ 164.15 $in.^4$ 52.49 $in.^4$
Flexibility		
shear connectors	μ	0.000003 $in.^2$/lbf
Constants		
	K_1 K_2 B_1 B_2	5.2665×10^{-3} $in.^{-2}$ 5.4667×10^{-3} $in.^{-2}$ 0.08281 $in.^{-4}$ 0.11734 $in.^{-4}$

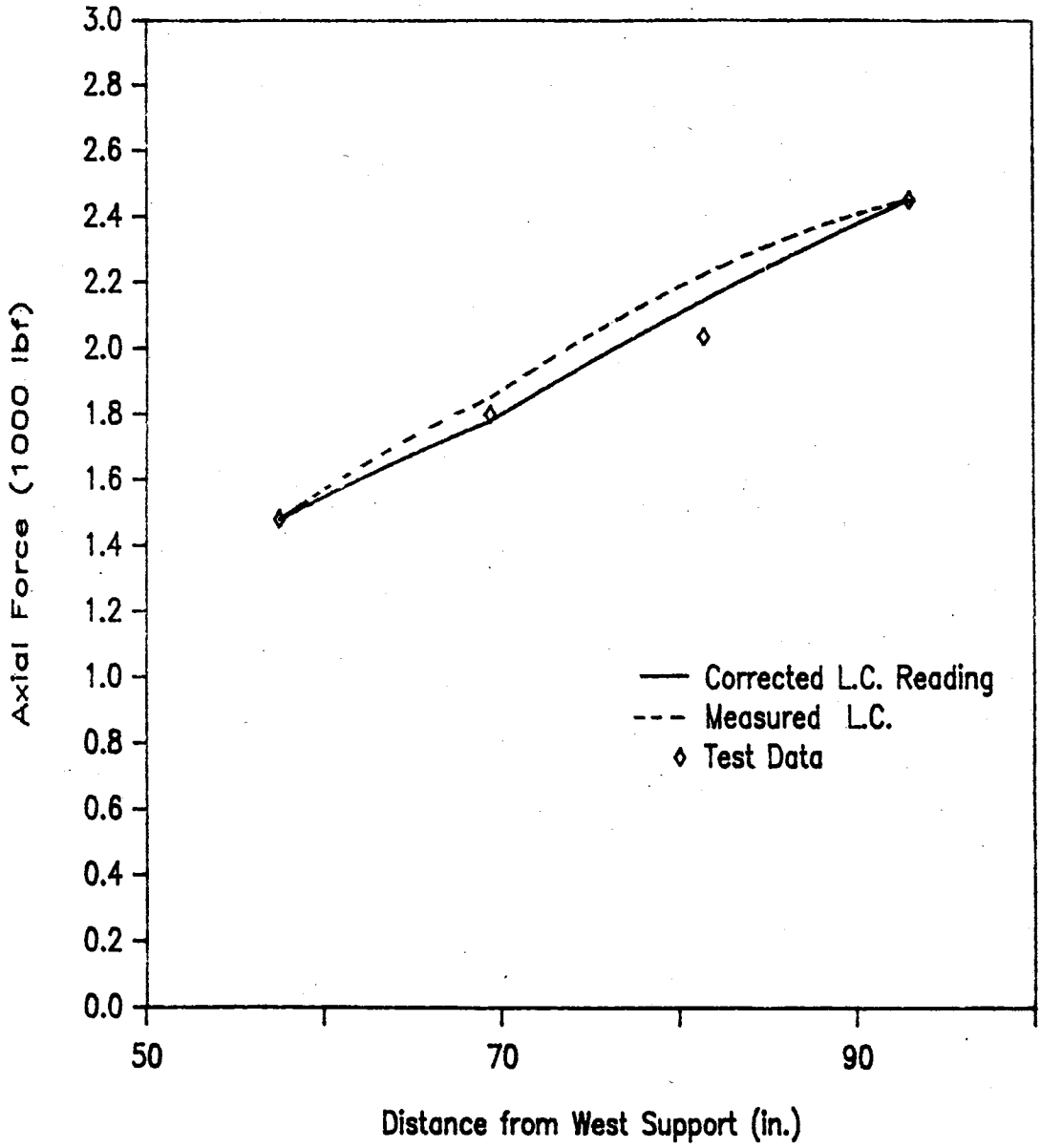

FIG. 23. Longitudinal Axial Force Distribution Between Section 8 and Section 5 for a Measured External Load of 0.75 kips and a Corrected Load of 0.70 Kips

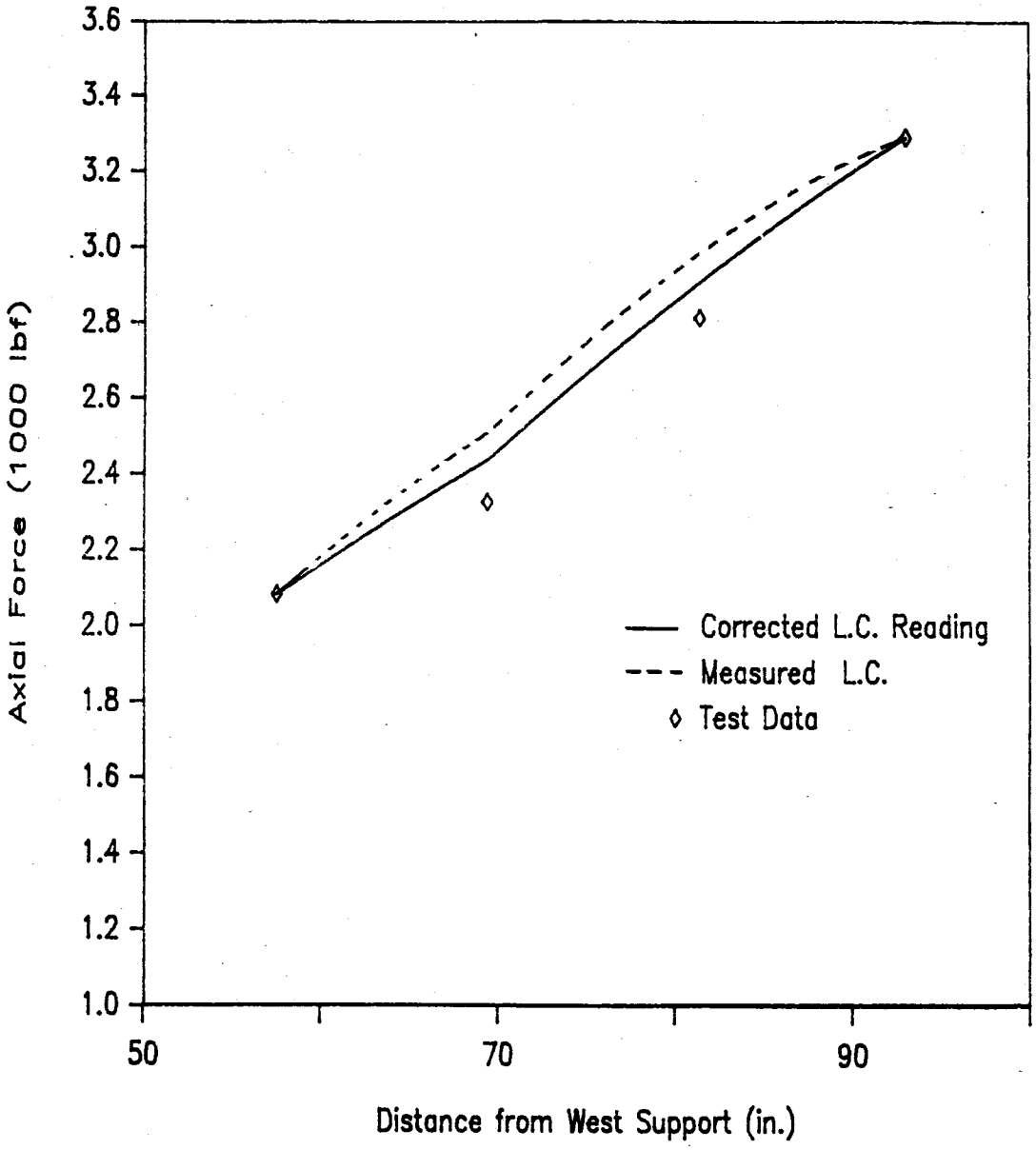

FIG. 24. Longitudinal Axial Force Distribution Between Section 8 and Section 5 for a Measured External Load of 1.00 Kips and a Corrected Load of 0.95 Kips

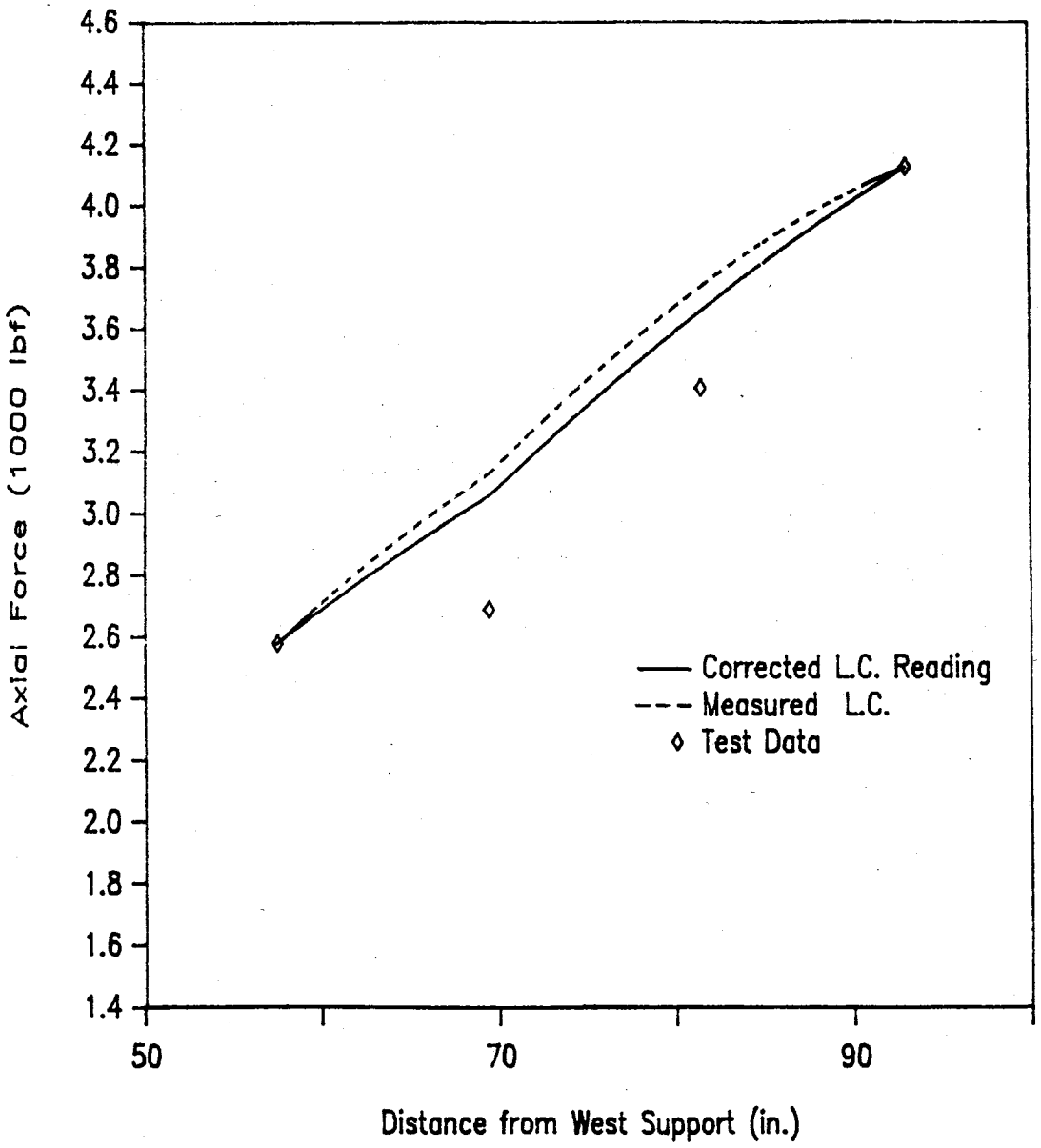

FIG. 25. Longitudinal Axial Force Distribution Between Section 8 and Section 5 for a Measured External Load of 1.25 Kips and a Corrected Load of 1.20 Kips

since the tensile modulus of elasticity of concrete decreases as the stress increases due to its non-linear stress-strain behavior, and during the analysis of the structure the modulus of elasticity of concrete was assumed to be constant.

Two different axial force distributions are shown in Figs. 23 to 25, and these correspond to two different external load magnitudes, thus, different shears and moments. Because during the experiment a small leakage in the hydraulic system was observed, the load in the model at the time when the strain gages were read is believed to be approximately 50 lbf lower than the load first recorded in the load cells. The axial force distribution labeled "corrected" corresponds to the measured applied load minus the load due to the error in strain readings observed in the load cells. Therefore, for Fig. 23 when the measured external force is 0.75 kips, the corrected force is 0.70 kips; for Figs. 24 and 25, the measured and corrected forces are 1.00 kips - 0.95 kips and 1.25 kips - 1.20 kips, respectively.

It can be seen from Figs. 23 to 25 that the distributions of axial forces corresponding to the corrected load cell readings yield a better approximation to the monitored behavior. As will be shown later, the corrected values also yield better results for the prediction of the section properties of the structure. For these reasons, in the following discussion of results, the applied load corrected for this error will be used.

Determination of Section Properties

The longitudinal distribution of moment of inertia, $I(x)$, for the model in the regions analyzed was obtained from the distribution of axial forces, $N(x)$, shown in Figs. 23 to 25. The procedure used to find $I(x)$ as a function of $N(x)$ was as follows: The bottom fiber stress in the steel stringer σ_b is given by

$$\sigma_b = \sigma_s + \frac{N(x)}{A_s} \tag{29}$$

where σ_s is the bottom fiber stress in the steel stringer due to bending only.

However, σ_b can also be found using the composite section properties. Therefore,

$$\sigma_b = \frac{M(x)\ d_b}{I_{comp}} \tag{30}$$

From Eq. 29 and Eq. 30,

$$\frac{I_{comp}}{d_b} = \frac{M(x)\ A_s}{A_s\ \sigma_s + N(x)} \tag{31a}$$

or

$$S_{comp} = \frac{M(x)\ A_s}{A_s\ \sigma_s + N(x)} \tag{31b}$$

To find σ_s in Eq. 31 the relationship of the internal forces acting on a composite section was used. From Eq. 1,

$$M_s = M(x) - N\ d_t - M_d \tag{32}$$

Solving for M_d, and using the assumption of equal curvature given in Eq. 2, results in

$$M_d = M_s \frac{E_d\ I_d}{E_s\ I_s}$$

For the steel-concrete sections, this yields

$$M_d = 0.044\ M_s \tag{33a}$$

and for the steel-epoxy sections,

$$M_d = 0.011\ M_s \tag{33b}$$

Recall,

$$\sigma_s = \frac{M_s\ d_{ss}}{I_s} \tag{34}$$

Therefore, using Eqs. 33a 33b, and Eq. 32, the bottom fiber steel stress due to bending only can be obtained, first for the steel-concrete sections,

$$\sigma_s = \frac{(M(x) - N(x)\ d_t)\ d_{ss}}{1.044\ I_s} \tag{35a}$$

and, for steel-epoxy sections,

$$\sigma_s = \frac{(M(x) - N(x)\ d_t)\ d_{ss}}{1.011\ I_s} \tag{35b}$$

The composite section moment of inertia, I_{comp}, can be obtained from Eq. 31a once d_b is defined. From the stress diagram and similar triangles relations,

$$\frac{d_b}{\sigma_b} = \frac{d_{ss}}{\sigma_s}$$

or

$$d_b = d_{ss}\ \frac{\sigma_b}{\sigma_s} \tag{36}$$

Using Eqs. 29, 31, and 36, the composite section moment of inertia becomes

$$I_{comp} = \frac{\left(\sigma_s + \frac{N(x)}{A_s}\right) M(x)\ A_s}{\sigma_s\ (A_s\ \sigma_s + N(x))} \tag{37}$$

The distribution of moments of inertia along the regions analyzed (section 8 to section 5) using Eq. 37 are shown in Figs. 26 to 28. Two different distributions are plotted in each figure, one corresponding to the uncorrected load cell measurements and the other to the corrected measurements. The dips in these figures represent the drop of inertia porperties across an interface as predicted by Newmark's partial interaction theory (11). These drops are drastic because of the equal curvature assumption and the modular ratio which cause a drop in the calculate moment of inertia.

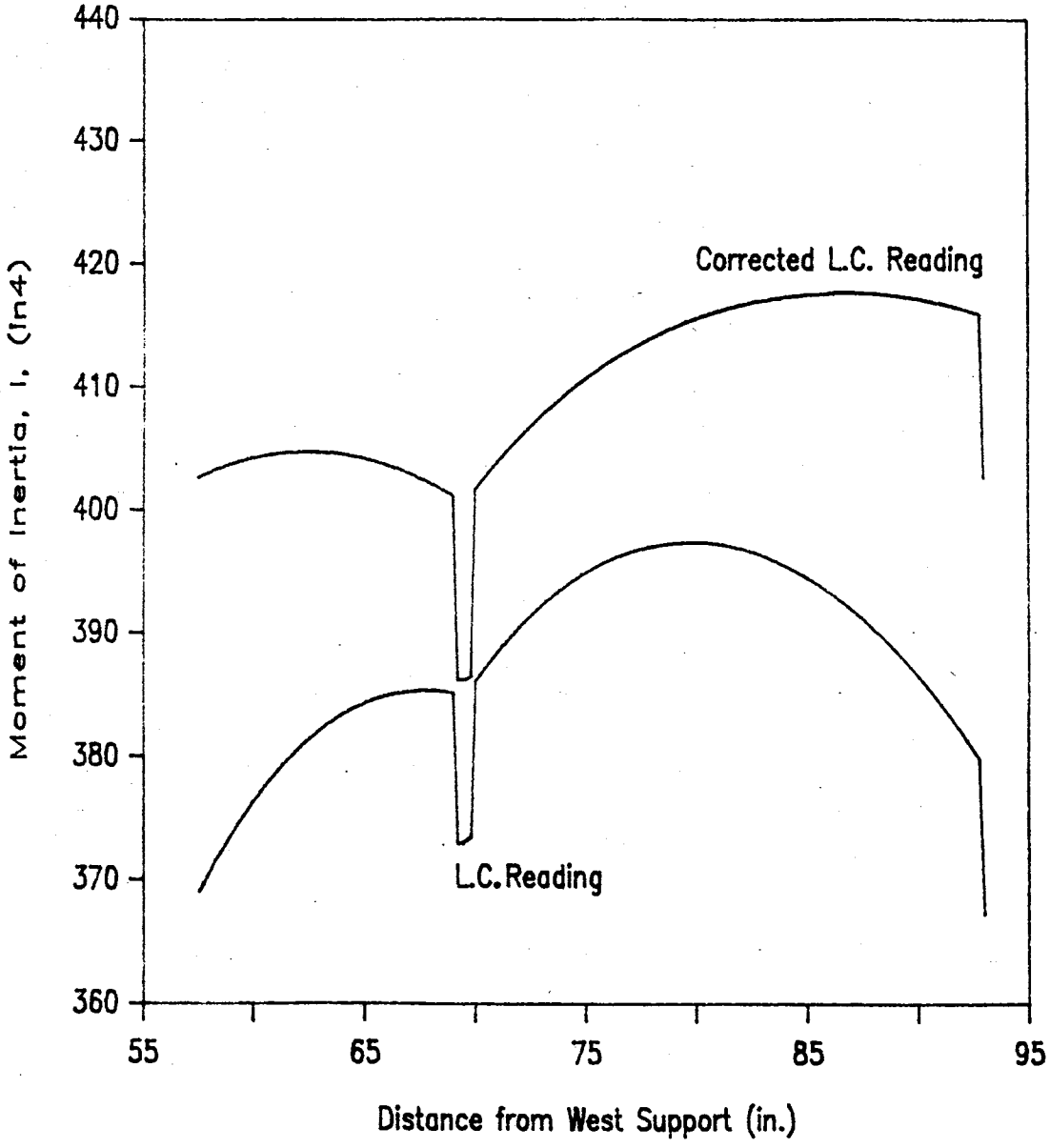

FIG. 26. Longitudinal Distribution of Moment of Inertia Between Section 8 and Section 5 for a Measured External Load of 0.75 Kips and a Corrected Load of 0.70 Kips

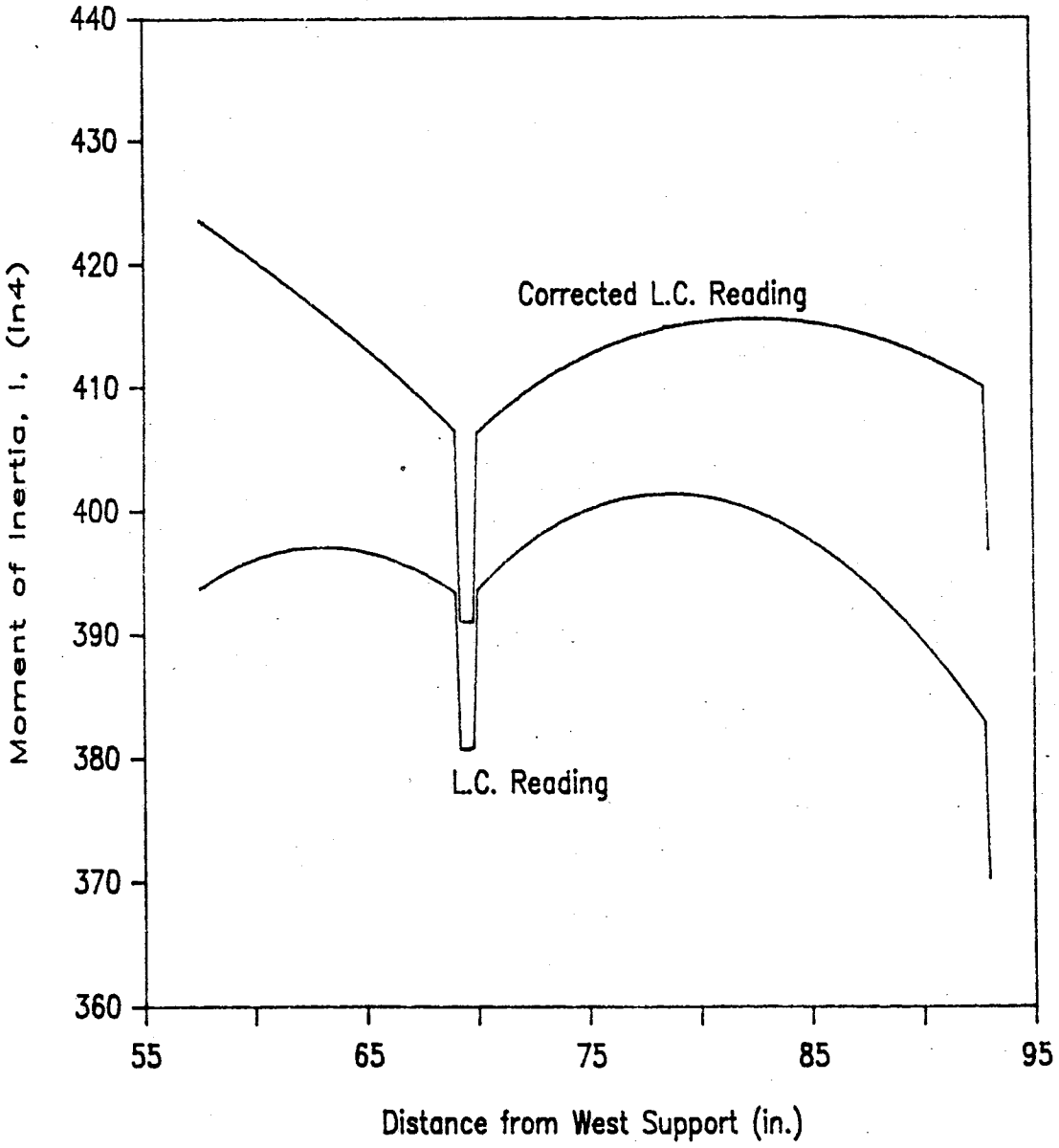

FIG. 27. Longitudinal Distribution of Moment of Inertia Between Section 8 and Section 5 for a Measured External Load of 1.00 Kips and a Corrected Load of 0.95 Kips

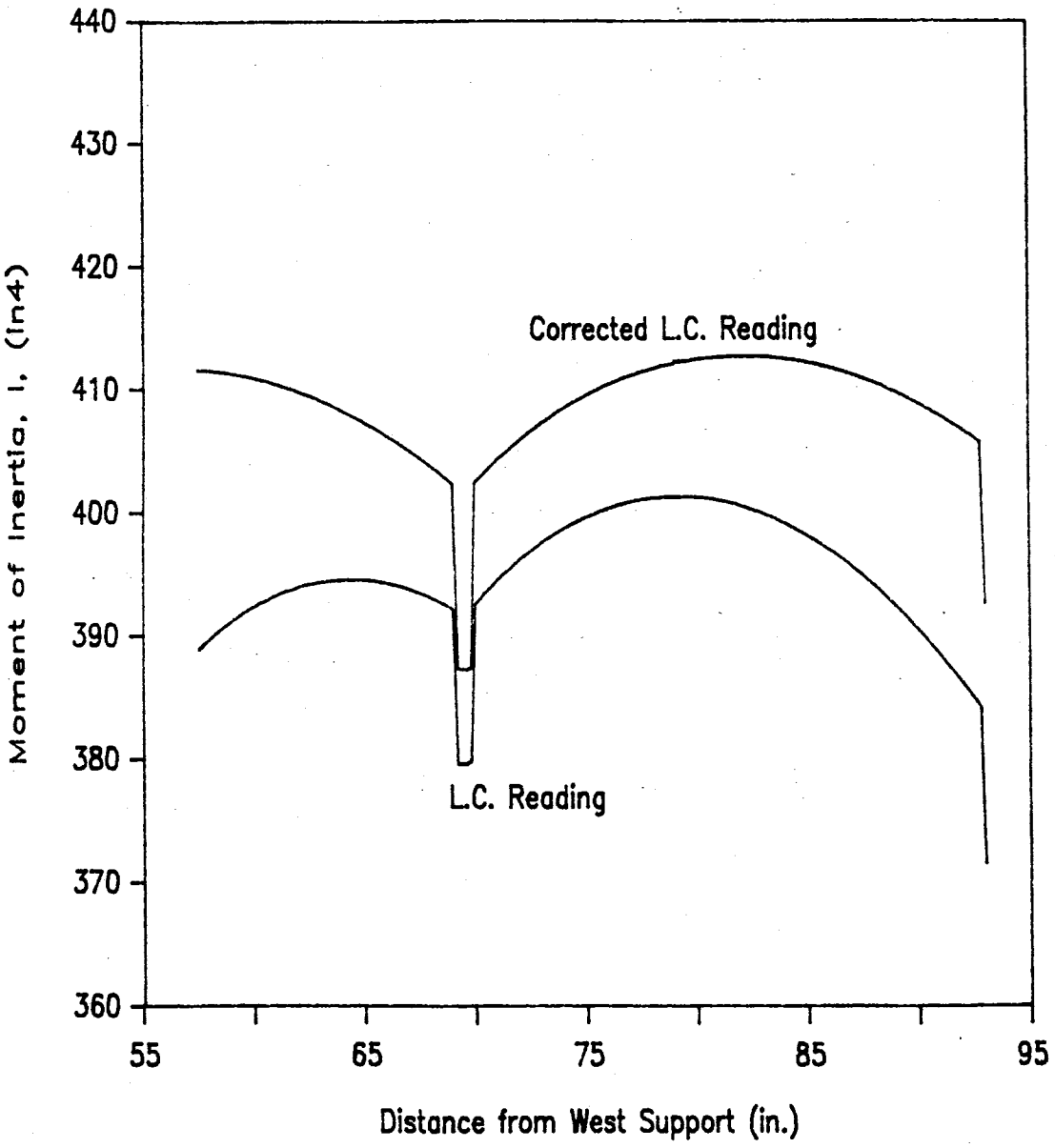

FIG. 28. Longitudinal Distribution of Moment of Inertia Between Section 8 and Section 5 for a Measured External Load of 1.25 Kips and a Corrected Load of 1.20 Kips

Because of symmetry the distribution of moments of inertia in the region between section 8 and section 7 was expected to be similar to the distribution of moments of inertia in the region between section 6 and section 5. It can be seen from Figs. 26 to 28 that, even though the distribution of I(x) shown for the corrected data was not exactly as expected, a more nearly symmetric distribution results from the corrected data than from the uncorrected data.

Fig. 29 shows a summary of all corrected distributions for the various external loads as well as values of the moment of inertia obtained from the linear extrapolation of the recorded strain data in Figs. B1 to B18. It can be seen from Fig. 29 that there is good agreement between the measured moment of inertia (from the corrected load cell readings) and the values obtained from the partial interaction theory. Fig. 29 also indicates that there is a reduction in section moment of inertia in the steel-concrete sections in areas near a shear key joint and that the maximum value for the moment of inertia occurs near midslab.

For the analysis of the model, average section properties were found from the distribution plotted in Fig. 29 and Fig. 30. It should be recalled that the bridge model was designed to have a higher section modulus at the midspan section (see Figs. 5,6). The average section properties obtained from the partial interaction analysis correspond to the midspan section only. Each concrete panel was divided into three regions with the following moments of inertia: 390 $in.^4$ for the shear key joint region, 404 $in.^4$ for the steel-concrete regions adjacent to the shear key joints, and 414 $in.^4$ for the midslab regions. Since the model was not instrumented in the end sections, the actual section properties in these regions could not be calculated from measured strain distributions. To account for the difference between the end and midspan sections a reduction factor based on the transformed area properties was used. The moment of inertia for the end regions was obtained using the following equation,

$$I_{end} = I_{midspan} \frac{I_{tae}}{I_{tam}} \qquad (38)$$

where

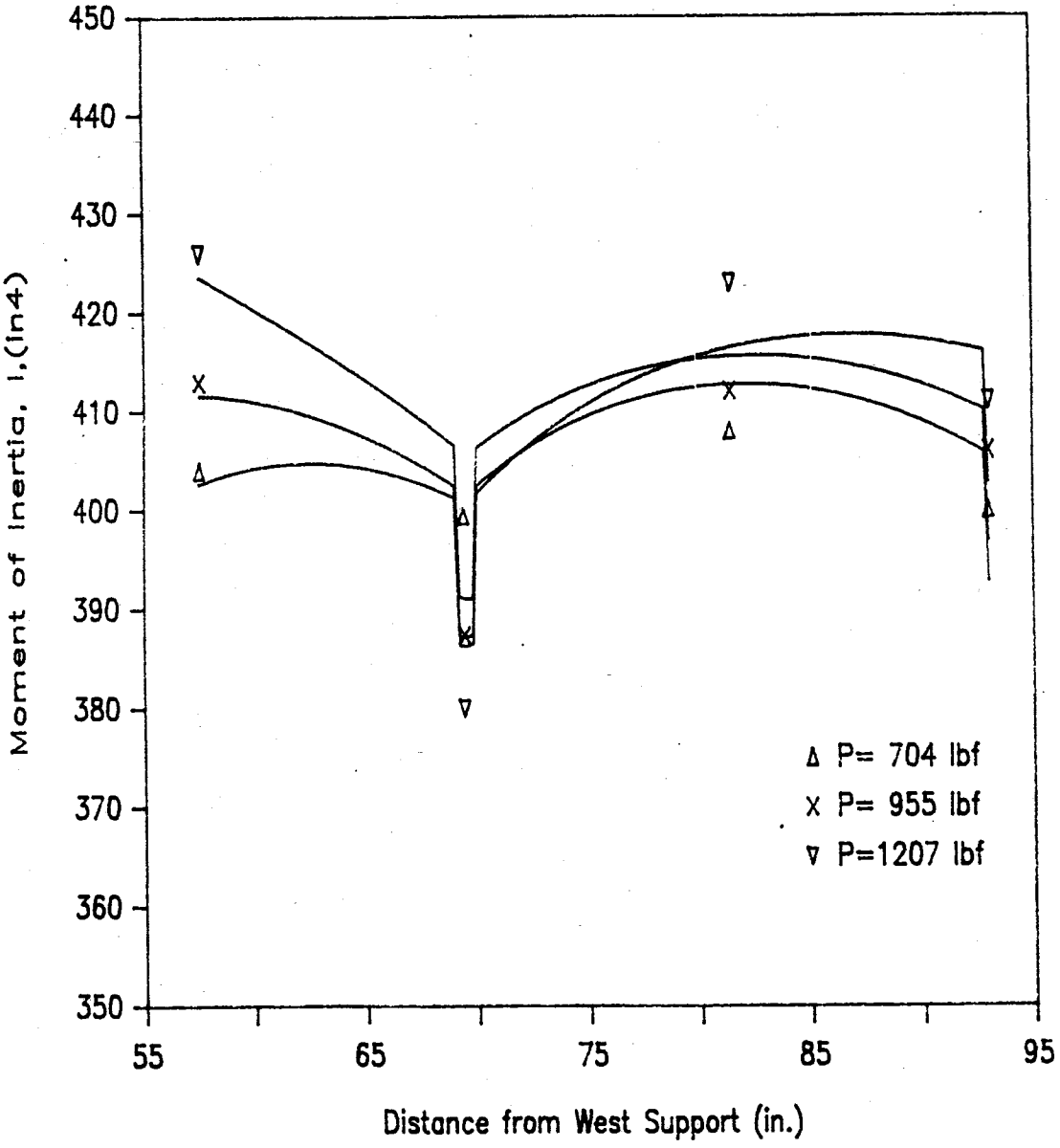

FIG. 29. Summary of the Longitudinal Distributions of Moment of Inertia Between Section 8 and Section 5 for the Corrected External Loads

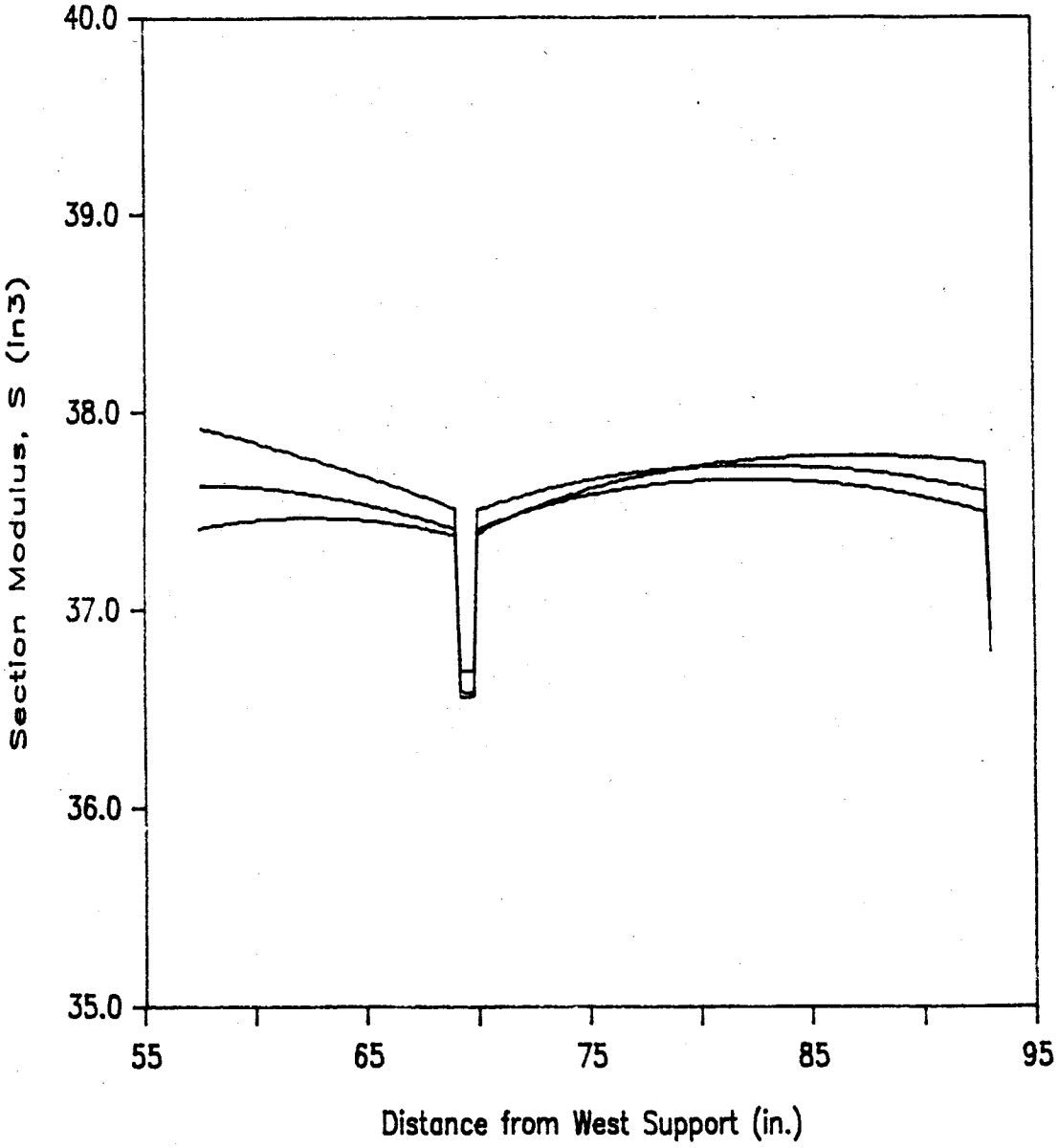

FIG. 30. Summary of the Longitudinal Distributions of Section Modulus Between Section 8 and Section 5 for the Corrected External Loads

I_{end} = moment of inertia at any region at an end section,

$I_{midspan}$ = average moment of inertia at a midspan region,

I_{tae} = transformed area moment of inertia at an end section, and

I_{tam} = transformed area moment of inertia at a midspan section

The values for the transformed area moments of inertia were obtained assuming that the modulus of elasticity of concrete in tension was equal to the modulus of elasticity in compression. The calculated values for I_{tam} and I_{tae} were 432 in.^{4} and 323 in.^{4}, respectively, as shown in Appendix C. From Eq. 38 the moment of inertia was calculated for each of the following three regions in the end sections of the model: midslab, joint, and regions adjacent to the joints. These calculated moments of inertia were 320 in.^{4}, 302 in.^{4}, and 291 in.^{4}, respectively. Fig. 31 shows an analytical model of the bridge with the six different values for the calculated moments of inertia. This analytical model is used later for the computation of vertical deflections.

For simplicity, average values for the section modulus of the model were obtained for the same regions in which the moments of inertia were calculated. The average values obtained for the section moduli for the midspan sections were 38.1 in.^{3}, 37.4 in.^{3}, and 36.6 in.^{3}, for the midslab regions, regions adjacent to the joints, and joint regions, respectively.

Development of Composite Action

To illustrate the amount of composite action developed in the model during the linear, or uncracked, phase of the experiment, a ratio of the axial force to the internal moment at each monitored section was calculated. It should be recalled that when composite action is present there is a transfer of axial forces from the steel stringer to the concrete deck, and these axial forces become zero as the composite action is lost.

The longitudinal distribution of the ratio Z of axial force to moment was determined from the strain diagrams shown in Figs. B1-B18 and Eq. 28. These distributions and the distribution predicted by the transformed area theory are shown in Fig. 32. The values of Z for the latter were found using the following relationship,

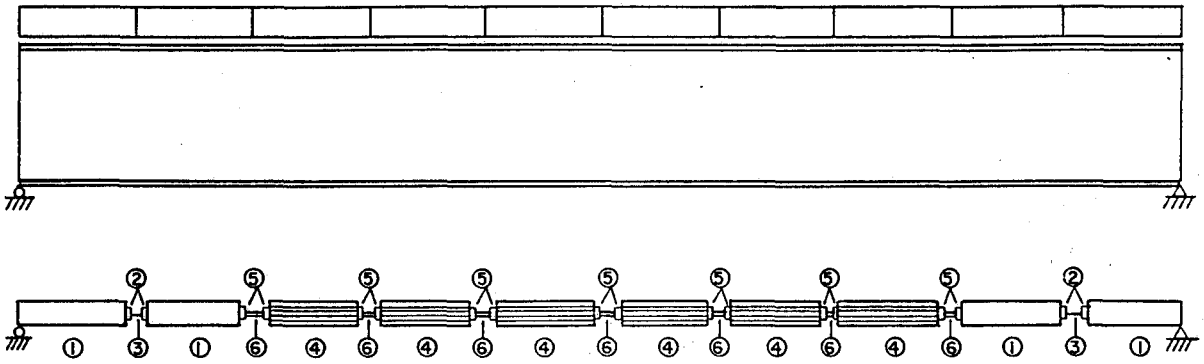

REGION	LENGTH (in.)	MOMENT OF INERTIA ($in.^4$)	SECTION MODULUS ($in.^3$)
1	19	320	
2	2	302	
3	1	291	
4	19	414	38.1
5	2	404	37.4
6	1	390	36.6

FIG. 31. Analytical Model of the Bridge Based on the Partial Interaction Theory

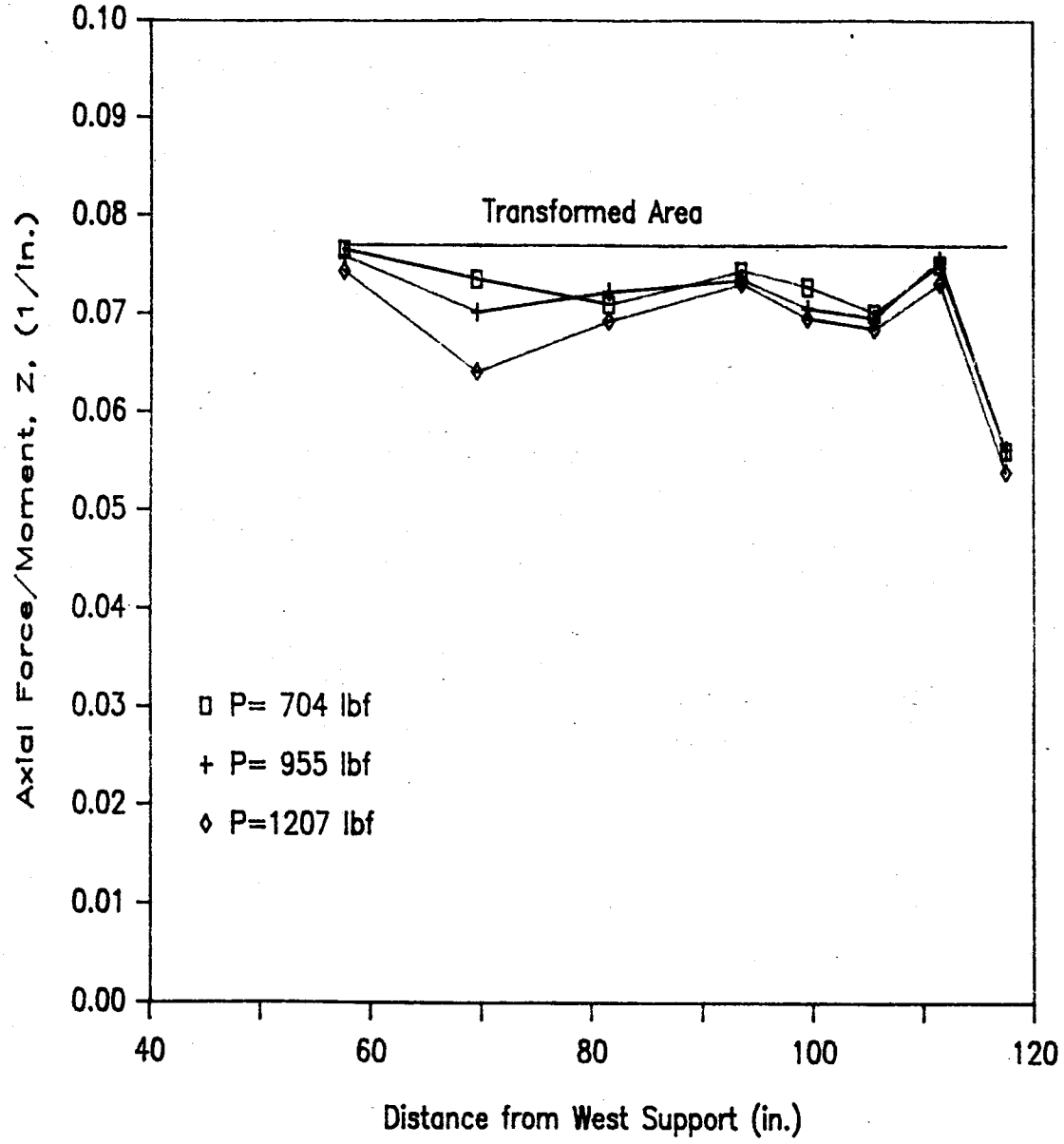

FIG. 32. Longitudinal Distribution of the Ratio of Axial Forces to the Internal Moments Between Section 8 and Section 5 for the Uncracked Load Sequence 2

$$\frac{N}{A_s} = \frac{M(x)}{I_{tam}} \quad (d_b - d_{ss})$$

from which the Z ratio can be found to be

$$\frac{N}{M(x)} = \frac{A_s}{I_{tam}} \quad (d_b - d_{ss}) \qquad . \quad (39)$$

From Eq. 39 it can be seen that the distribution of Z is uniform according to the transformed area theory, but the measured data varies longitudinally since the moments of inertia and position of the centroid along the length of the beam vary (see Fig. 29). While the calculated values of Z are significantly reduced at midspan, section 1, these are not considered to indicate a reduction of section modulus. At this stage no cracks had been observed, and the model continued to exhibit linear behavior. It is believed that the concentrated load applied to the lower flanges of the stringers caused local stress concentrations which, superimposed on the linear flexural stress distribution, resulted in a non-linear stress distribution at sections near to the concentrated load.

Timoshenko (17) discusses the influence of a concentrated load in the distribution of flexural stresses for a simply supported beam with a narrow rectangular cross section. It is shown in the discussion of Ref. 17 that the flexural stress distribution is non-linear near the point of application of a concentrated force, and that the non-linear effects vanish some distance away from the point of application of the load. When the stresses predicted by the theory of mechanics of materials are compared to the actual generated stresses at the location of the concentrated load, the theory predicts higher stresses. However, at a small distance away from the point of application of the load the effect is reversed, and the generated stresses become higher than those predicted by the theory of mechanics of materials.

In general, the pattern of the distribution of strains observed in the monitored sections of the model was similar to the effects of the concentrated load discussed in Ref. 17. Because the function describing the non-linear distribution of strains at section 1 was not known, the actual values for Z could not be computed at this location. However, the use of a linear strain distribution to calculate the axial forces acting on this section is considered to be a conservative assumption. As is shown in Fig.

32, despite the approximation of the values of N in section 1, the values of Z at this section were still smaller when compared to other locations.

From Fig. 32 it can be seen that the transformed area theory predicts a higher development of composite action than what was observed. However, a better prediction of the distribution of Z can be obtained if a different modulus of elasticity for the concrete is used. It is suggested in Ref. 2 that the modulus of elasticity of the concrete in tension is about 67 per cent of the modulus of elasticity in compression. If this reduction is taken into account for the computations of section properties using transformed area theory (see Appendix C), a better prediction of Z is obtained as is shown in Fig. 33.

Deflections

For the analysis of deflection of the structure two analytical models were used. The first model is shown in Fig. 31, and it was based on the results obtained from partial interaction theory. The second model, shown in Fig. 34, was based on the transformed area theory with a modified value for the modulus of elasticity of concrete. Fig. 35 to Fig. 38 are plots of the measured deflections in the structure compared to the deflections predicted by the two models for the uncracked load sequence 2. The values for deflection obtained during the experiment and predicted analytically are tabulated in Table 7. The results show that the values obtained for deflections from both models are equal, and the predicted deflections are very close to the measured deflections

Part 2: Model After Cracking of the Concrete Deck

Cracking Pattern

The cracking pattern of the model structure has been briefly discussed in Chapter III and is graphically shown in Fig. 18. Fig. 39 shows the cracking pattern of the model with the corrected magnitudes for the external loads on each stringer and induced internal moments. In general it was observed that the distribution of cracks in the concrete deck of the model

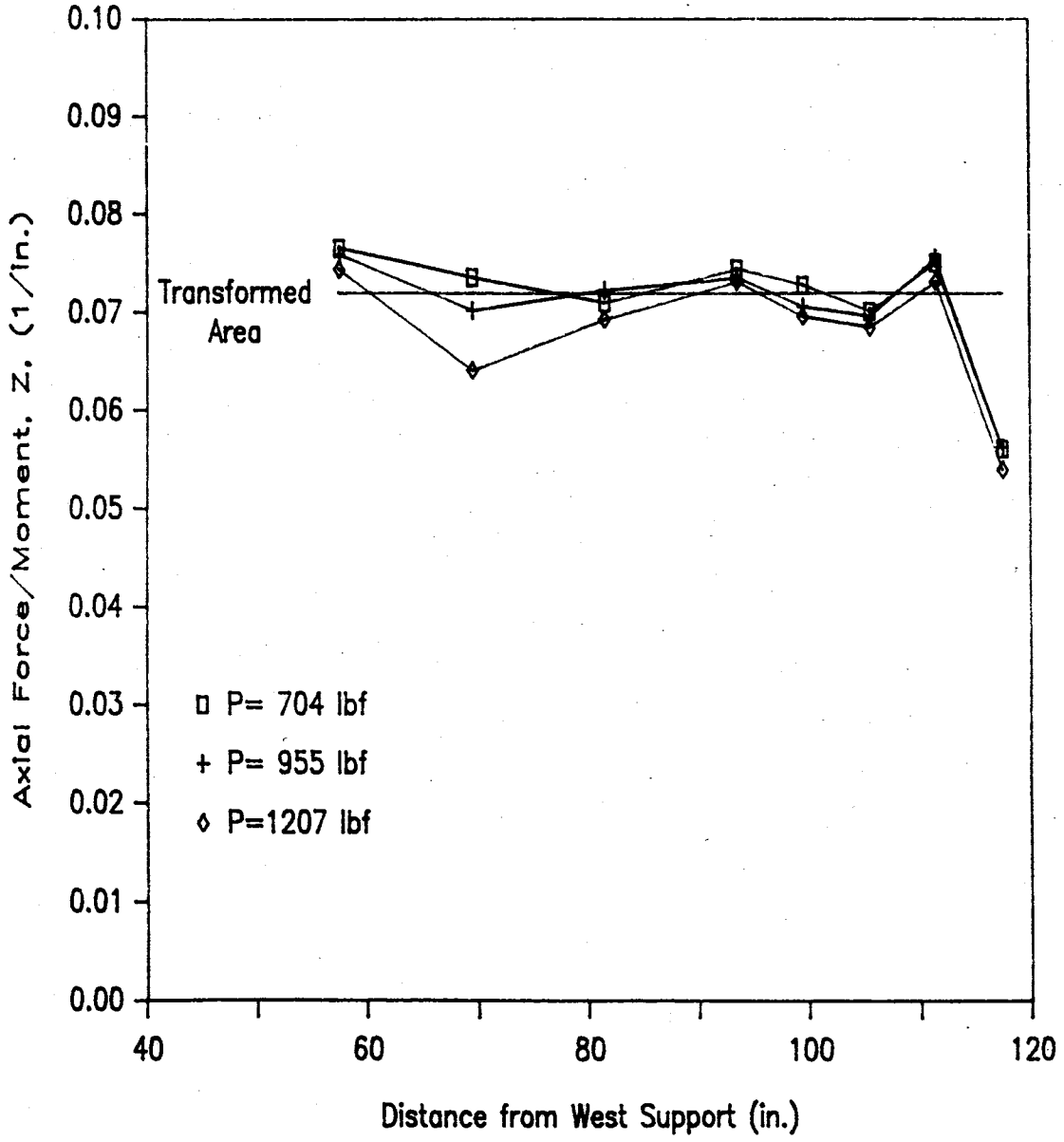

FIG. 33. Measured Longitudinal Distribution of Z Compared to the Distribution Given by the Transformed Area Theory Using a Reduced Modulus of Elasticity for Concrete.

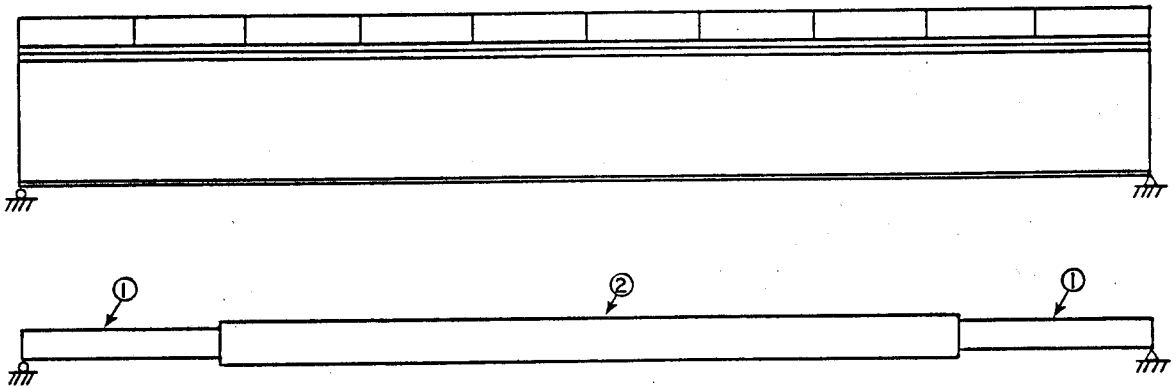

REGION	LENGTH (in.)	MOMENT OF INERTIA ($in.^4$)	SECTION MODULUS ($in.^3$)
1	40	293.8	30.9
2	155	389.9	36.9

FIG. 34. Analytical Model of the Bridge Based on the Transformed Area Theory

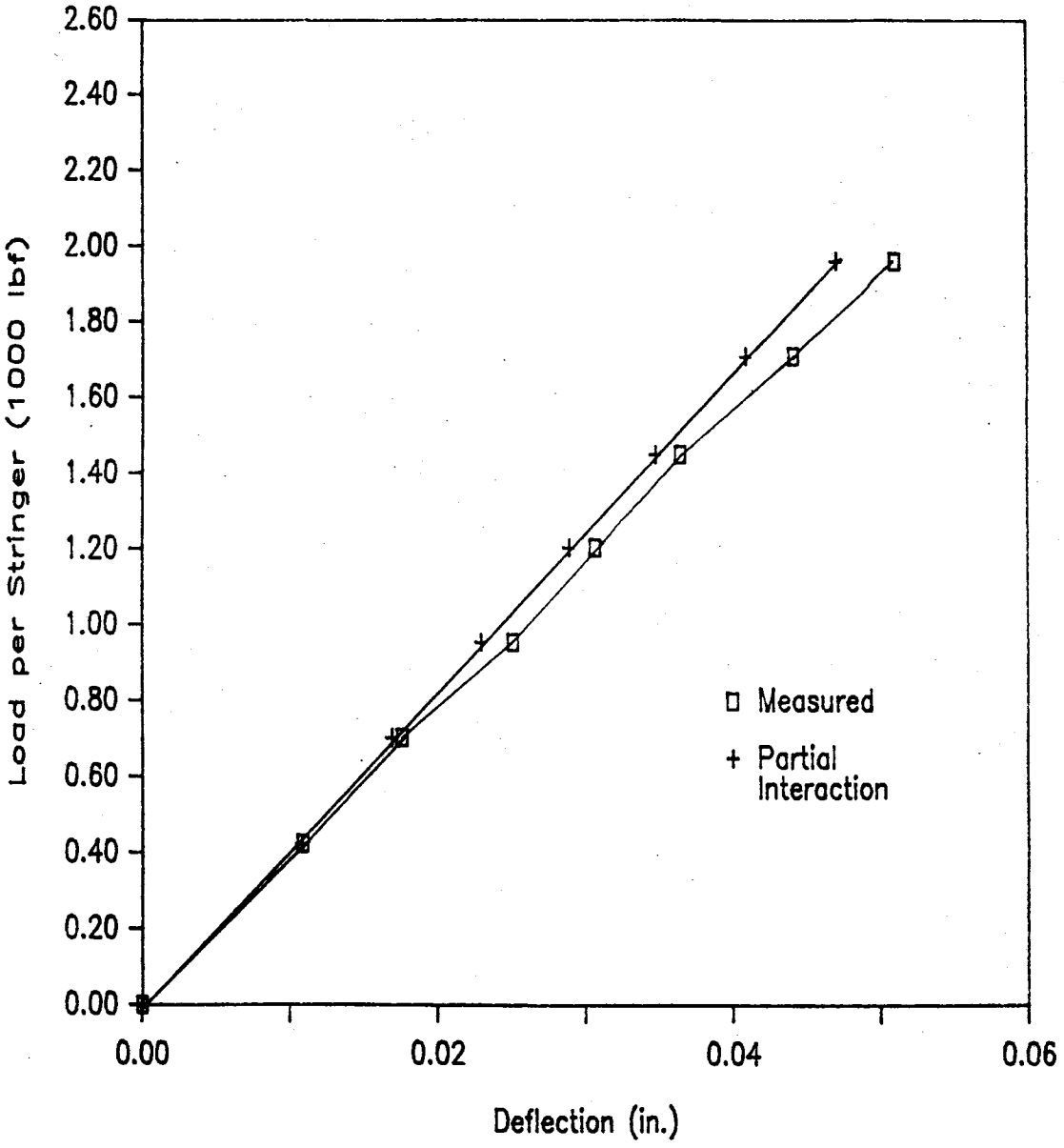

FIG. 35. Comparison Between Results from the Partial Interaction Model and the Deflections Measured at Midspan for the Uncracked Load Sequence 2

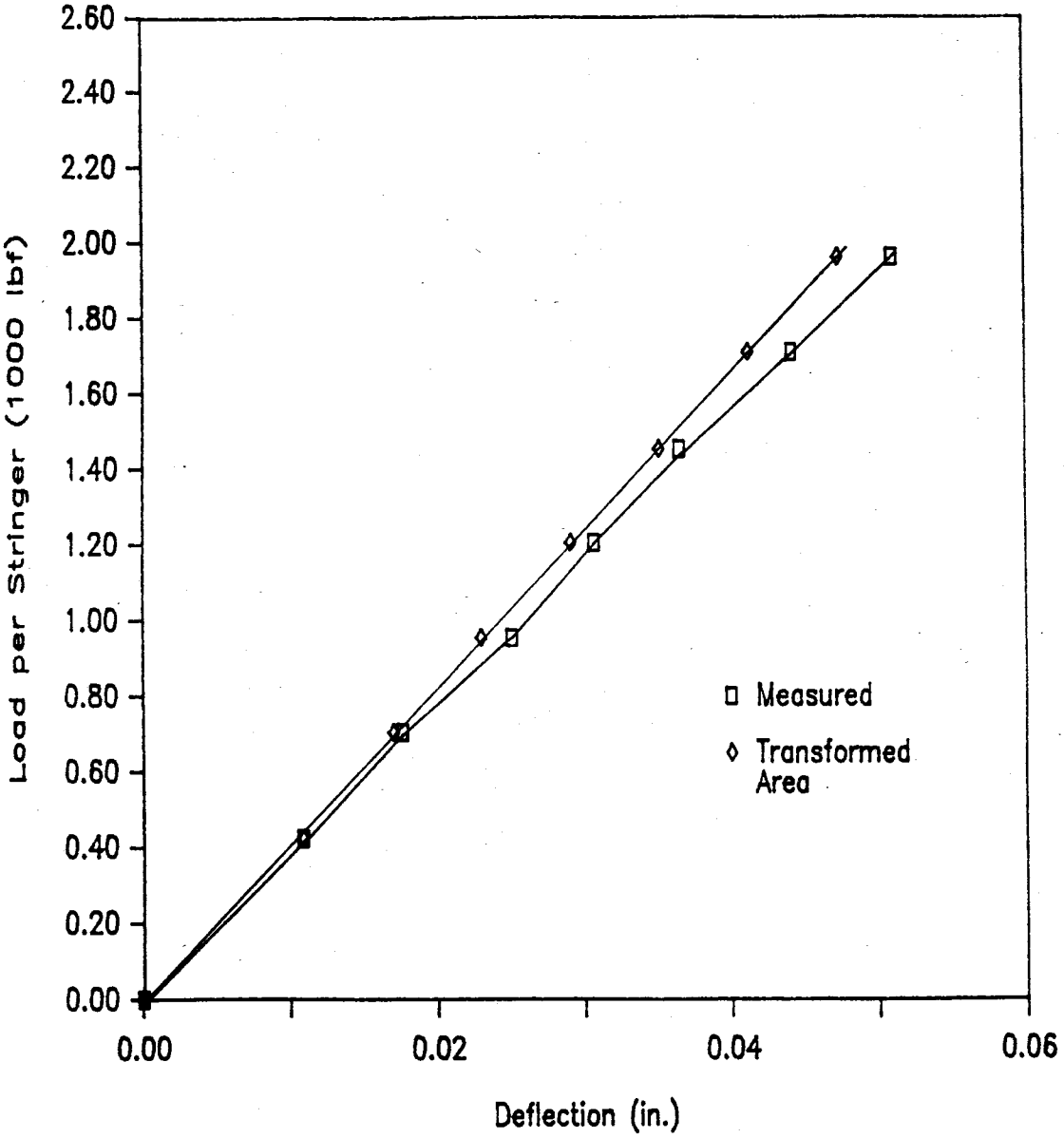

FIG. 36. Comparison Between Results from the Transformed Area Model and the Deflections Measured at Midspan for the Uncracked Load Sequence 2

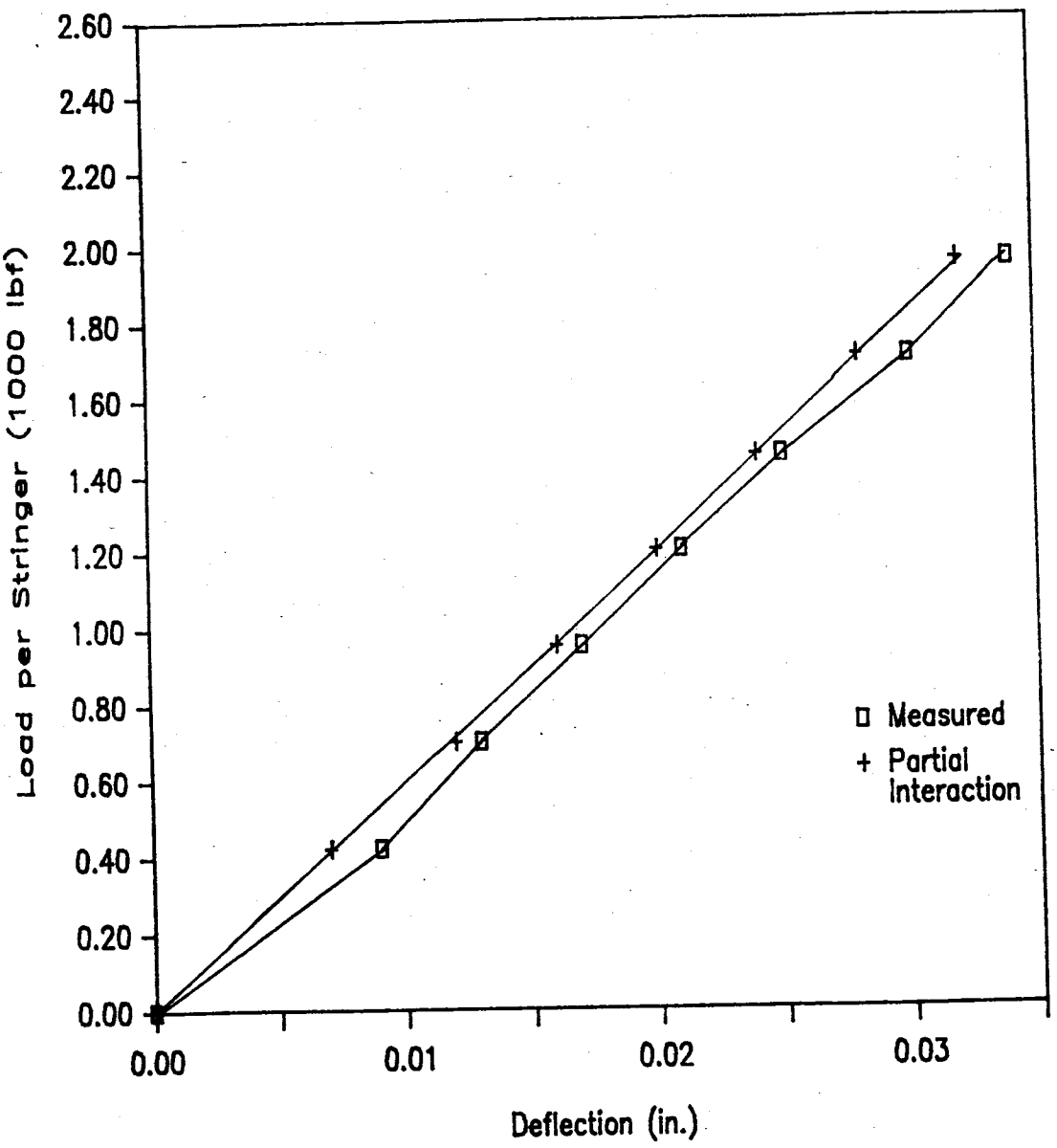

FIG. 37. Comparison Between Results from the Partial Interaction Model and the Deflections Measured at Section 8 for the Uncracked Load Sequence 2

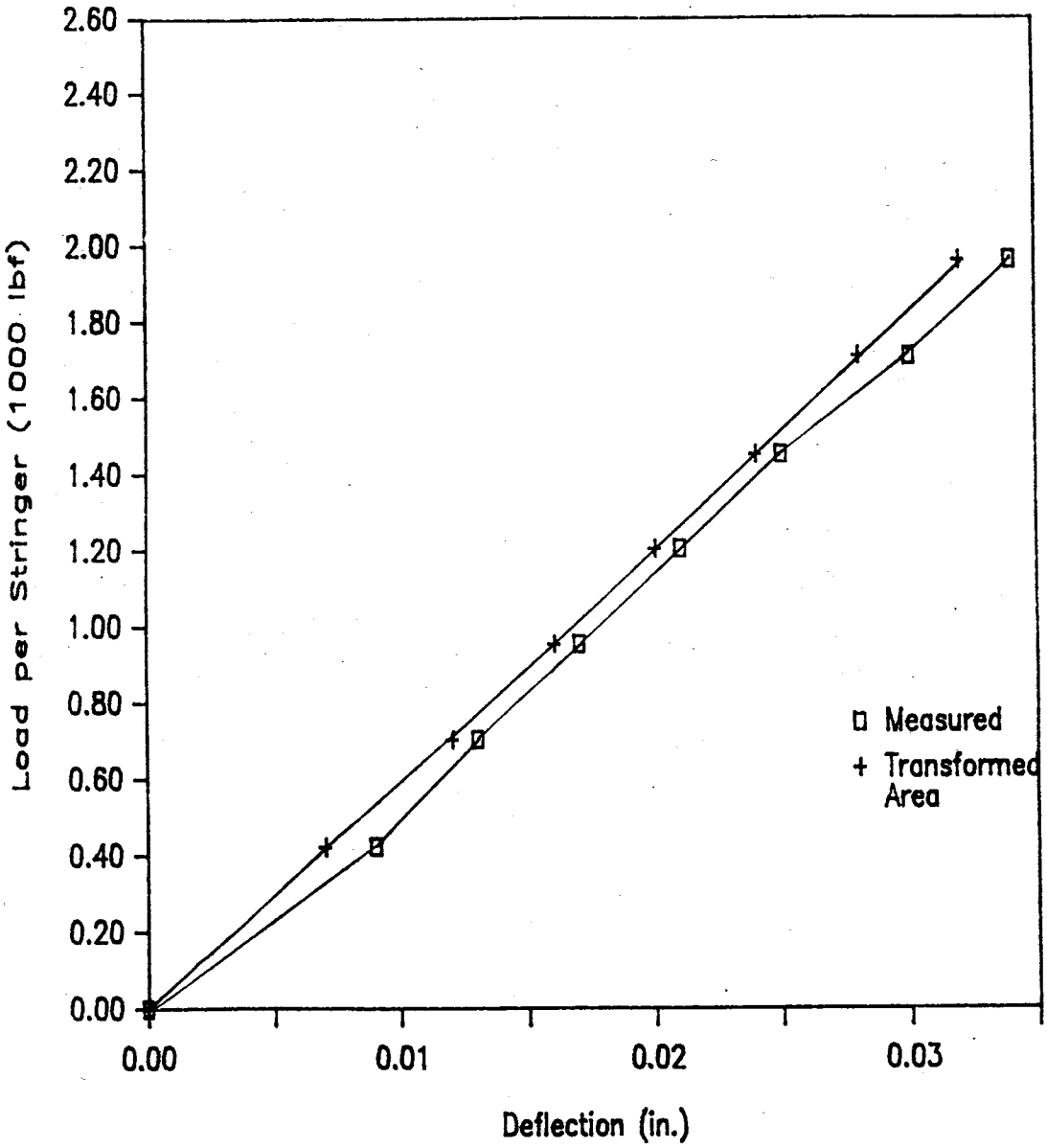

FIG. 38. Comparison Between Results from the Transformed Area Model and the Deflections Measured at Section 8 for the Uncracked Load Sequence 2

TABLE 7. Measured and Theoretical Deflections at Midspan and 57.5 in. from the West Support on Stringer 1 for the Uncracked Load Sequence 2

CORRECTED LOAD (lbf)	DEFLECTION (in.)					
	AT SECTION 8			AT MIDSPAN		
	MEASURED	THEORETICAL		MEASURED	THEORETICAL	
		MODEL 1	MODEL 2		MODEL 1	MODEL 2
453	0.009	0.007	0.007	0.0109	0.0108	0.0109
704	0.013	0.012	0.012	0.0176	0.0169	0.0170
955	0.017	0.016	0.016	0.0251	0.0229	0.0230
1207	0.021	0.020	0.020	0.0307	0.0289	0.0291
1454	0.025	0.024	0.024	0.0365	0.0348	0.0351
1710	0.030	0.028	0.028	0.0441	0.0409	0.0473
1961	O.034	0.032	0.032	0.051	0.047	0.047

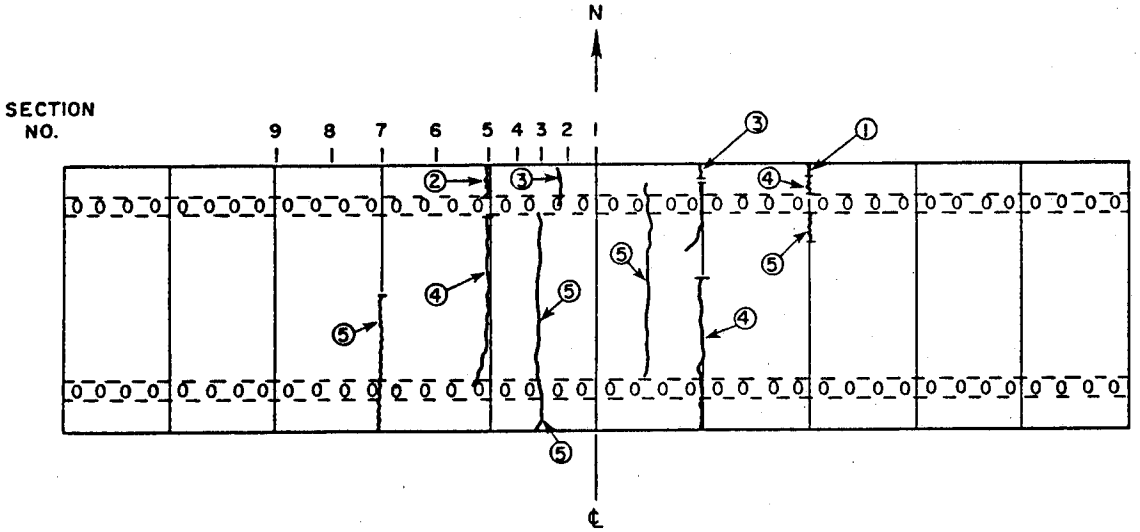

CRACK #	LOAD (kips)	INTERNAL MOMENT (kip.in.) @								
		SECTION 1	SECTION 2	SECTION 3	SECTION 4	SECTION 5	SECTION 6	SECTION 7	SECTION 8	SECTION 9
1	4.224	248	235	223	210	197	172	147	121	96
2	4.374	257	244	231	218	204	178	152	126	100
3	4.864	286	271	257	242	227	198	169	140	111
4	5.103	300	284	269	254	239	208	177	147	116
5	7.190	422	401	379	358	336	293	250	207	164

FIG. 39. Cracking Pattern of the Concrete Deck for the Corrected External Loads

did not agree with the distribution predicted by the theory of mechanics of materials, and that the final cracking pattern was symmetric about the midspan.

Two analytical models to study the behavior of the structure were presented in Part 1 of this chapter, one based on the partial interaction theory and the other on transformed area theory. When the first approach is used to compute tensile stresses in the concrete slab, extrapolated strain data was not used because slip deformations were not monitored during the test, even though from the positive moment test they are known to be small (12). Approximate top fiber stresses in the deck can be obtained using assumptions already discussed in Part 1 for partial interaction theory.

The maximum top fiber stresses in the concrete can be expressed as,

$$\sigma_{max} = \sigma_c + \frac{N(x)}{A_c} \tag{40}$$

where

σ_c is the stress in the concrete slab due to bending only.

Using Eq. 32, 33a, and 33b

$$\sigma_{max} = \frac{(M(x) - N(x)\ d_t)\ d_{cc}}{k_c} + \frac{N(x)}{A_c} \tag{41}$$

where

d_{cc} is the distance from the centroid of the deck to the extreme fibers, and

$$K_c = 1 + \frac{E_s I_s}{E_c I_c} \tag{42}$$

After the development of a crack in the concrete, or a release of axial forces in the deck, the curvature in the steel stringer and the curvature of the concrete deck will not be equal, therefore, the stresses in the concrete cannot be predicted using Eq. 41.

To determine the approximate magnitude of the external load at which significant cracking in the model's deck started, the ratio of the measured axial force to the total internal moment at each section, Z, has been used. As is shown in Fig. 40, the distribution of Z at an external load of 4860 lbf

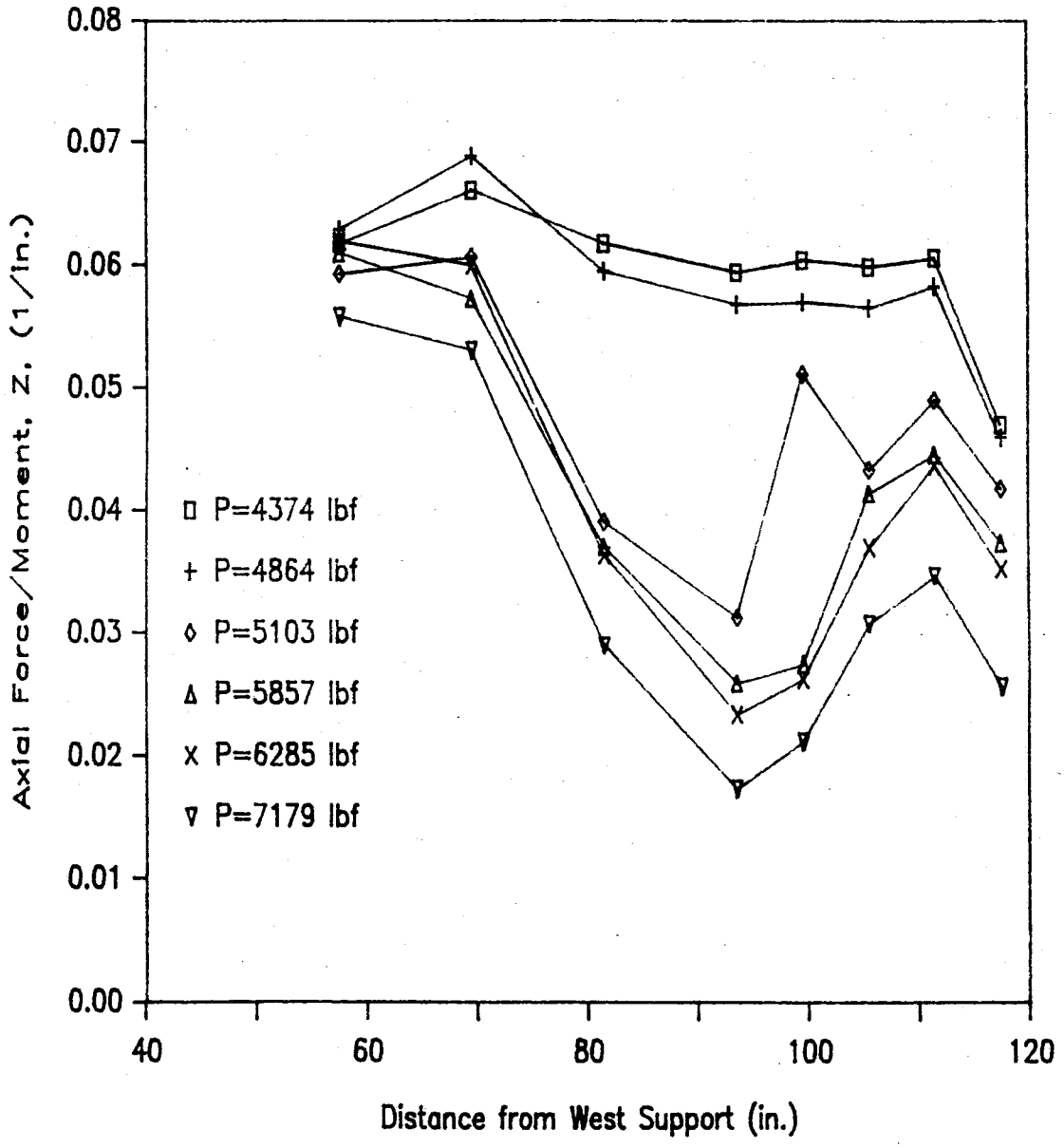

FIG. 40. Longitudinal Distribution of the Ratio of Axial Forces to the Internal Moments Between Section 8 and Section 5 for the Cracked Load Sequence 2

in one stringer is almost constant throughout the monitored length in the model. A significant drop in Z can be observed for the next higher load, 5100 lbf, as a result of loss of composite action due to the development of a crack. Therefore, if the variation in modulus of elasticity of concrete due to the increment in loading is ignored, it can be assumed that the model behaved linearly up to a load of 4860 lbf per stringer. The cracking stress at this magnitude at section 5 as calculated by Eq. 41 was 286 psi.

Tensile stresses in the concrete deck can be predicted in a simpler form using the model based on transformed area theory. Stresses in the concrete are obtained from the following equation,

$$\sigma_{max} = \frac{M(x)\ d_c}{n\ I_{tam}} \qquad (43)$$

where

n_c = modular ratio, E_s / E_c(tension) and

d_c = distance from the centroid of the deck to the extreme top concrete fibers

The cracking tensile stress predicted by Eq. 43 at section 5 at an applied load of 4860 lbf per stringer is 263 psi. Based on the cracking stresses predicted by the two analytical models, the cracking moment in the structure can be defined as the internal moment that generates a tensile stress of approximately $3\ f_c$.

It is important to notice that the first major cracks developed at the shear key joints adjacent to the midspan joint despite the fact that these points were not the most highly stressed areas in the model. However, the shear key joints are considered the weakest areas in the structure as a result of the discontinuities in the deck reinforcement. The influence of the applied load at the midspan section reducing the stresses generated in that location is thought to be the reason that cracks were not observed at the midspan joint.

The behavior of the model after cracking of the concrete deck could not be predicted by the partial interaction theory since the equal curvature requirement for the deck and the stringer at a cracked section is not met. Transition from non-composite to composite behavior resulted in a complicated distribution of internal forces in the structure, and a mathematical analysis of this problem was beyond the scope of this study.

Cracks and Composite Action

It is well known that when a crack develops in the deck of a composite structure subjected to negative moments, the composite action is locally lost. The length of the area of reduced composite action is usually assumed to be equal to the entire negative moment region for design purposes. In this experiment the length of the area of reduced composite action due to the presence of cracks at the midspan slabs was approximately 8 ft, or 36 slab thicknesses (36 t), as is shown in Fig. 40 for one-half of the tested structure. However, if the external loads in the model had been increased up to a magnitude at which the cracking moment was reached in section 7, or 65.5 in. away from the west support, the length of area of reduced composite action for the model could have increased 4 more feet (2 ft at each side). This effect taken to the limit, provided that the design forces are not exceeded, results in the cracking of the entire negative moment region as current design practice assumes. On the other hand, if the cracking moment is never reached in sections outside the crack-affected regions, the length of the area of reduced composite action is not expected to increase; therefore, the design assumption may be too conservative.

No problems at the ends due to the method of restraining the supports were observed. Despite the higher uplift forces at the ends resulting from restraining the model beams to the reaction floor, no failures were observed at the concrete-steel interface. Furthermore, all strain measurements were made in the cover-plated sections of the model bridge. Except for the reported cracking due to higher slab stresses, no difference was observed in the behavior of the deck panels over cover-plated portions of the girder, compared to those panels near the girder ends.

CHAPTER V

APPLICATIONS

Design Example

To illustrate the application of the findings to design, consider a 5-span continuous bridge on an important highway route which is scheduled for deck replacement. The capacity of the structure also needs to be increased to sustain loads greater than the original design loads. It is proposed to replace the deck using precast concrete panels and to develop full composite action in the structure by welding shear studs to the top flanges of the steel stringers. Epoxy mortar will be used to seal the joints between the panels and to transmit the shear forces from the studs to the concrete deck.

Details of the structure to be repaired are shown in Fig. 41. It is proposed to use precast panels 44 ft long, 5 ft wide, and 8 in. thick, and a concrete strength of 4500 psi. The design live load of the bridge is the AASHTO HS20 loading.

Design Procedure

The design procedure to be used will consider that composite action is developed along the entire length of the structure, except in those regions affected by the cracked concrete deck. For design purposes it is assumed that the cracking stress of concrete subjected to tensile stress is $3\sqrt{f_c}$, or 201 psi, based on the experimental findings. The section properties of the structure must be determined to find what moment will induce a bending stress equal to the design cracking tensile stress of concrete.

The transformed area theory can be used to determine the section properties of the bridge. However, since the deck will experience tensile stresses, the modulus of elasticity of concrete used to find the transformed areas is taken as 0.67 the compression modulus of concrete as suggested in Ref. 2.

The section properties are determined as follows:

From the cross section shown in Fig. 42 and using AASHTO section 10.38.3.1 (15),

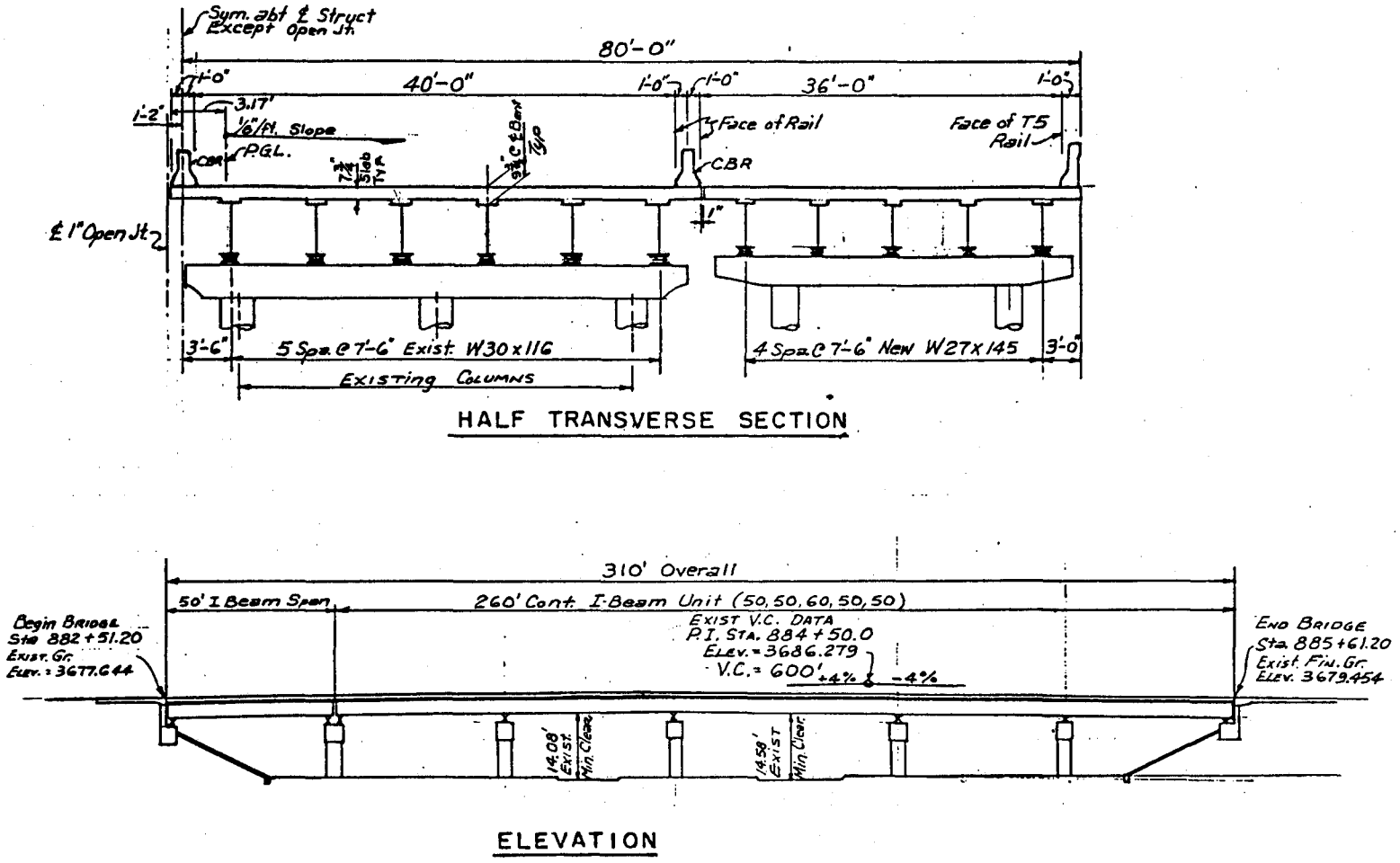

FIG. 41. Details of the Structure to be Repaired

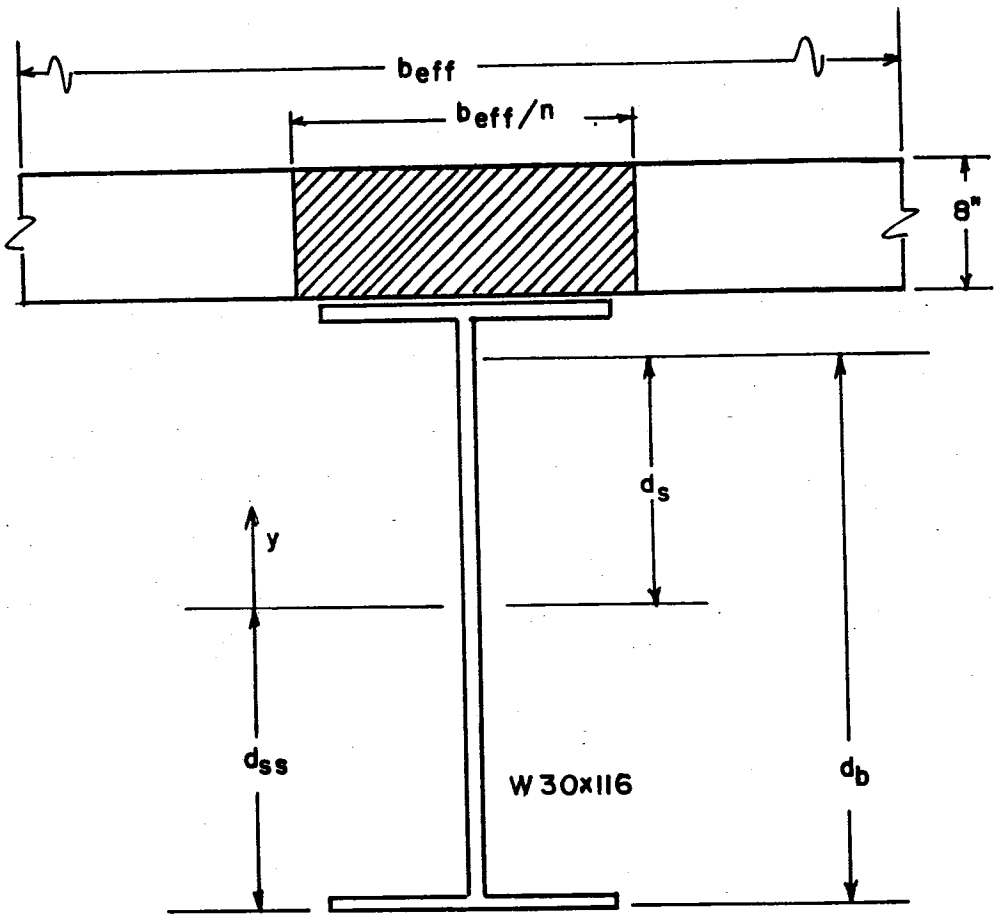

FIG. 42. Cross Section Details of the Structure to be Repaired

b_{eff}:

1/4 span length	= 180 in.
Distance between girders	= 90 in. (controls)
12 slab thicknesses	= 96 in.

The modulus of elasticity of concrete in compression, E_{cc}, can be obtained using the recommendations given in Section 10.38.1.3 of AASHTO (15).

For f'_c = 3600 psi to f'_c = 4500 psi,

$$n_c = 8$$

Then

$$E_{cc} = \frac{E_s}{n} = \frac{29{,}000 \text{ ksi}}{8} = 3625 \text{ ksi}$$

Therefore, for the modulus of elasticity of concrete in tension, E_{cs},

$$E_{cs} = (3625 \text{ ksi})\ (0.67) = 2417 \text{ ksi}$$

and the modular ratio for the structure in tension, n_t, is

$$n_t = \frac{29{,}000 \text{ ksi}}{2417 \text{ ksi}} = 12$$

From Fig. 42,

$$\frac{b_{eff}}{n_t} = \frac{90 \text{ in.}}{12} = 7.50 \text{ in.}$$

Table 8 shows the calculations used to find the transformed area section properties.

TABLE 8. Calculation of Section Properties for the Bridge to be Repaired

SECTION	AREA $in.^2$	y in.	Ay $in.^3$	Ay^2 $in.^4$	Io $in.^4$
Girder	34.2	0.	0.	0.	4390.0
Deck	60.0	19.75	1185.0	23,403.0	320.0
Total	94.2	19.75	1185.0	23,403.0	4710.0

$$d_b = d_s + d_{ss} = \frac{\Sigma Ay}{\Sigma A} + 15 \text{ in.} = 27.58 \text{ in.}$$
$$I = \Sigma Ay^2 + \Sigma I_o - \Sigma A\, d_s = 13{,}207. \text{ in.}^4$$
$$S_{top} = I / (38.75 \text{ in.} - 27.58 \text{ in.}) = 1182.3 \text{ in.}^3$$
$$S_{bot} = I / (27.58 \text{ in.}) = 478.9 \text{ in.}^3$$

Once the section properties are known, the cracking moments can be obtained. Recall,

$$\sigma_{cr} = \frac{M_{cr}}{n_t S_{top}}$$

where

σ_{cr} = cracking tensile stress of concrete, and
M_{cr} = cracking moment.

then

$$M_{cr} = \sigma_{cr}\, n\, S_{top}$$
$$= (201 \text{ psi})(12)(1{,}182.3 \text{ in.}^3)$$
$$= 2{,}851{,}708 \text{ lb-in.}$$
$$= 238.6 \text{ kip-ft}$$

The next step is to determine the design moments for the structure. Fig. 43 shows the live load moment envelope of the 5-span bridge for an HS20 loading. The envelope was obtained from a computer program (8) which considers impact loading as well as distribution factors as recommended by AASHTO for this geometry.

From Fig. 43 the cracking points in the tension areas, or locations where the design moments are approximately equal to the cracking moment, can be obtained. For one half of the structure these were located at 45 ft, 55 ft, 95 ft, and 105 ft from the left end, approximately.

The length of the area of reduced composite action, l, can be obtained from the recommendations of this study,

$$l = 18\ t$$

then, $l = 144$ in. $= 12$ ft

or $l/2 = 6$ ft

Since cracking will occur at a joint first, choose l/2 equal to 10 ft or 2 slab lengths. Then each crack-affected region can be delimited by two boundary points. Assuming that composite action is completely lost within the crack-affected region, the distribution of section properties is as follows,

distance from the support ft	design assumption
0-35	composite
35-65	non-composite
65-85	composite
85-115	non-composite
115-145	composite
145-175	non-composite
175-195	composite
195-225	non-composite
225-260	composite

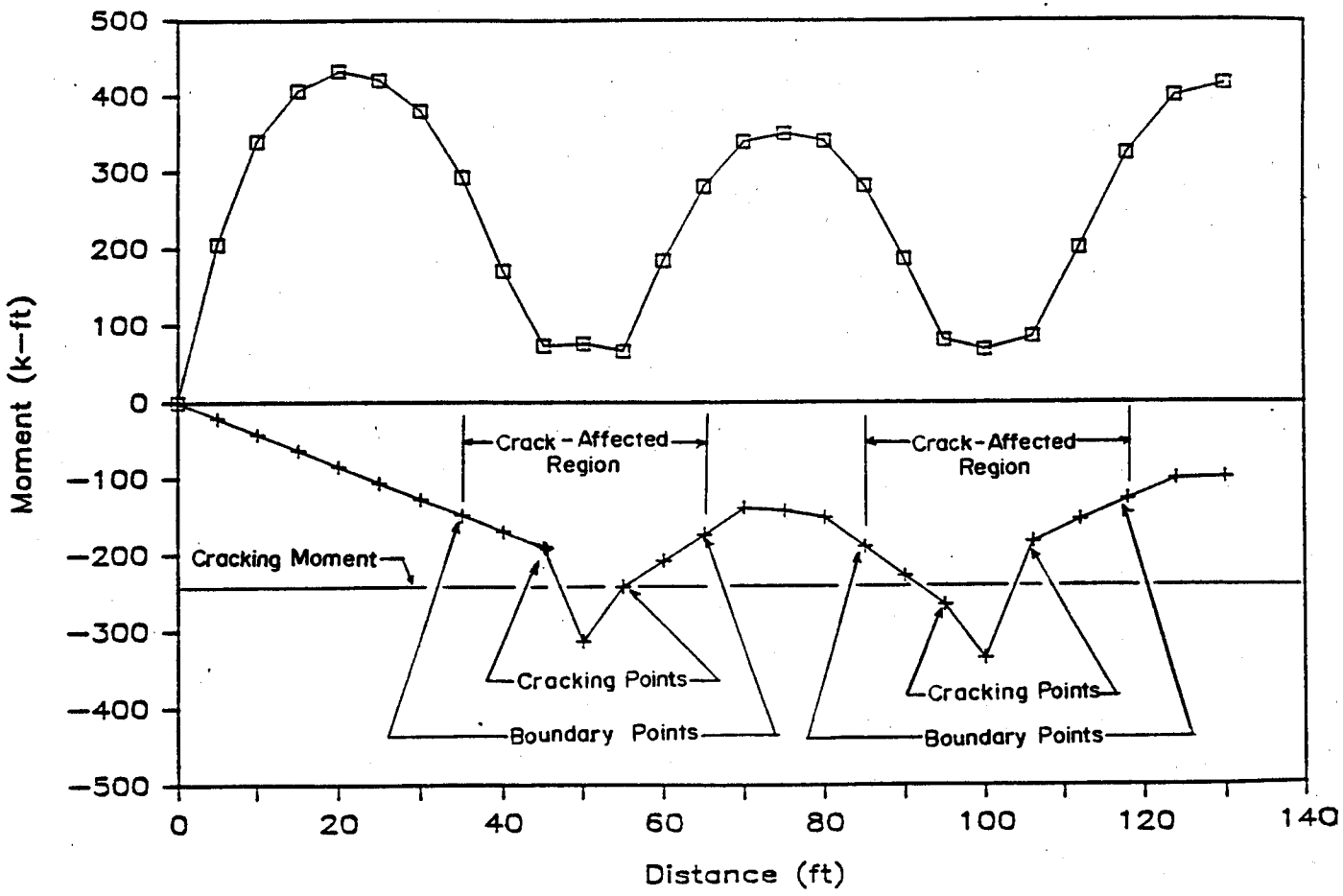

FIG. 43. Live Load Moment Envelope for One-Half of the Structure to be Repaired

The moment envelope shown in Fig. 43 considers a bridge with uniform section properties only. When different section properties are used for the analysis of the structure, a redistribution of moments will occur, and the live load moment envelope of the bridge will be different from that shown in Fig. 43. With respect to the actual moment envelope of the structure with non-uniform section properties three factors must be considered:

1. If the redistributed negative moments at the boundary points are higher than the cracking moment, the length of the crack-affected region will increase and a new moment envelope must be computed.
2. If the maximum negative moment is higher than the moment before the redistribution of loads, then the maximum allowable stress in the steel stringer should be checked.
3. Since the section properties at the supports will be lower than the section properties in the positive moment regions, it is possible that the behavior of the structure will approach that of a series of simply supported beams. Thus, higher positive moments are expected in the positive moment regions if cracking occurs.

The moment envelope for the structure with non-uniform section properties was not available for this design example. To check for the maximum flexural stresses developed in the bridge after the redistribution of loads had taken place, it was assumed that the critical positions for the truck and lane loadings were equal to those that yielded maximum moments in the uniform structure. Based on this assumption, the bending stresses developed at locations considered to be critical were calculated on the first span at the left end of the structure. The critical locations were considered to be the sections with maximum positive moment, maximum negative moment, and the boundary points.

Table 9 shows the live load moments and live load bending stresses at the critical locations. It can be seen that the most highly stressed region for the structure with non-uniform section properties is the boundary point, even though other sections have higher moments. Also, it is important to notice that after the loads are redistributed, the magnitude of the negative moments is reduced at the locations studied.

It may be concluded that when composite action is taken into account in areas outside the crack-affected regions in the continuous bridge, the capacity of the structure is increased. When the design loads generated in the uniform non-composite structure are compared with the non-uniform composite structure, a redistribution of forces occurs. The non-uniform structure tends to relieve moments from the weaker non-composite regions and redistribute them to the stronger composite regions. However, special attention should be paid to the boundary points, since these locations may be more highly stressed after the redistribution of moments. Other aspects that most be considered for the application of this method of design are the effect of the overload on the structure and the fatigue of concrete in tension. These aspects are beyond the scope of this design example, however.

TABLE 9. Bending Live Load Moments and Stresses at the Critical Locations Measured from the Left End for the Structure to be Repaired

DISTANCE	BENDING MOMENT (kip-ft)		BENDING STRESS (ksi)	
(ft)	COMPOSITE	NON-COMPOSITE	COMPOSITE	NON-COMPOSITE
20	465.97	432.07	11.68	17.72
35	351.24	293.15	14.40	12.02
35	-124.71	-149.44	6.13	9.73
50	-221.79	-312.80	9.09	12.83

CHAPTER VI

CONCLUSIONS AND RECOMMENDATIONS

The test structure studied in this experiment was a composite steel-concrete stringer bridge with a deck made of precast concrete panels with shear key joints and shear transfer mechanisms grouted with an epoxy mortar. Results of the experiment show that the behavior under negative moments was different from the behavior of the same structure under positive moment loading reported in Ref. 12.

Two different analytical models were developed in this investigation to study the behavior of the structure during the linear, uncracked, phase of the experiment, so that the cracking pattern of the deck could be predicted. The first model was based on the partial interaction theory, and its main purpose was to analyze the significance of the shear key joints in the behavior of the structure. The second model was a simpler approach to the problem, being based on the transformed area theory. Both models were found to closely predict the behavior of the structure observed during the test.

Conclusions

The analytical model based on the partial interaction theory showed that the changes in section properties at the shear key joint locations were not significant. The structure was divided into several regions, and six different values of section moment of inertia were used during this analysis. Three of the section moments of inertia were used to model the end sections of the bridge, and the other three to model the midspan sections. Each concrete panel was divided into three regions: midslab, joint, and the region adjacent to the joints. The lengths of the various regions along the structure were 19 in., 1 in. (0.5 in. at each end of a panel), and 4 in. (2 in. at each end of a panel). The results of the analysis show that the reductions in moment of inertia relative to the average maximum moment of inertia were only of 6.2 per cent for the shear key joint regions and 2.4 per cent for the regions adjacent to the shear key joints. Reductions in bottom section modulus were found to be even smaller than the reductions of moments

of inertia. Bottom section modulus reductions were 2 per cent for the joint regions and less than 1 per cent for the regions adjacent to the joints; both relative to the section modulus of the midslab region.

It was observed that for the prediction of deflections of the structure, the drops in moments of inertia due to the presence of the joints could be significant if several joints are included in the partial interaction analysis; as in this experiment where nine joints were included. However, the model based on transformed area theory showed that equally good results can be obtained using the simpler model of the structure which neglects the effects of the joints.

The section properties for the second model were obtained using the assumption that the modulus of elasticity of concrete in tension was 67 per cent of the compressive modulus, and that the presence of the shear key joints could be neglected. This last assumption was considered to be valid based on the results obtained from the first model.

The discontinuity of reinforcing steel in the concrete deck at the shear key joints caused weak points at these areas which resulted in cracking at these locations. The cracking stress was calculated to be 286 psi from the first model and 263 psi from the second. A maximum cracking stress of approximately $3\sqrt{f'_c}$, is recommended to be used for the purposes of design. It was observed that after a crack develops, composite action is reduced over an area approximately 18 slab thicknesses long per crack; half of the length on each side of the crack. It was also observed that as the external load was increased the section properties of the structure approached those of the steel stringer alone.

In general it is concluded that:

1. The change in section properties at the epoxy shear key joints is small, however, the change may be significant if partial interaction theory is used for the analysis of the structure.
2. The transformed area theory predicts satisfactorily the behavior of the structure in negative moment regions if the modulus of elasticity of concrete in tension is taken to be 67 per cent of the compressive modulus.
3. The cracking stress at the shear key joints may be assumed to be approximately $3\sqrt{f'_c}$.

4. The length of the area of reduced composite action can be taken as approximately 18 slab thicknesses for structures with section properties similar to the prototype for the model tested.
5. The length of the area for reduced composite action can be expected to increase only after a section outside the crack-affected region cracks.

Recommendations

From the results of this investigation rough design rules can be obtained. However, it is important to notice that a design alternative has been presented for the design of composite steel stringer-concrete bridges with a deck made of precast concrete panels when the maximum live load negative moments in the structure do not significantly exceed the design cracking moment. The alternatives presented to the engineer for the design for steel-concrete bridges can be summarized as follows:

1. neglecting the composite action in the entire negative moment region,
2. when precast concrete panels are used, to prestressing the concrete panels and post-tensioning the entire negative moment region to provide composite action throughout the entire structure, or
3. predicting the extent of the cracking of the concrete deck and the length of the area of reduced composite action, and neglecting composite behavior only within this region.

The design procedure recommended for alternative 3 is explained in Chapter V, "Applications".

More research is recommended to determine the actual length of the reduced composite action for structures with significantly different section properties from those of the prototype structure (see Ref. 12). Also, more research is needed to study the effects of cracks of the concrete deck on the fatigue life of the structure and the effects of temperature and creep on the cracking of the concrete deck.

To minimize the potential damage due to cracking of the concrete deck and subsequent corrosion in the reinforcing steel, it is recommended that all composite action be neglected in the crack-affected region, and that only the minimum amount of shear transfer mechanisms required to hold the deck and stringer together be provided. Finally, it is recommended that the crack-affected regions be delineated by well articulated and waterproofed joints.

REFERENCES

1. "AASHO Interim Specifications, 1971," American Association of State Highway Officials, (AASHO), Washington D.C, 1971.

2. Ammed A. E., discussion of "Tensile Strength of Concrete," by Jerome M. Raphael, American Concrete Institute Journal, ACI, Vol. 82, No 1, Jan.-Feb. 1985, pp. 94-95.

3. Biswas M., Osegueda R. A., and Noel J. S., "Scale-Model Test for Full-Depth Precast Concrete Panel-Decked Composite Bridge Span," Transportation Research Record, Second Bridge Engineering Conference, Transportation Research Board, Vol. 1, No 950, Sep. 24-26, 1984.

4. "Composite Steel Concrete Construction," Report of the Subcommittee on the State-of-the-Art Survey of the Task Committee on Composite Construction of the Committee on Metals of the Structural Division, Journal of the Structural Division, American Society of Civil Engineers, Vol. 100, No ST5, May 1974, pp. 1085-1139.

5. Fullmer, J. M. "Shear Connectors in Epoxy Mortar," Unpublished Report, Texas A&M University, College Station, Texas.

6. Handbook of Composite Construction Engineering, Edited by Gajanan M. Sabnis, Van Nostrand Reinhold Company, New York, N.Y., 1979.

7. Hyma, W. R., "Replacing Timber Decks on Railroad Bridges with Prestressed Concrete Slabs," Concrete International, American Concrete Institute, Vol. 1, No. 5, May 1979, pp. 18-21.

8. Jones H. L., Furr H. L., Ingram L. L., and Harris W. D., "Automated Design of Prestressed Concrete Beams Made Continuous for Live Load - Volume Two, Program Documentation," Texas Transportation Institute, Report No. TTI-2-5-73-22-1F, Oct. 1974

9. Knowles R. P., Composite Steel and Concrete Construction, Halsted Press Book, John Wiley and Sons, New York, 1973.

10. Manual of Steel Construction, 8th ed., American Institute of Steel Construction (AISC), Chicago, Illinois, 1980.

11. Newmark N. H., Siess C. P., and Viest I. M., "Test and Analysis of Composite Beams with Incomplete Interaction," Proceedings, Society for Experimental Stress Analysis, Vol. 9, No 1, 1951.

12. Osegueda R. A., and J. S. Noel, "Positive Moment Tests for Precast Concrete Panel-Decked Composite Bridges," Research Report 324-1, Texas Transportation Institute, Texs A&M University, March 1986.

13. Sherman J., "Continuous Composite Steel and Concrete Beams," Transactions, American Society of Civil Engineers, Vol. 119, 1954, pp. 810-828.

14. Standard Specifications for Highway Bridges, 7th ed., American Association of State Highway Officials, (AASHO), Washington D.C., 1957.

15. Standard Specifications for Highway Bridges, 13th ed., American Association of State Highway and Transportation Officials (AASHTO), Washington D.C., 1983.

16. The Consulting Engineers Group, Inc., "Connections for Modular Precast Concrete Bridge Decks," Interim Report Submitted to the United States Department of Transportation, Federal Highway Administration, Glenview, Illinois, Dec. 1982.

17. Timoshenko S. and Goodier J. N., Theory of Elasticity, 3rd ed., McGraw-Hill Book Company, New York, 1970.

18. Viest I. M. and Siess C. P., "Composite Construction for I-Beam Bridges," Proceedings, Highway Research Board, Vol. 32, 1953, pp. 161-179.

APPENDIX A

NOTATION

A_c = cross-sectional area of concrete in the deck

A_d = cross-sectional area of the deck

A_e = cross-sectional area of the epoxy mortar in the deck at the shear key joints

A_s = cross-sectional area of the steel stringer

b_{eff} = effective width of the deck

B = a constant depending on the section properties of the composite section and the flexibility of the shear connectors

BT = parameter used during the solution of the distribution of axial forces

c = constant in the solution of a differential equation depending on the boundary conditions of the structure

C = a constant depending on the section properties of the composite section and the internal moment at a specific section

d_b = distance from the centroid of the composite section to the bottom fibers of the steel stringer

d_c = distance from the centroid of the composite section to the centroid of the deck

d_{cc} = distance from the centroid of the deck to the extreme fibers of the deck

d_s = distance from the centroid of the composite section to the centroid of the steel stringer

d_{ss} = distance from the centroid of the steel stringer to the extreme fibers of the stringer

d_t = distance from the centroid of the stel stringer to the centroid of the deck

D = parameter used in the solution of the distribution of axial forces

e = distance from the top fibers of the steel stringer to the bottom fibers of the deck

E_c = modulus of elasticity of concrete

E_d = modulus of elasticity of deck

E_e = modulus of elasticity of epoxy mortar

E_s = modulus of elasticity of the steel stringer

EA = a constant depending on the sectional properties of the composite section

$\overline{EI}$ = a constant depending on the sectional properties of the composite section

f'_c = compressive strength of concrete

I_c = moment of inertia of a section of concrete in the deck

I_{comp} = moment of inertia of the composite section

I_d = moment of inertia deck

I_e = moment of inertia of a section of epoxy mortar in the shear key joints

I_s = moment of inertia of a steel stringer

I_{tae} = transformed area moment of inertia at an end section

I_{tam} = transformed area moment of inertia at a midspan section

I(x) = longitudinal distribution of moment of inertia

k_c = parameter relating the curvature of the steel stringer and the curvature of the concrete deck

K = constant depending on the material and section properties

l = length of the crack-affected region

L = length of a region of study

M = bending moment

M_{cr} = bending moment that will crack the concrete deck

M_d = internal moment acting in the deck

M_s = internal moment acting in the steel stringer

M(x) = longitudinal distribution of bending moments

n = steel-concrete modular ratio

N = interior axial force acting in a composite section

N_d = interior axial force acting in the deck of the structure

N_s = interior axial force acting in the steel stringer

N(x) = longitudinal distribution of axial forces

$\overline{N}$ = axial force boundary conditions at a region of study

P = externally applied load on a stringer

R	=	product of the length of a region of study and the respective B parameter for that region
s	=	slip displacement
S	=	hyperbolic sine of the product of two parameters
S_{comp}	=	bottom section modulus of the composite structure
t	=	thickness of the concrete deck
T	=	hyperbolic cotangent of the product of two paramters
V	=	constant shear in the structure due to the application of a concentrated force at midspan
Z	=	ratio of the axial force at a section to the internal moment at that section
ε_{slip}	=	slip strain
ε_b	=	strain at the bottom fibers of the steel stringer
μ	=	flexibility of the shear connectors per unit length
σ_b	=	flexural stress at the bottom fibers of the steel stringer
σ_c	=	extreme fiber stress in the deck due to bending only
σ_{cr}	=	cracking stress of the concrete deck
σ_{max}	=	maximum top fiber stress in the concrete deck
σ_s	=	extreme fiber stress in the steel stringer due to bending only
ΣEI	=	a constant depending on the sectional properties of the composite section

APPENDIX B

STRAIN DIAGRAMS

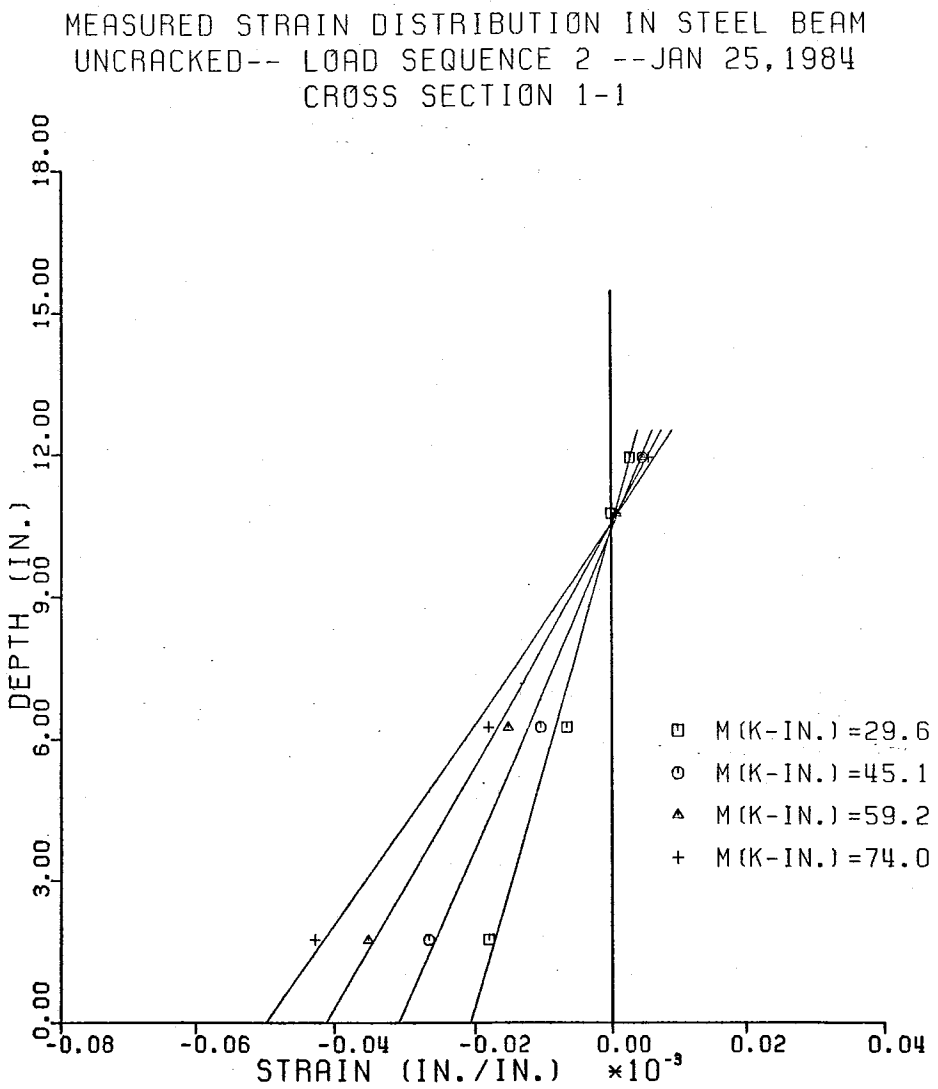

FIG. B1. Measured Strain Distribution in Stringer 1 for the Uncracked Load Sequence 2 at Monitored Section 1 for Loads 1-4.

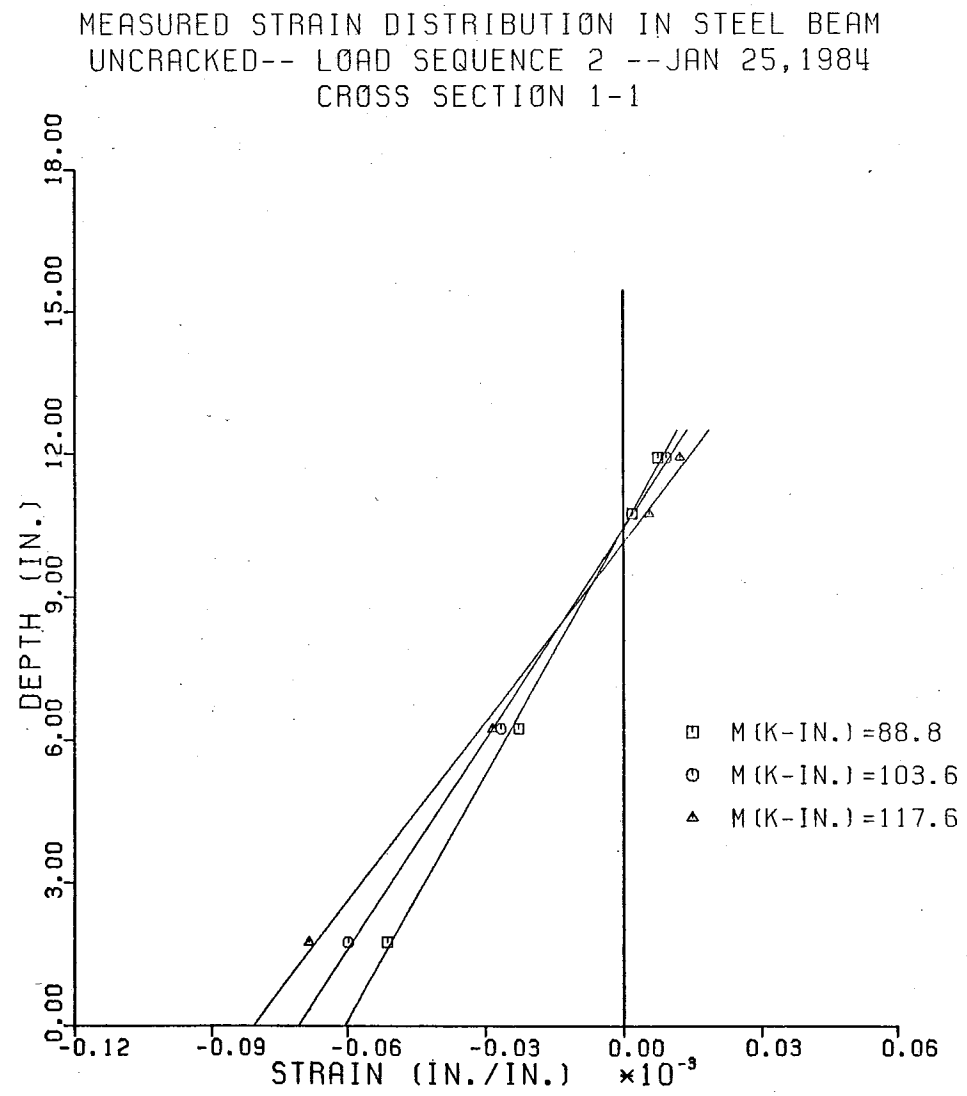

FIG. B 2. Measured Strain Distribution in Stringer 1 for the Uncracked Load Sequence 2 at Monitored Section 1 for Loads 4-7

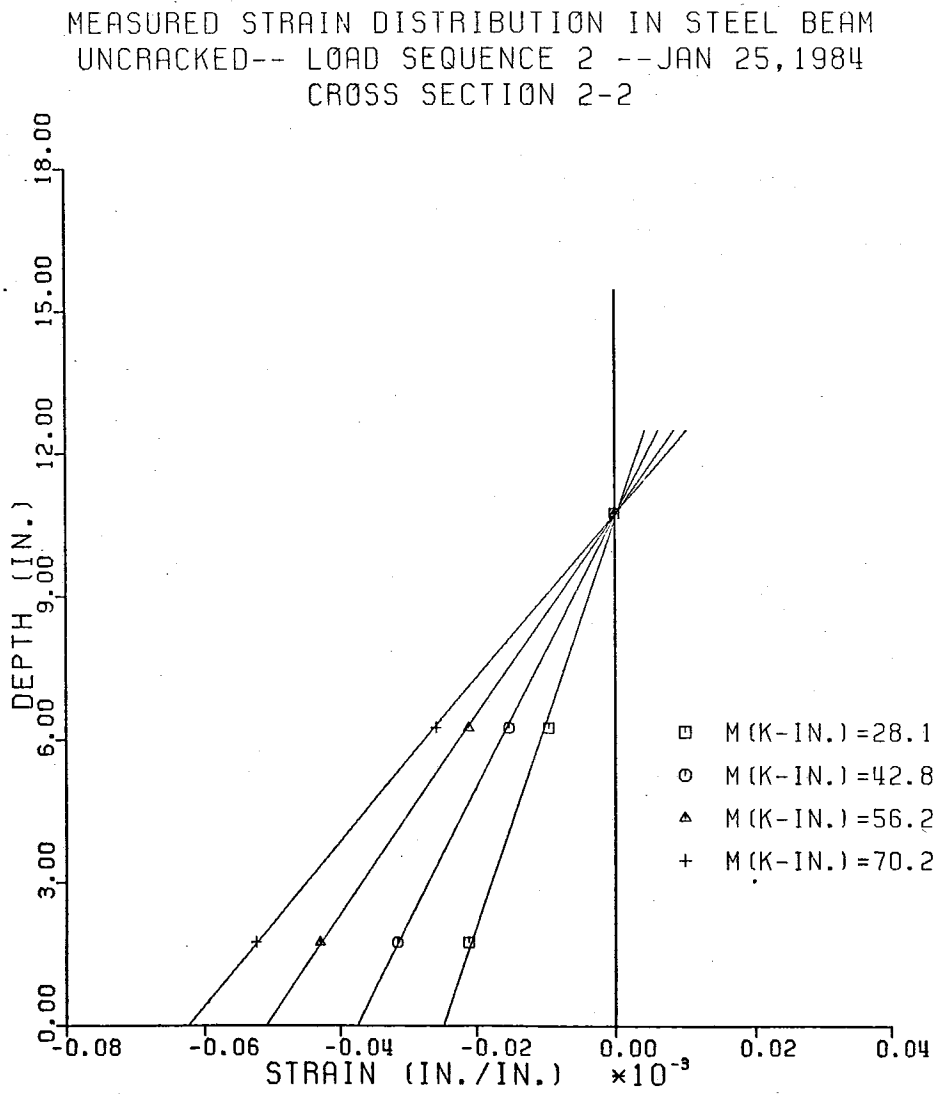

FIG. B3. Measured Strain Distribution in Stringer 1 for the Uncracked Load Sequence 2 at Monitored Section 2 for Loads 1-4.

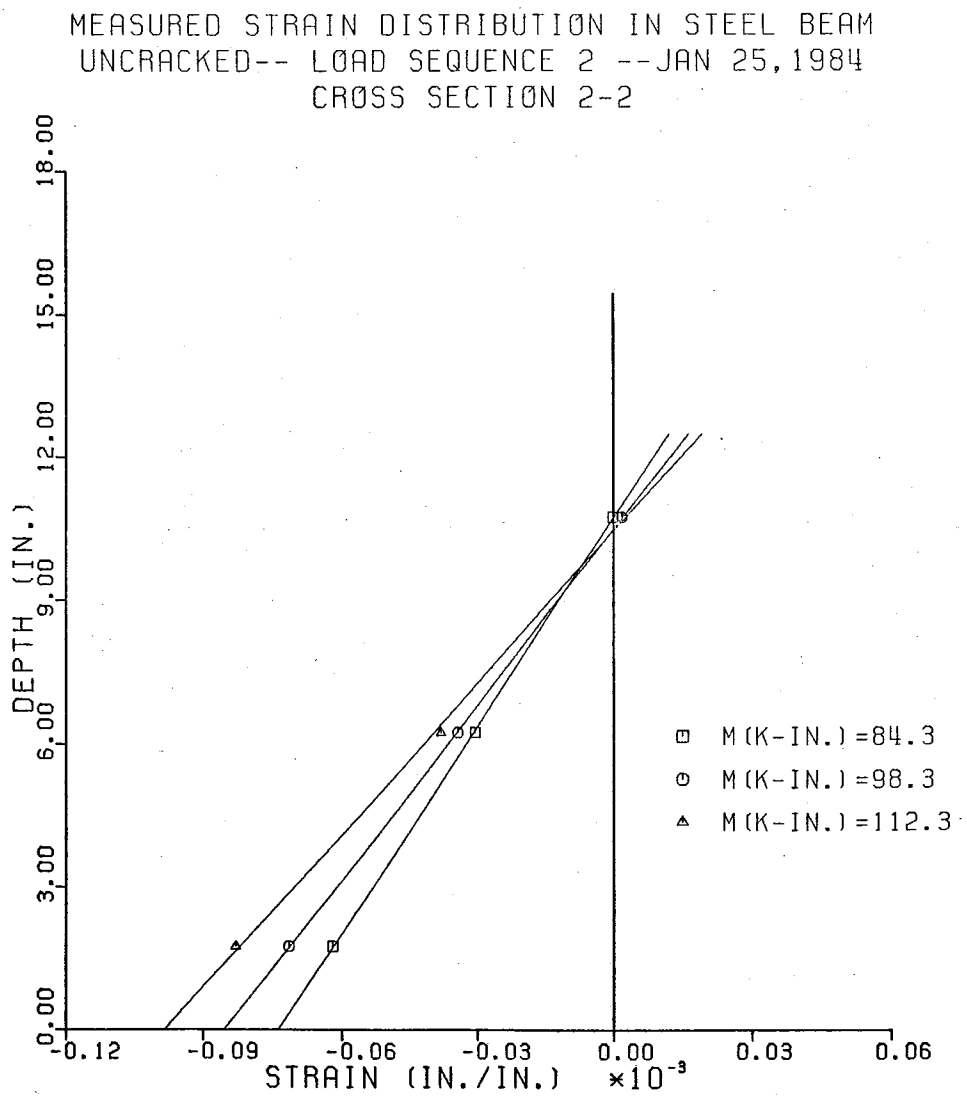

FIG. B 4. Measured Strain Distribution in Stringer 1 for the Uncracked Load Sequence 2 at Monitored Section 2 for Loads 5-7.

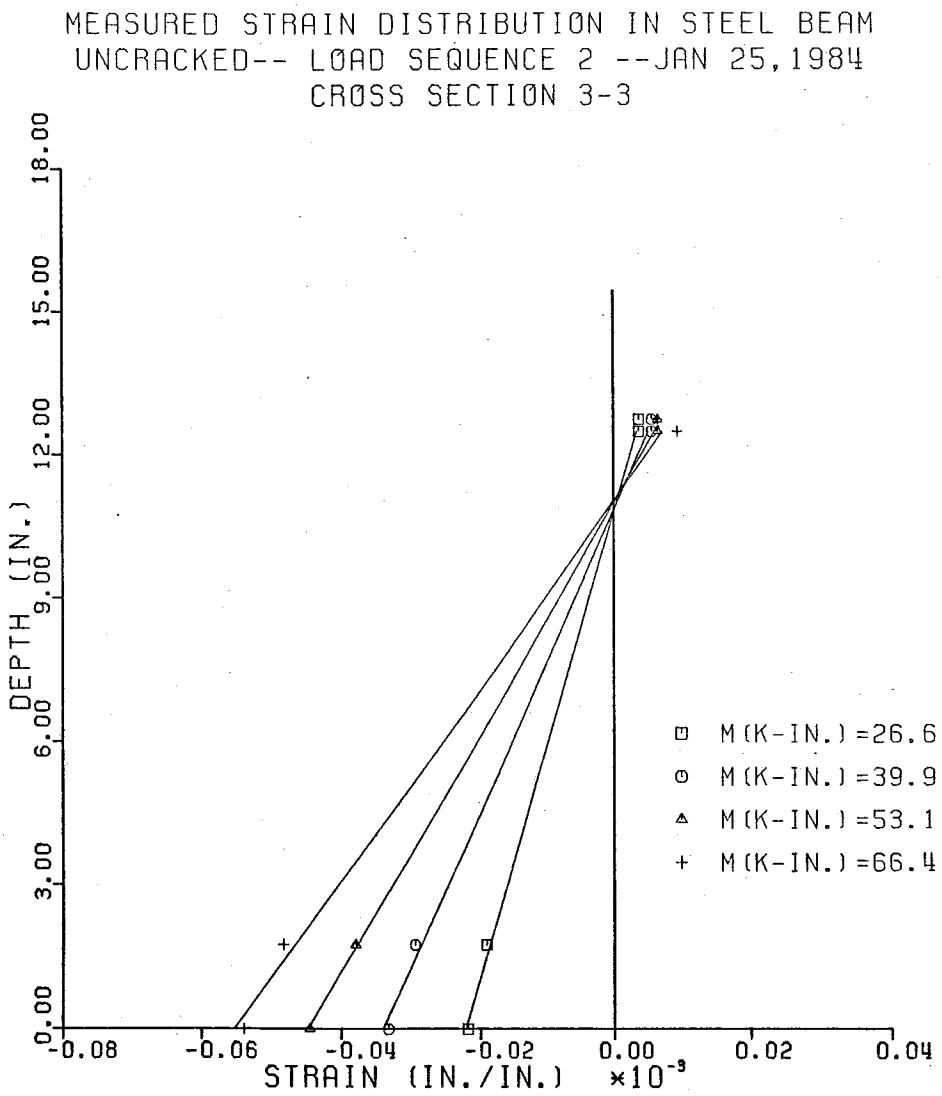

FIG. B5. Measured Strain Distribution in Stringer 1 for the Uncracked Load Sequence 2 at Monitored Section 3 for Loads 1-4.

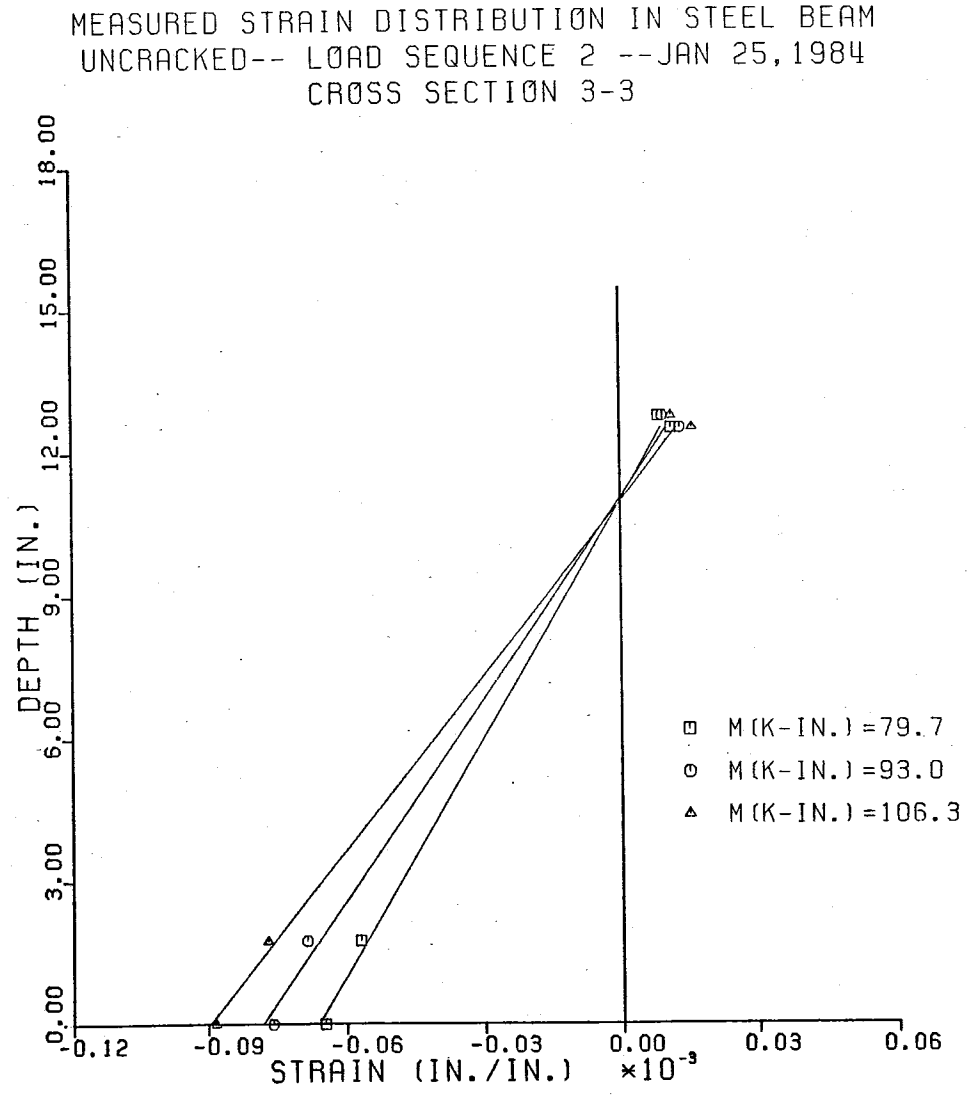

FIG. B6. Measured Strain Distribution in Stringer 1 for the Uncracked Load Sequence 2 at Monitored Section 3 for Loads 5-7

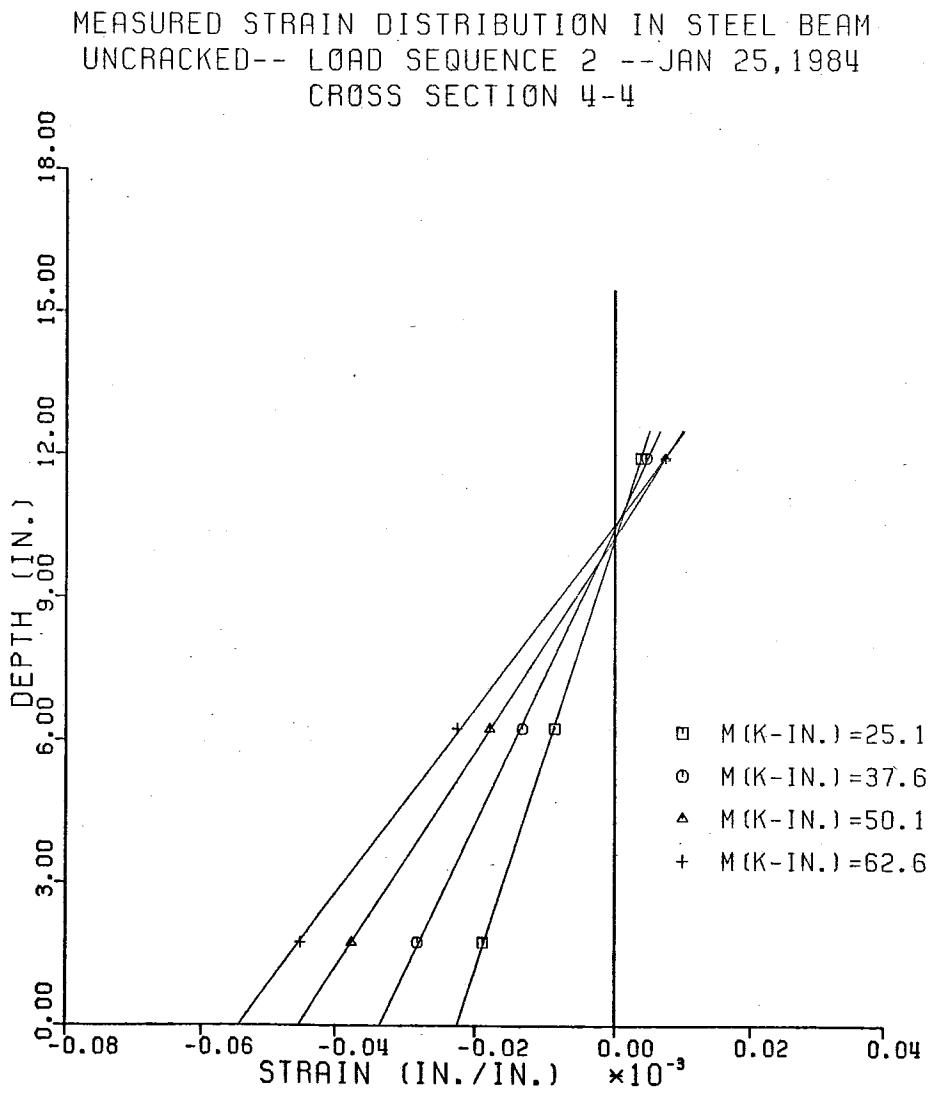

FIG. B 7. Measured Strain Distribution in Stringer 1 for the Uncracked Load Sequence 2 at Monitored Section 4 for Loads 1-4.

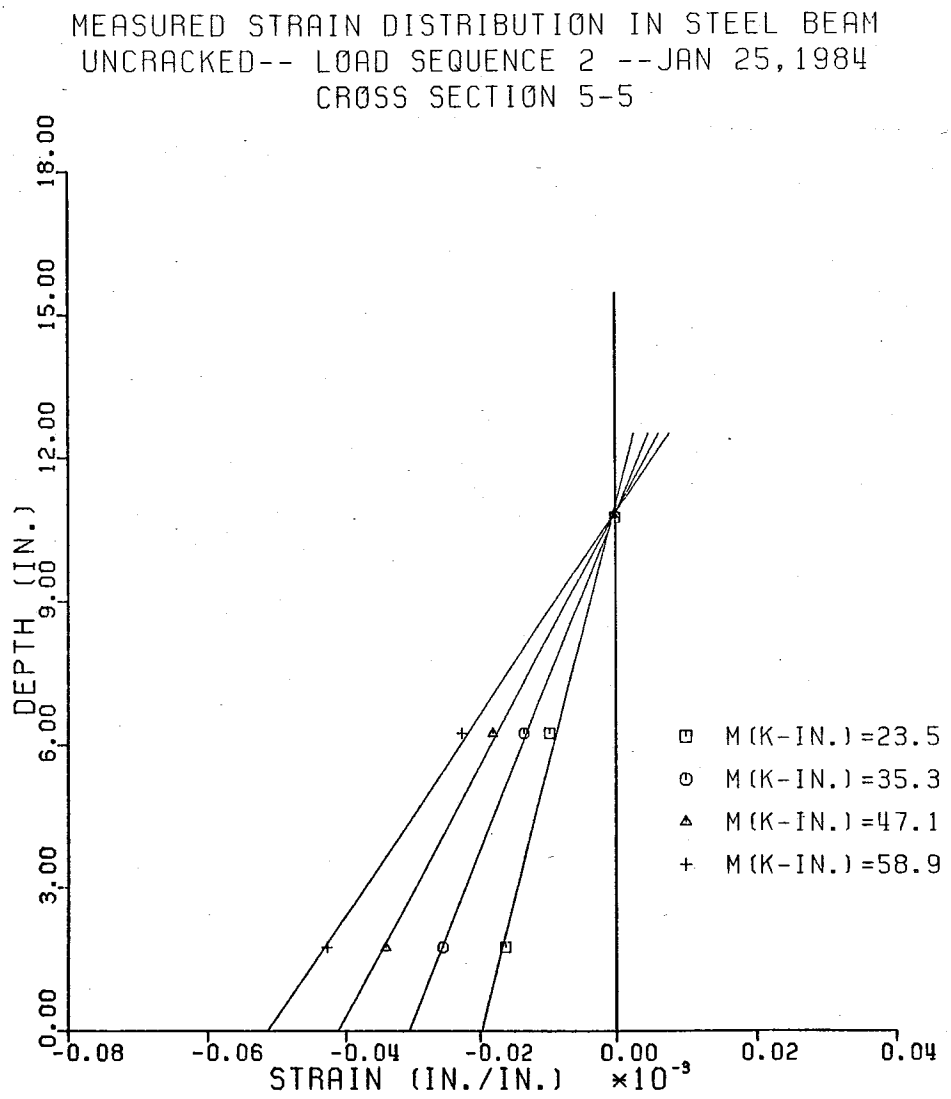

FIG. B 9. Measured Strain Distribution in Stringer 1 for the Uncracked Load Sequence 2 at Monitored Section 5 for Loads 1-4

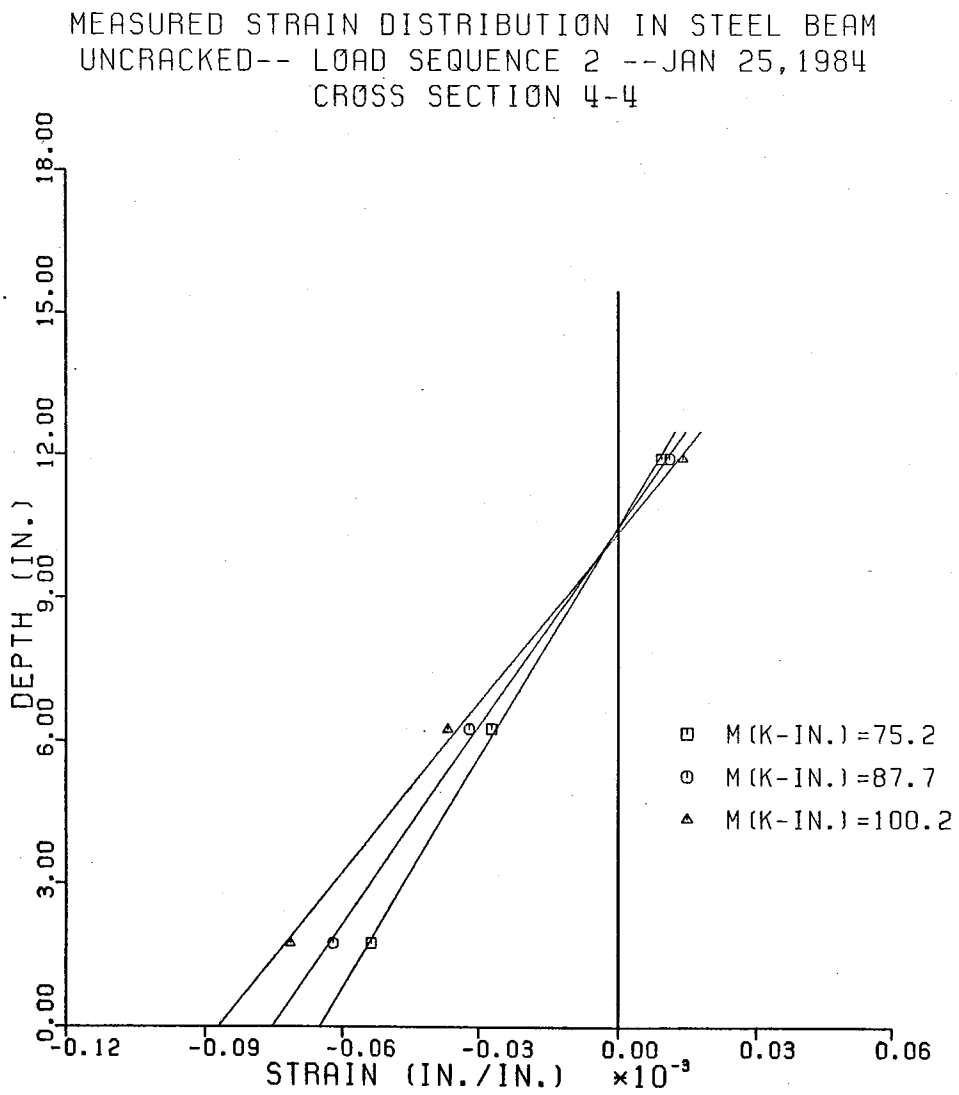

FIG. B8. Measured Strain Distribution in Stringer 1 for the Uncracked Load Sequence 2 at Monitored Section 4 for Loads 5-7.

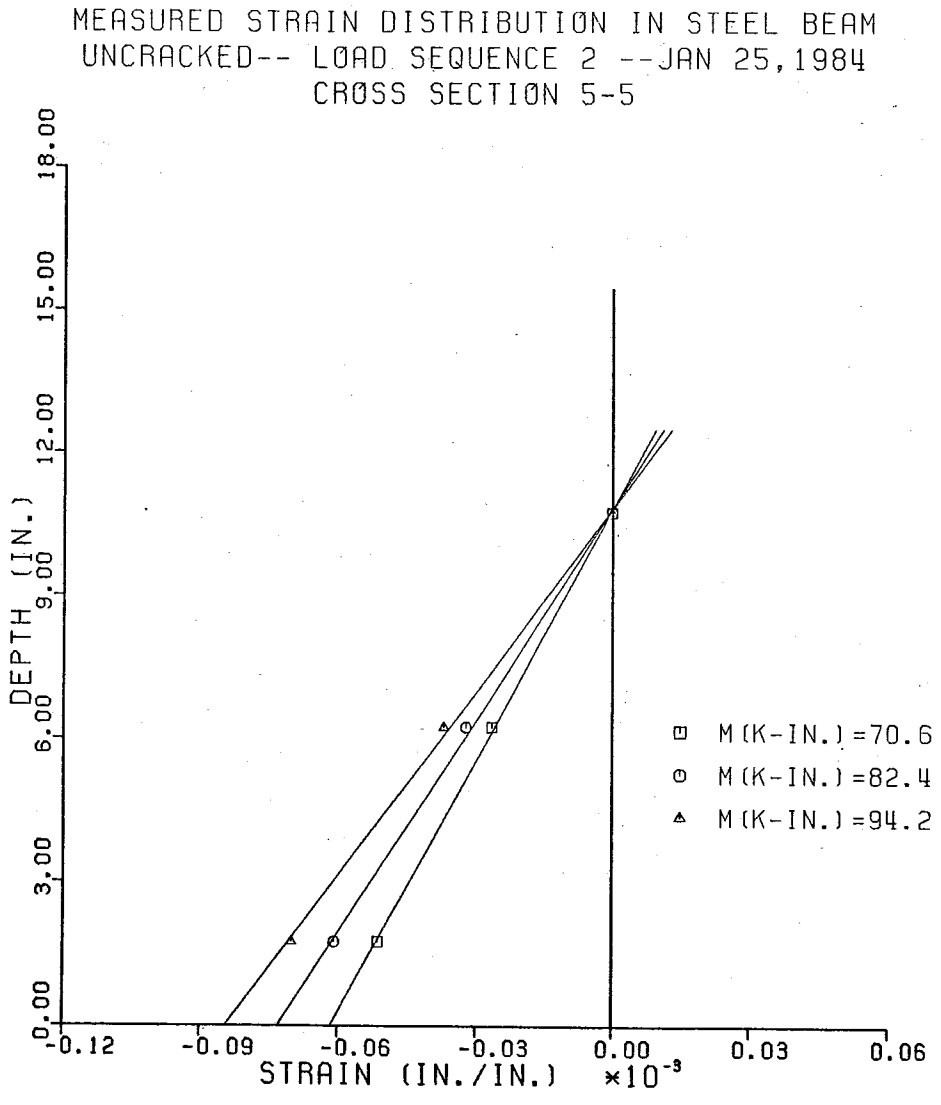

FIG. B10. Measured Strain Distribution in Stringer 1 for the Uncracked Load Sequence 2 at Monitored Section 5 for Loads 5-7.

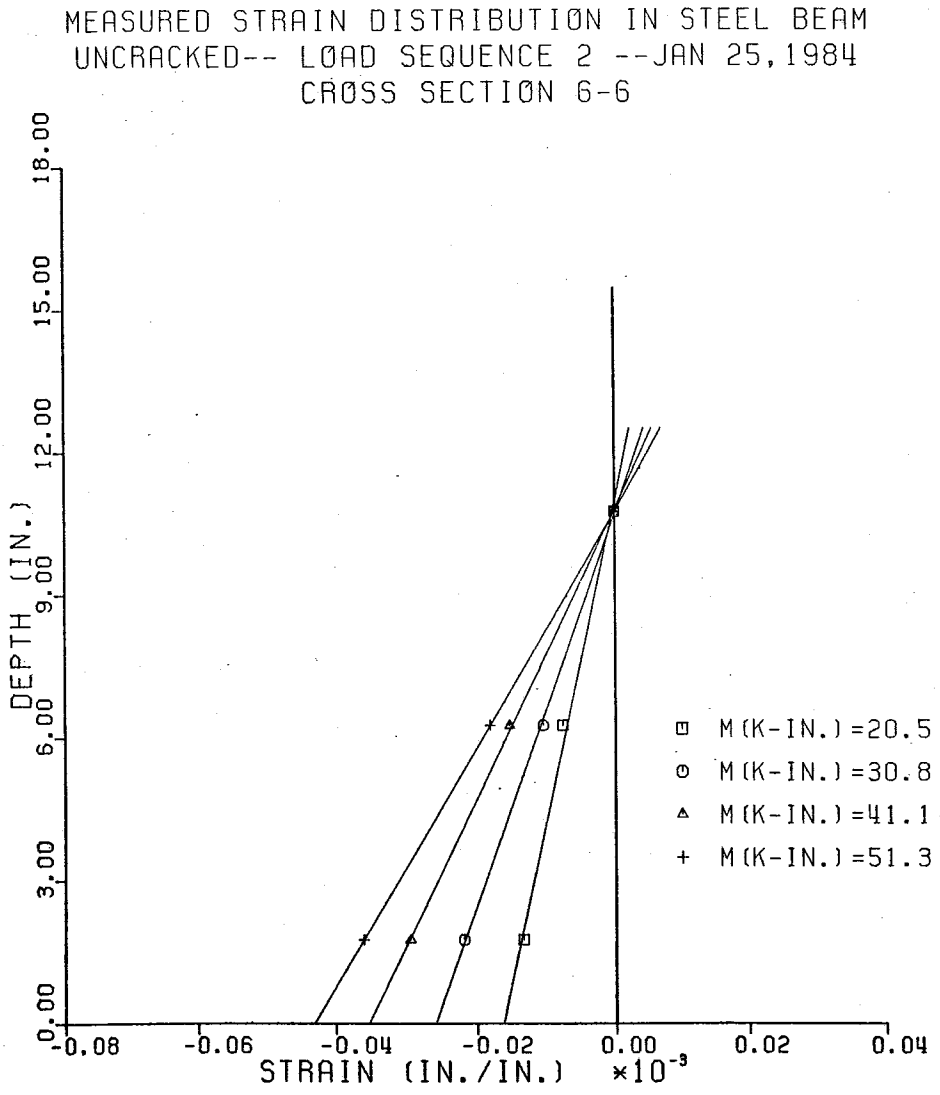

FIG. B11. Measured Strain Distribution in Stringer 1 for the Uncracked Load Sequence 2 at Monitored Section 6 for loads 1-4

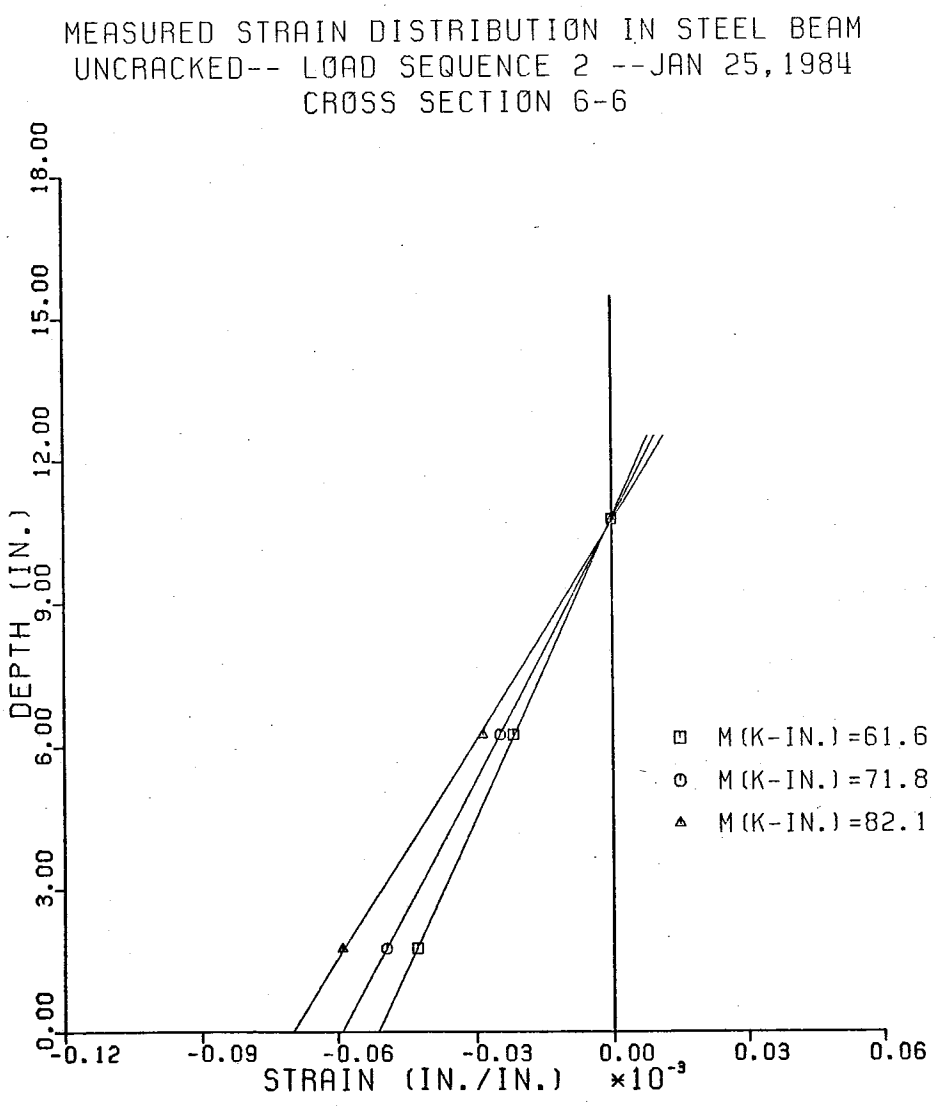

FIG. B12. Measured Strain Distribution in Stringer 1 for the Uncracked Load Sequence 2 at Monitored Section 6 for Loads 5-7.

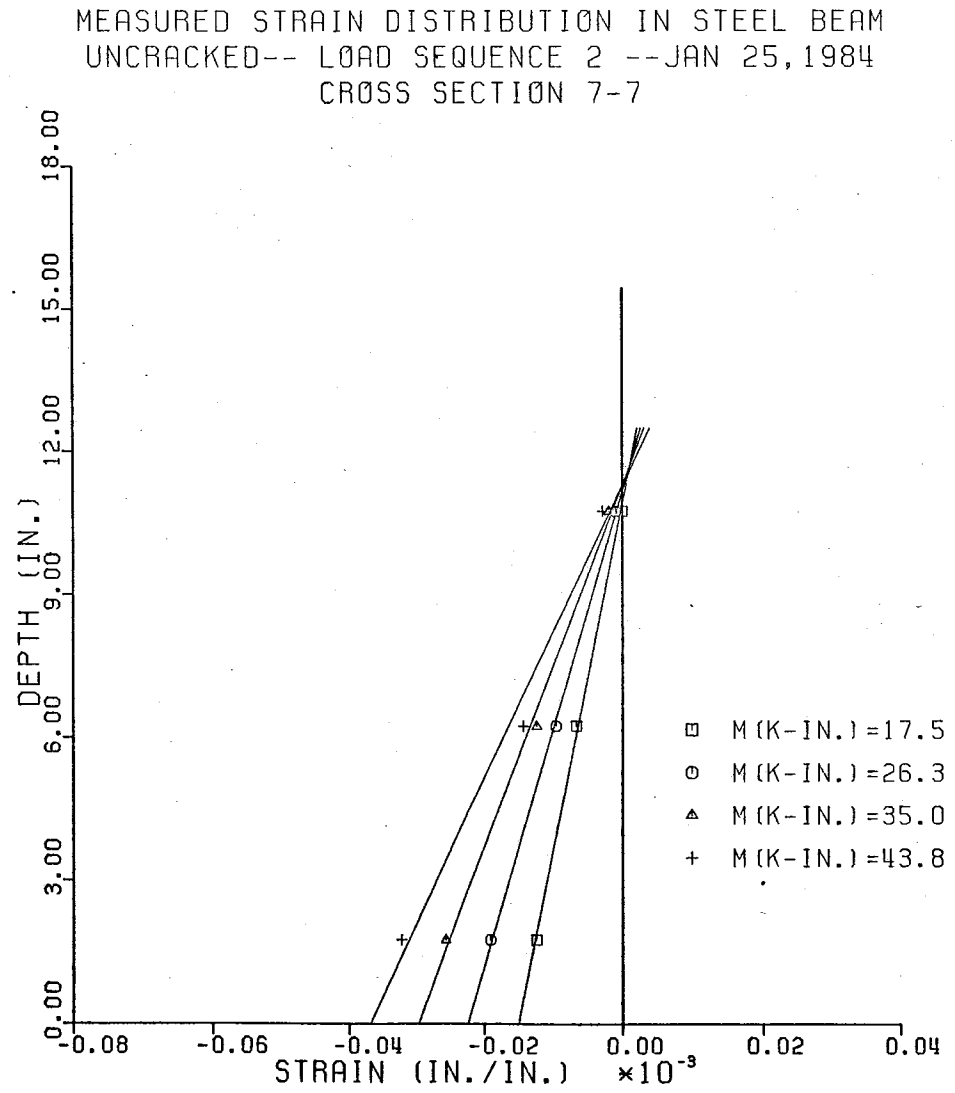

FIG. B13. Measured Strain Distribution in Stringer 1 for the Uncracked Load Sequence 2 at Monitored Section 7 for Loads 1-4.

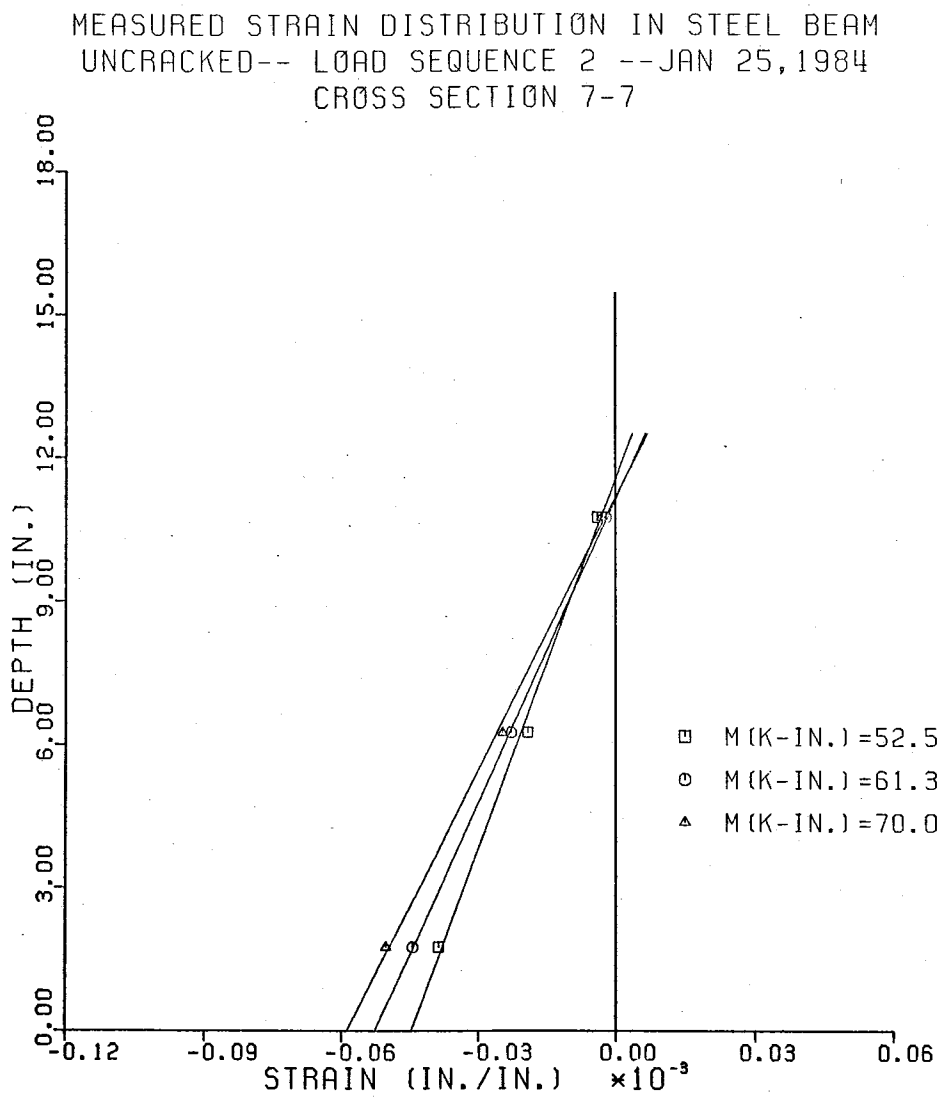

FIG. B14. Measured Strain Distribution in Stringer 1 for the Uncracked Load Sequence 2 at Monitored Section 7 for Loads 5-7.

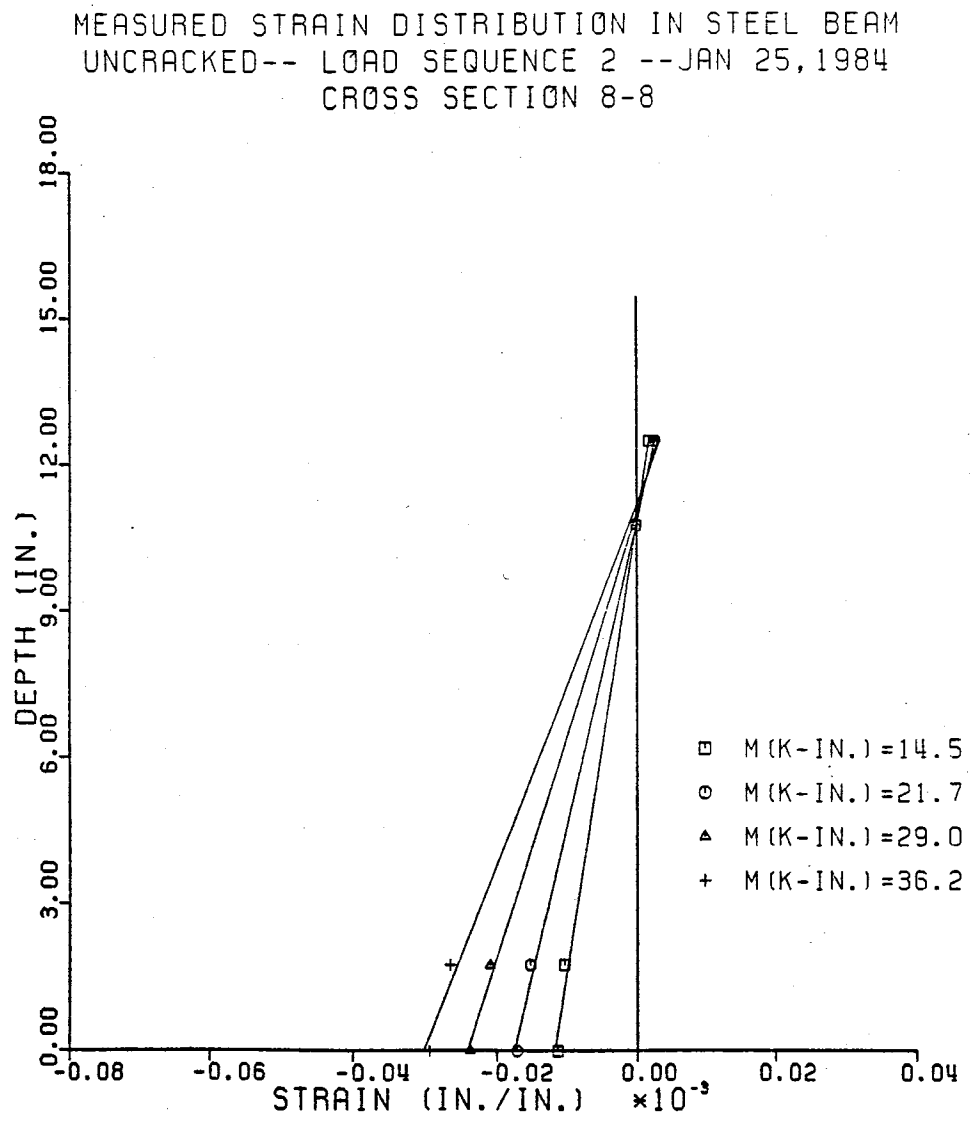

FIG. B15. Measured Strain Distribution in Stringer 1 for the Uncracked Load Sequence 2 at Monitored Section 8 for Loads 1-4.

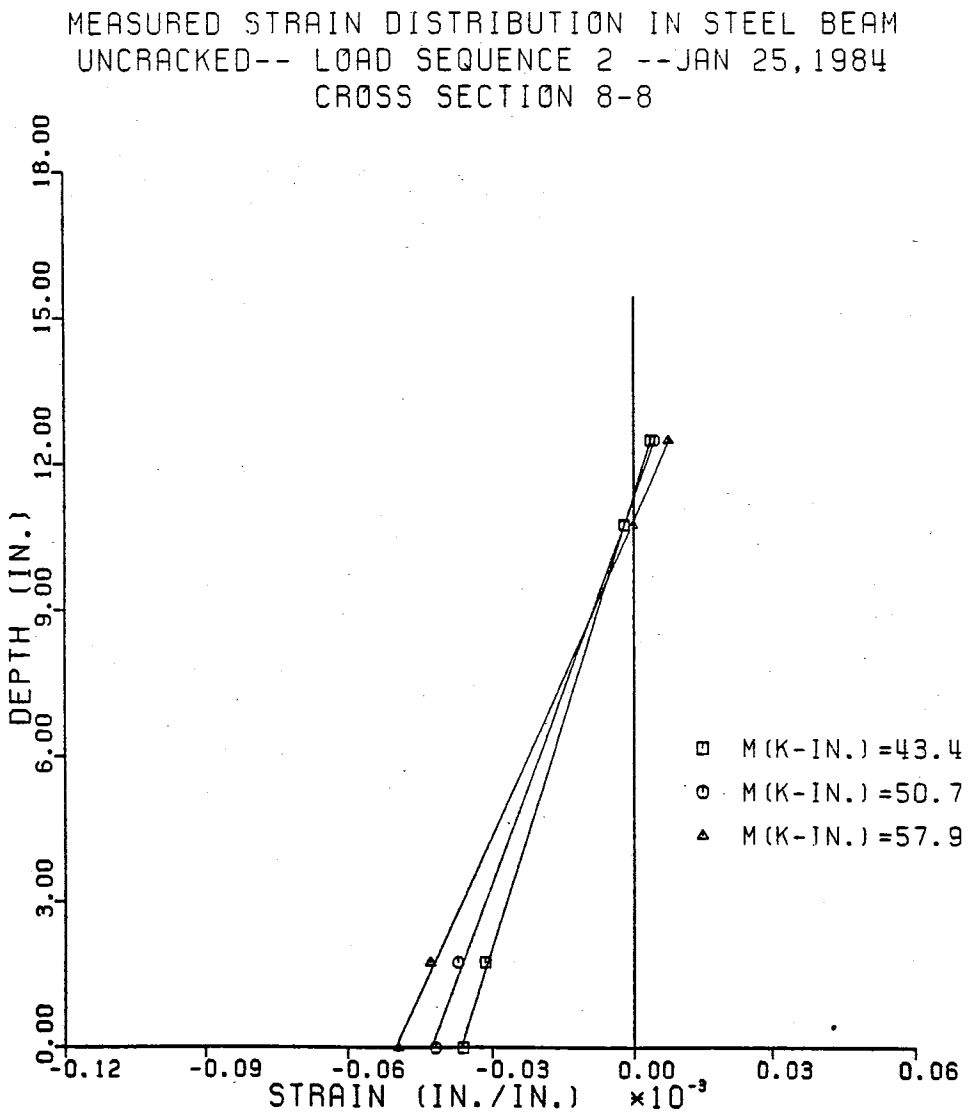

FIG. B16. Measured Strain Distribution in Stringer 1 for the Uncracked Load Sequence 2 at Monitored Section 8 for Loads 5-7.

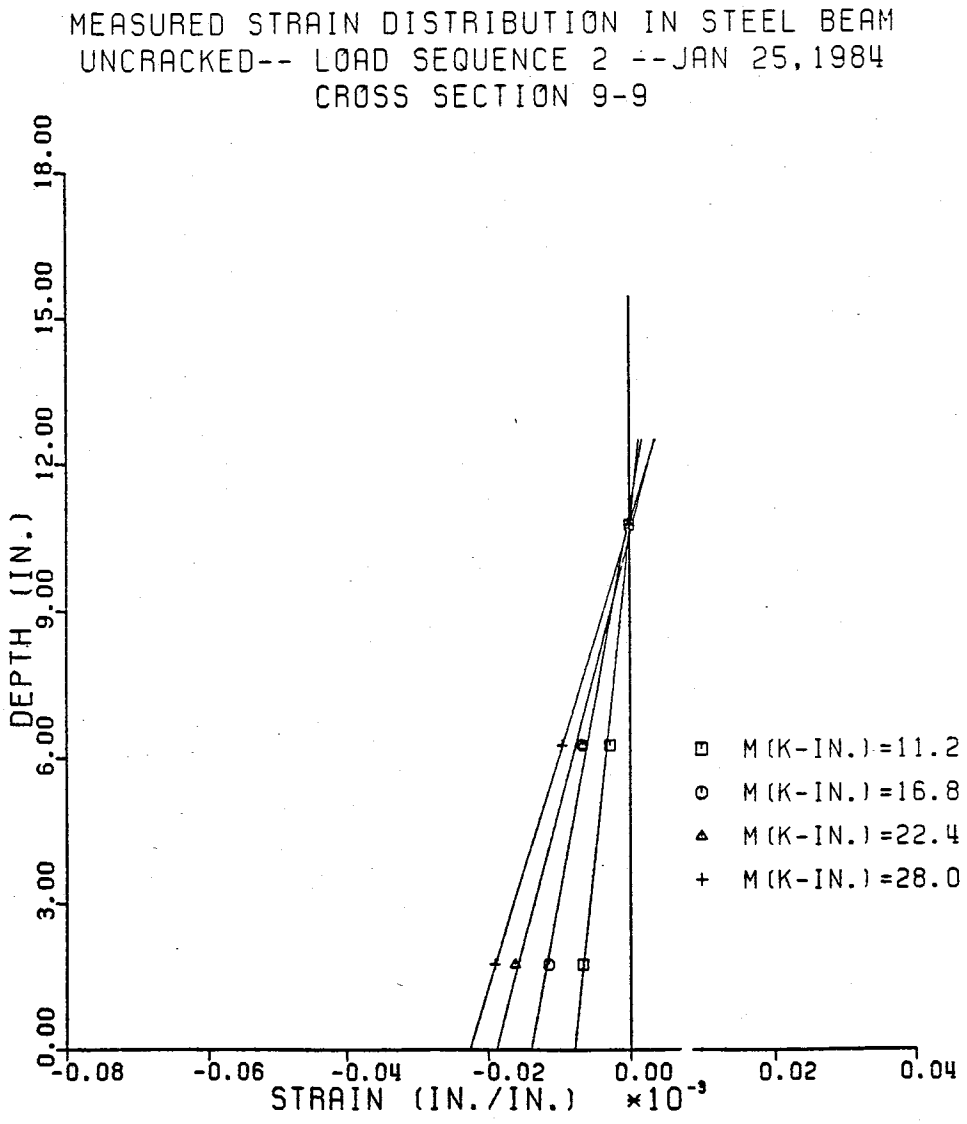

FIG. B17. Measured Strain Distribution in Stringer 1 for the Uncracked Load Sequence 2 at Monitored Section 9 for Loads 1-4.

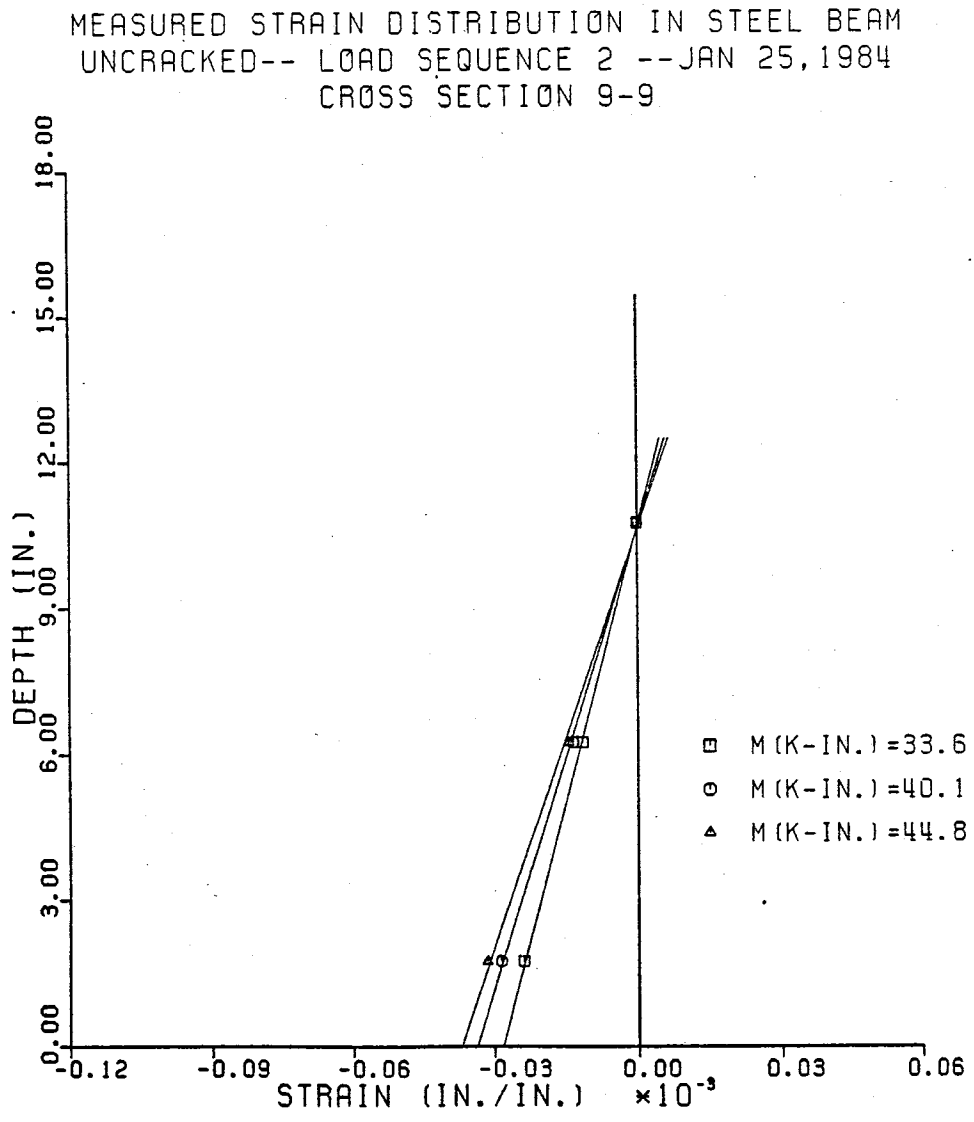

FIG. B18. Measured Strain Distribution in Stringer 1 for the Uncracked Load Sequence 2 at Monitored Section 9 for Loads 5-7.

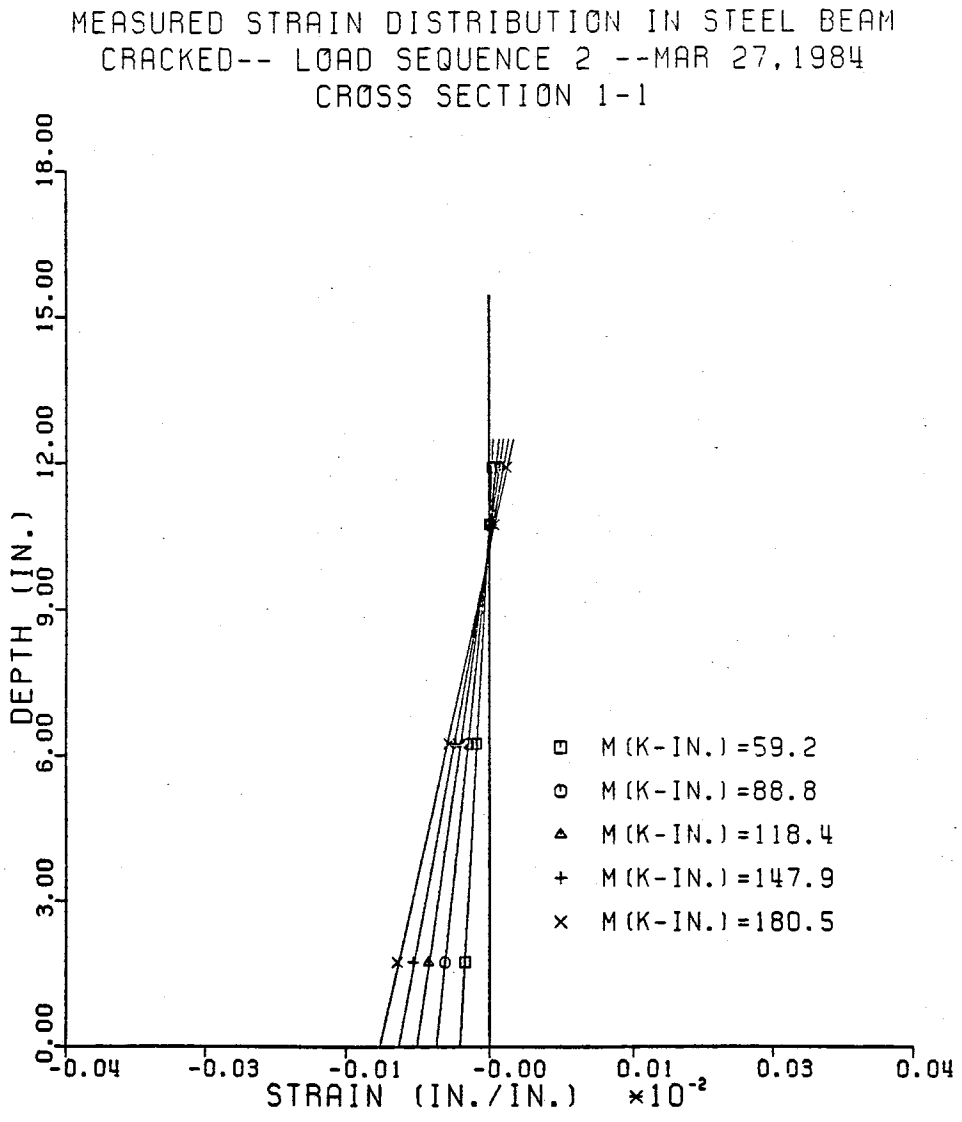

FIG. B19. Measured Strain Distribution in Stringer 1 for the Cracked Load Sequence 2 at Monitored Section 1 for Loads 1-5

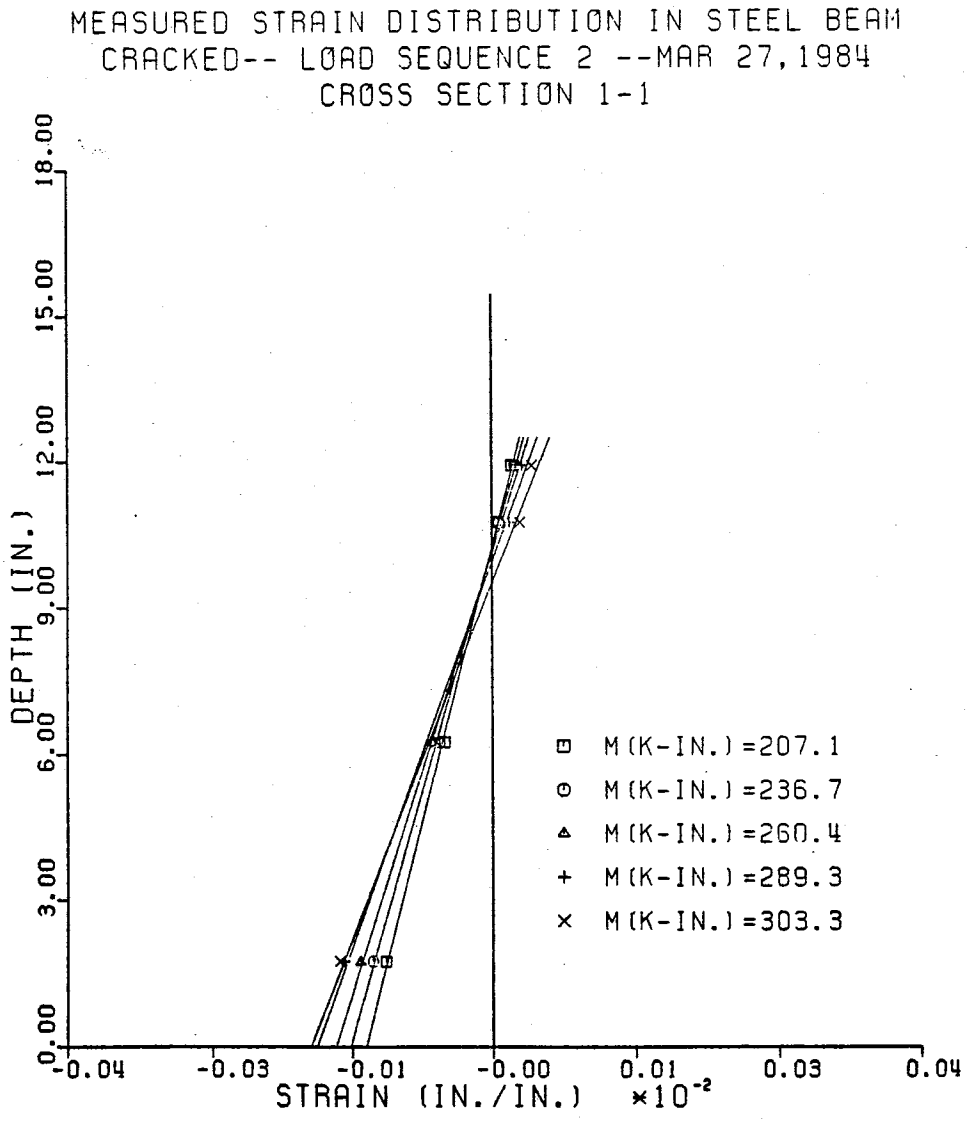

FIG. B20. Measured Strain Distribution in Stringer 1 for the Cracked Load Sequence 2 at Monitored Section 1 for Loads 6-10

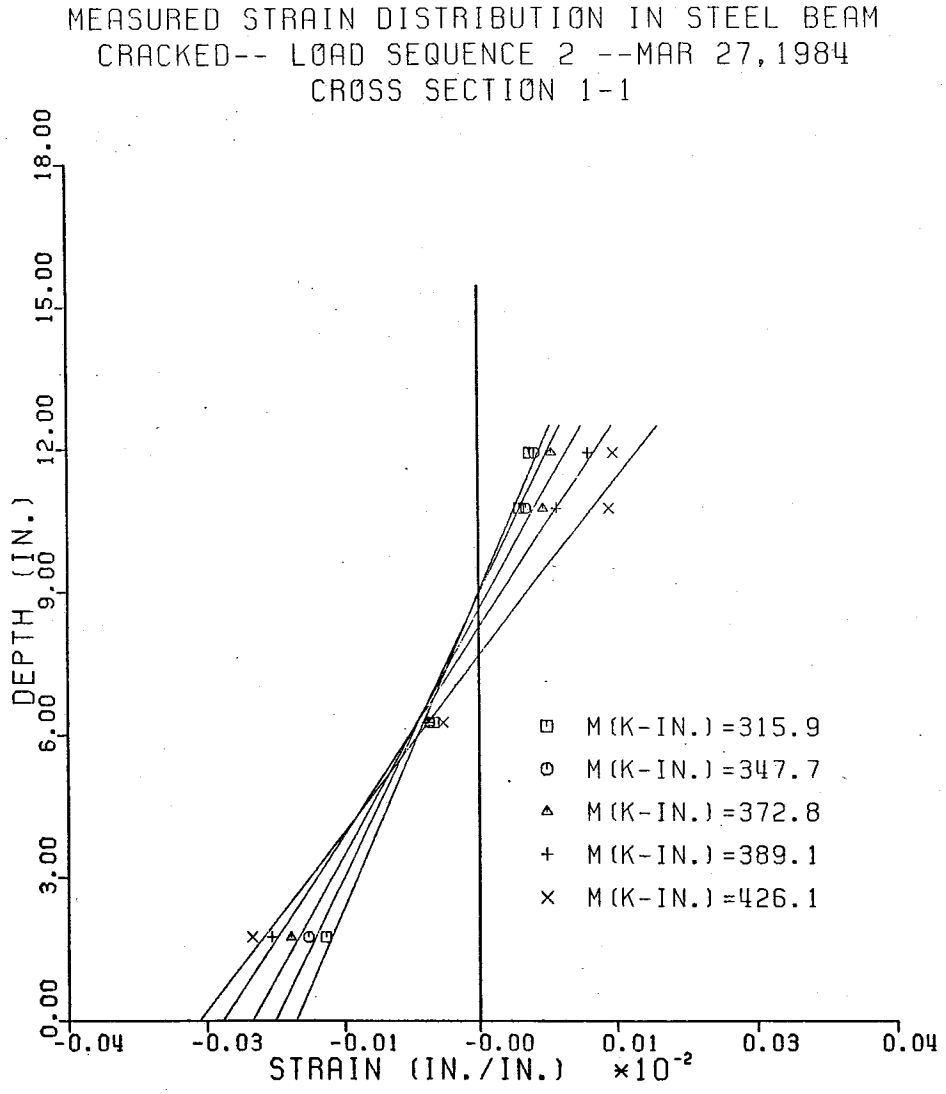

FIG. B21. Measured Strain Distribution in Stringer 1 for the Cracked Load Sequence 2 at Monitored Section 1 for Loads 11-15.

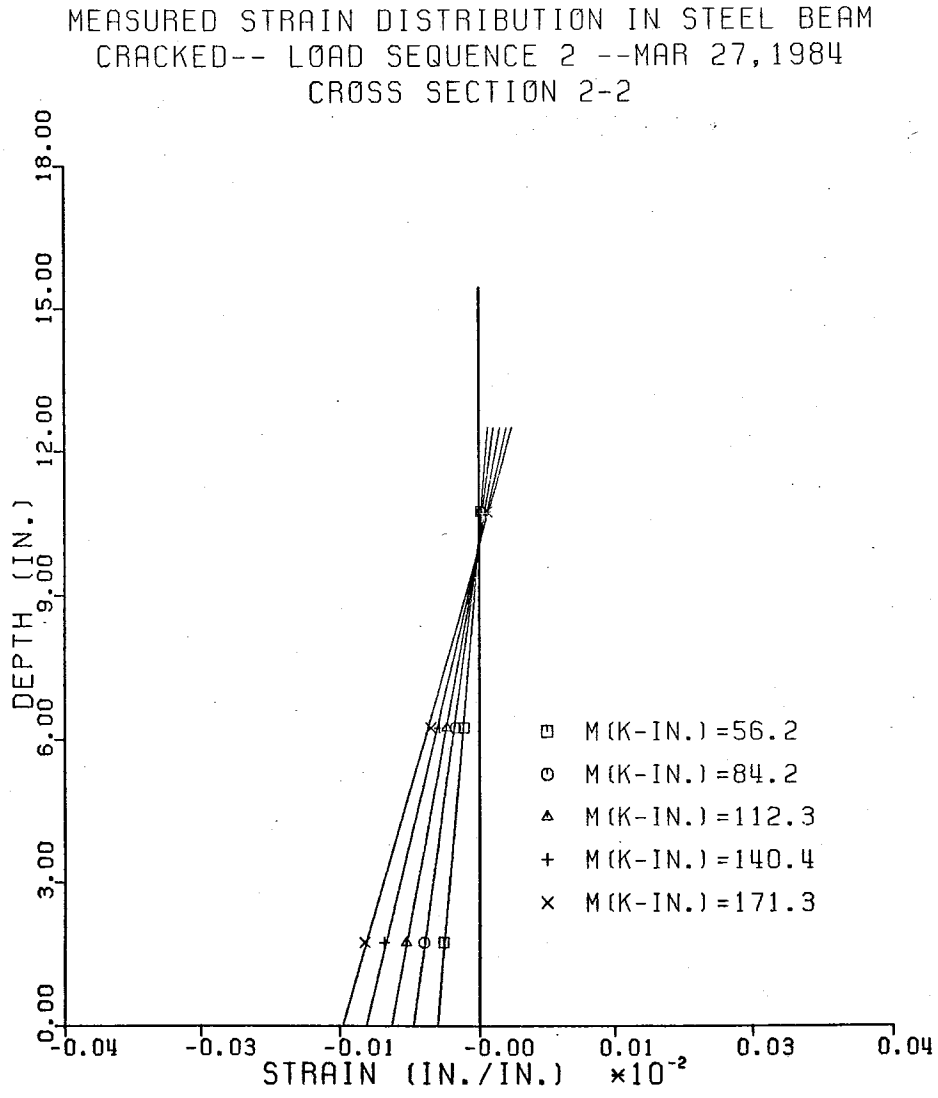

FIG. B22. Measured Strain Distribution in Stringer 1 for the Cracked Load Sequence 2 at Monitored Section 2 for Loads 1-5.

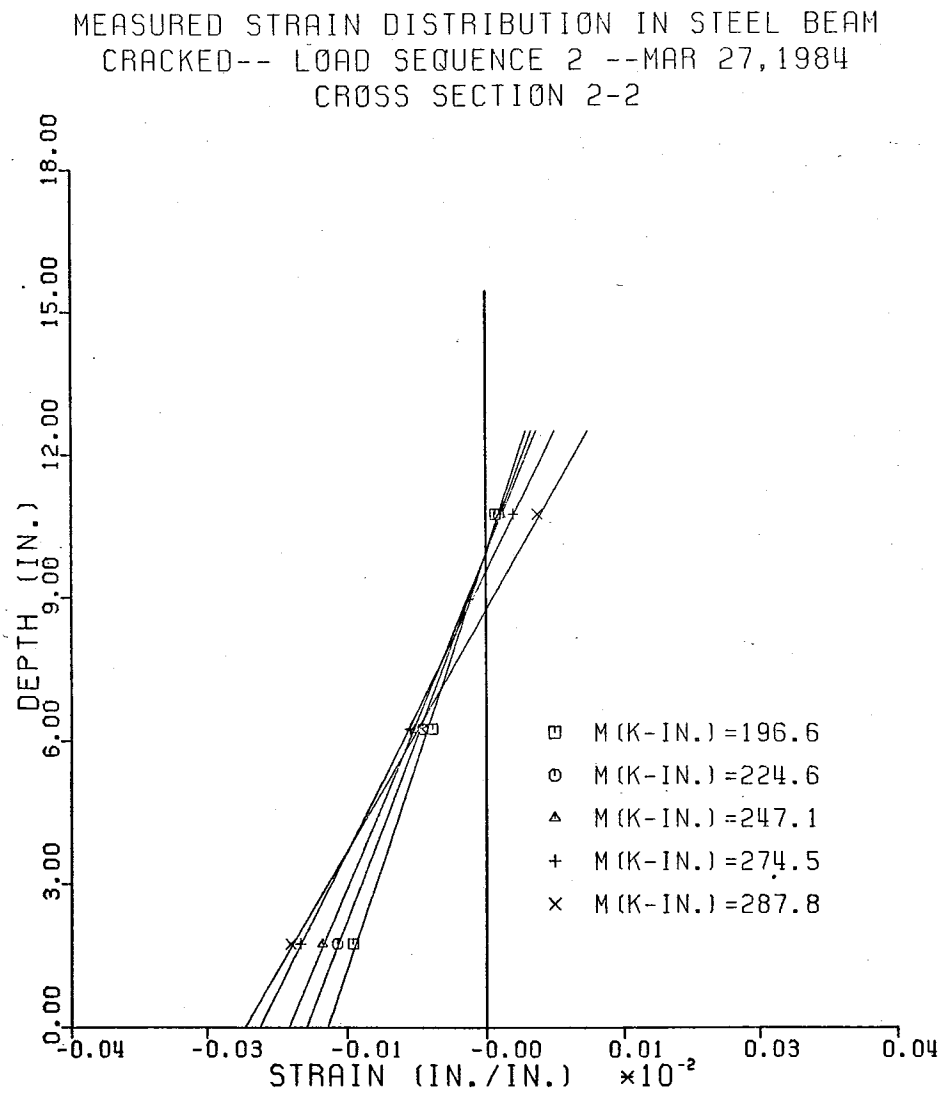

FIG. B23. Measured Strain Distribution in Stringer 1 for the Cracked Load Sequence 2 at Monitored Section 2 for Loads 6-10

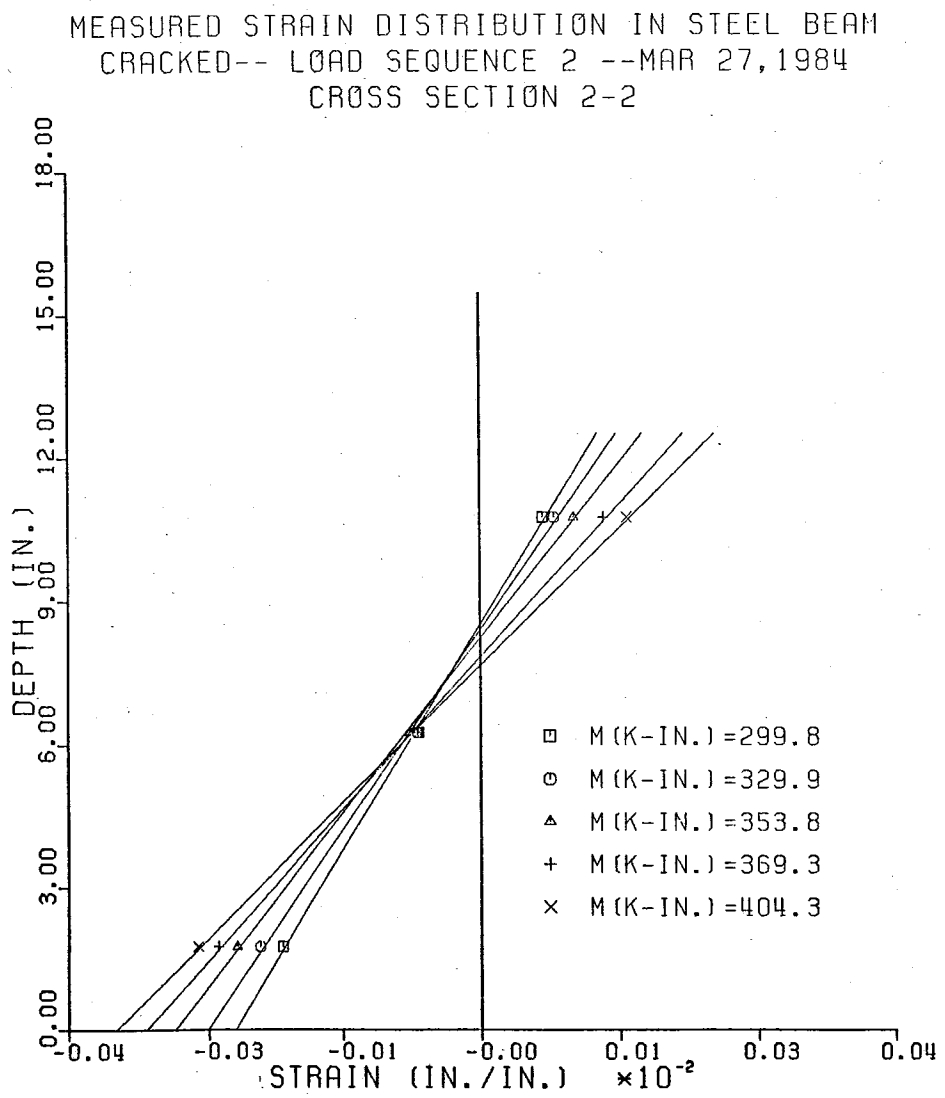

FIG. B24. Measured Strain Distribution in Stringer 1 for the Cracked Load Sequence 2 at Monitored Section 2 for Loads 11-15

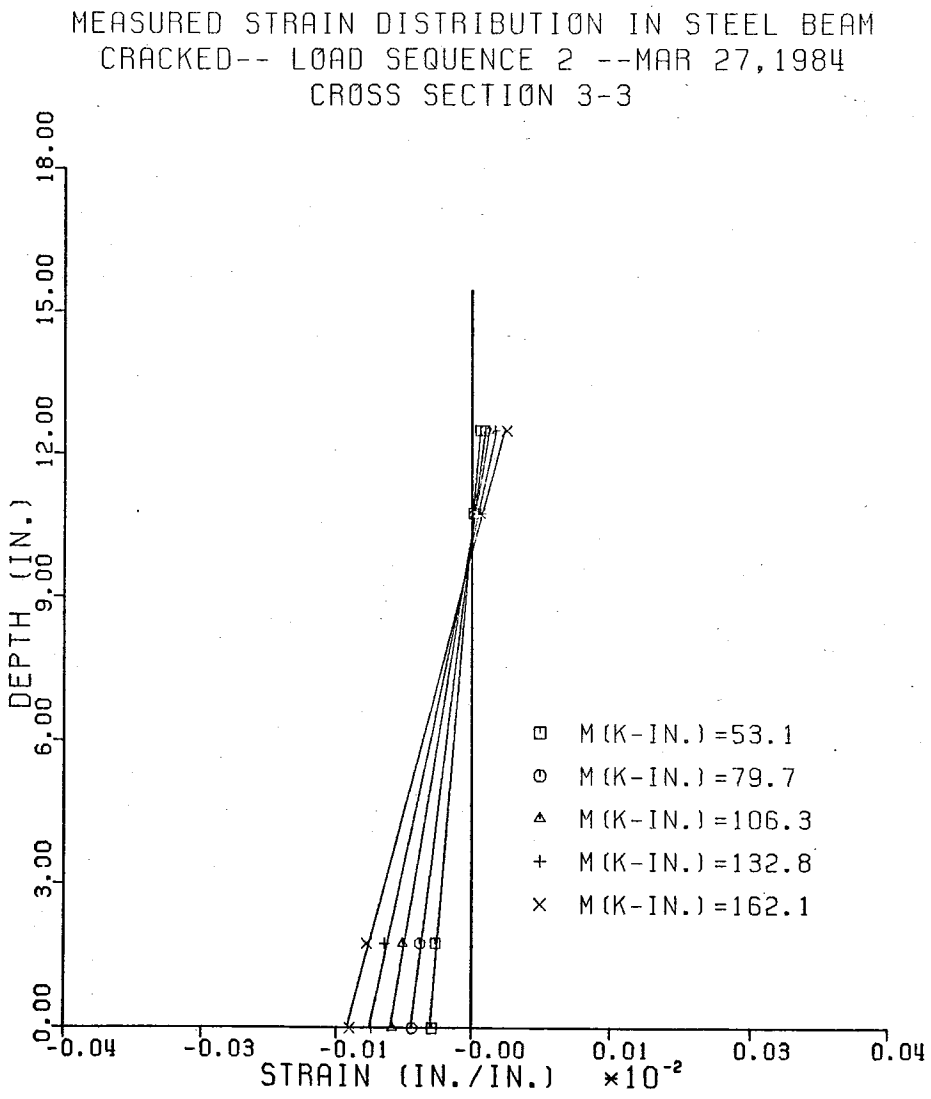

FIG. B25. Measured Strain Distribution in Stringer 1 for the Cracked Load Sequence 2 at Monitored Section 3 for Loads 1-5.

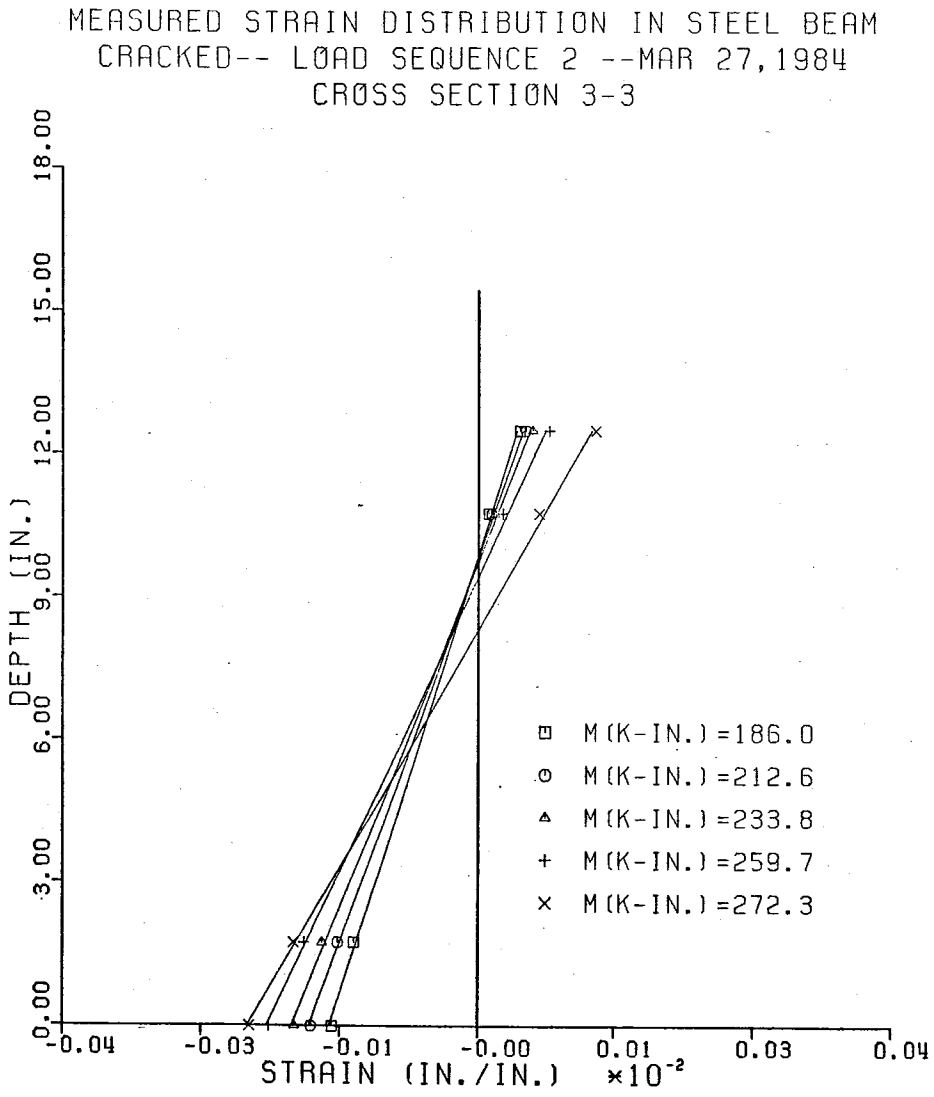

FIG. B26. Measured Strain Distribution in Stringer 1 for the Cracked Load Sequence 2 at Monitored Section 3 for Loads 6-10.

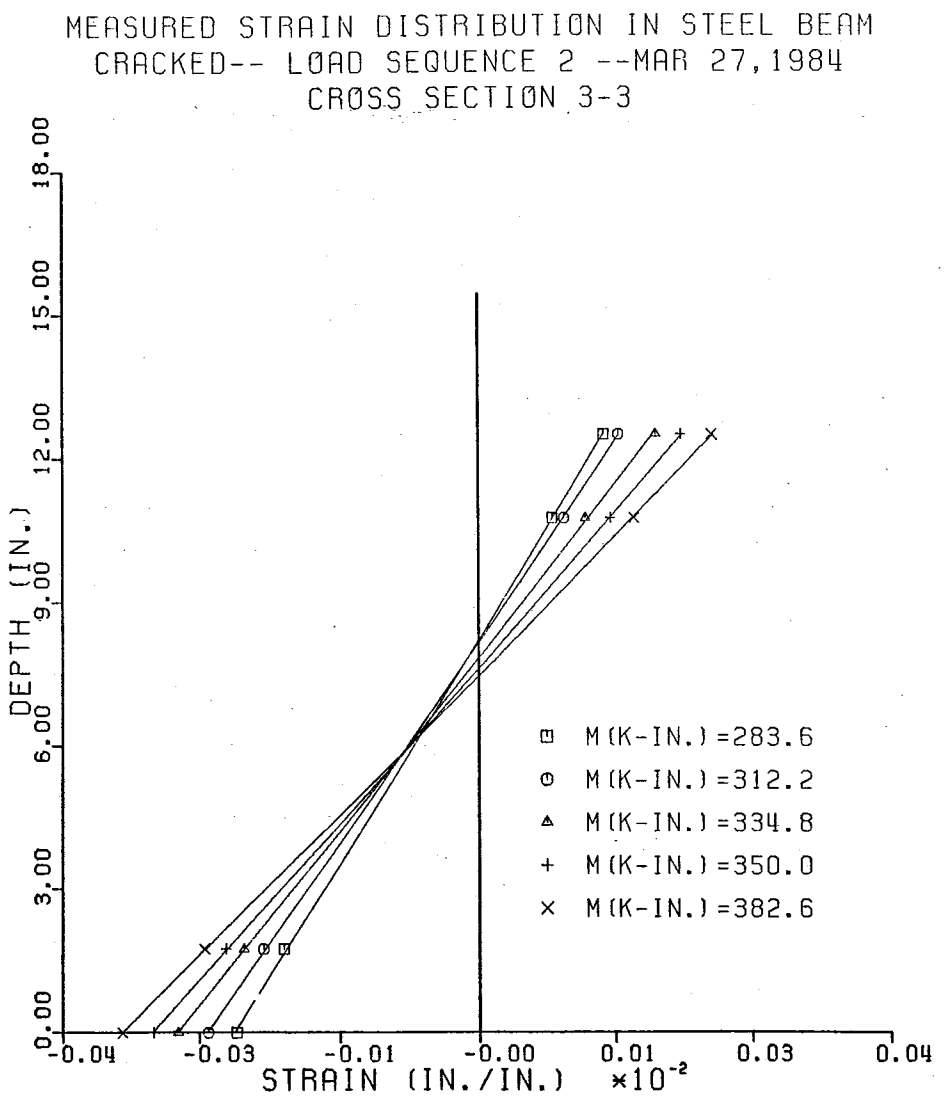

FIG. B27. Measured Strain Distribution in Stringer 1 for the Cracked Load Sequence 2 at Monitored Section 3 for Loads 11-15.

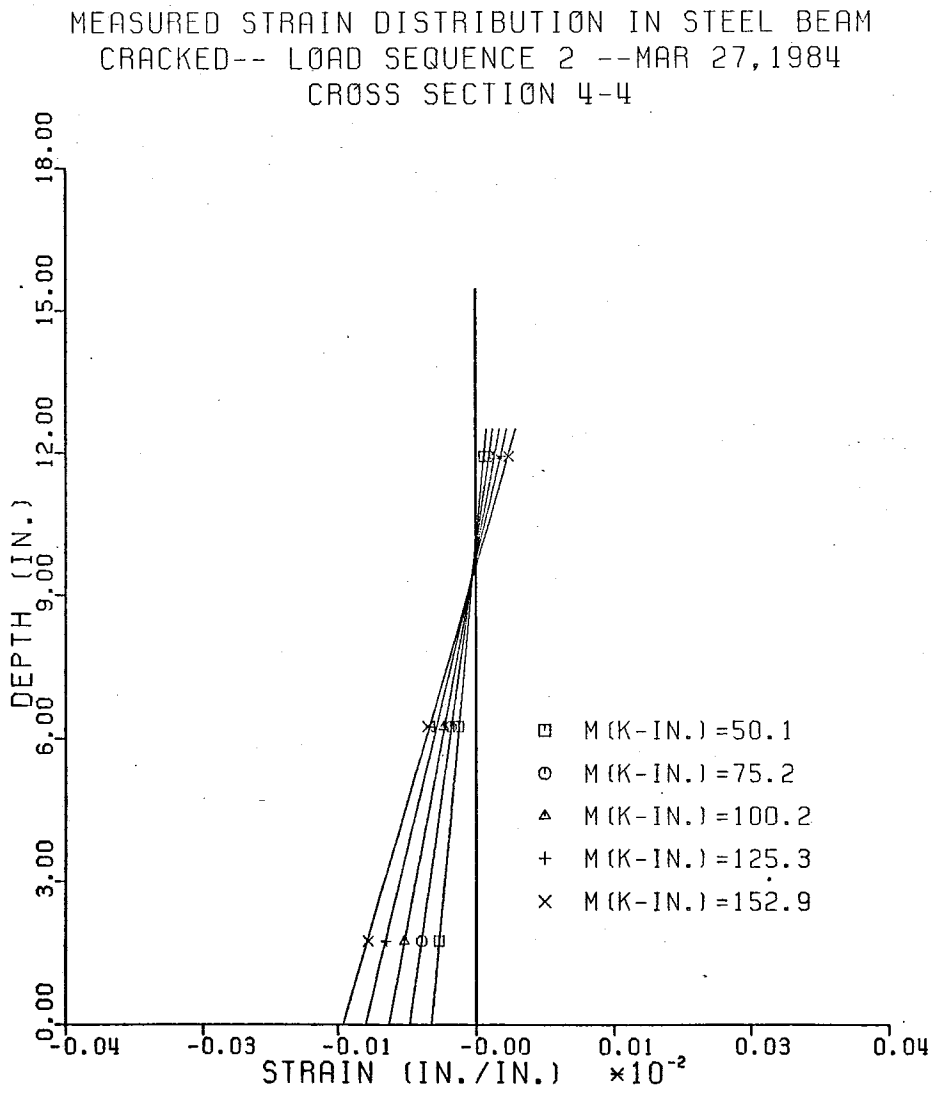

FIG. B28. Measured Strain Distribution in Stringer 1 for the Cracked Load Sequence 2 at Monitored Section 4 for Loads 1-5.

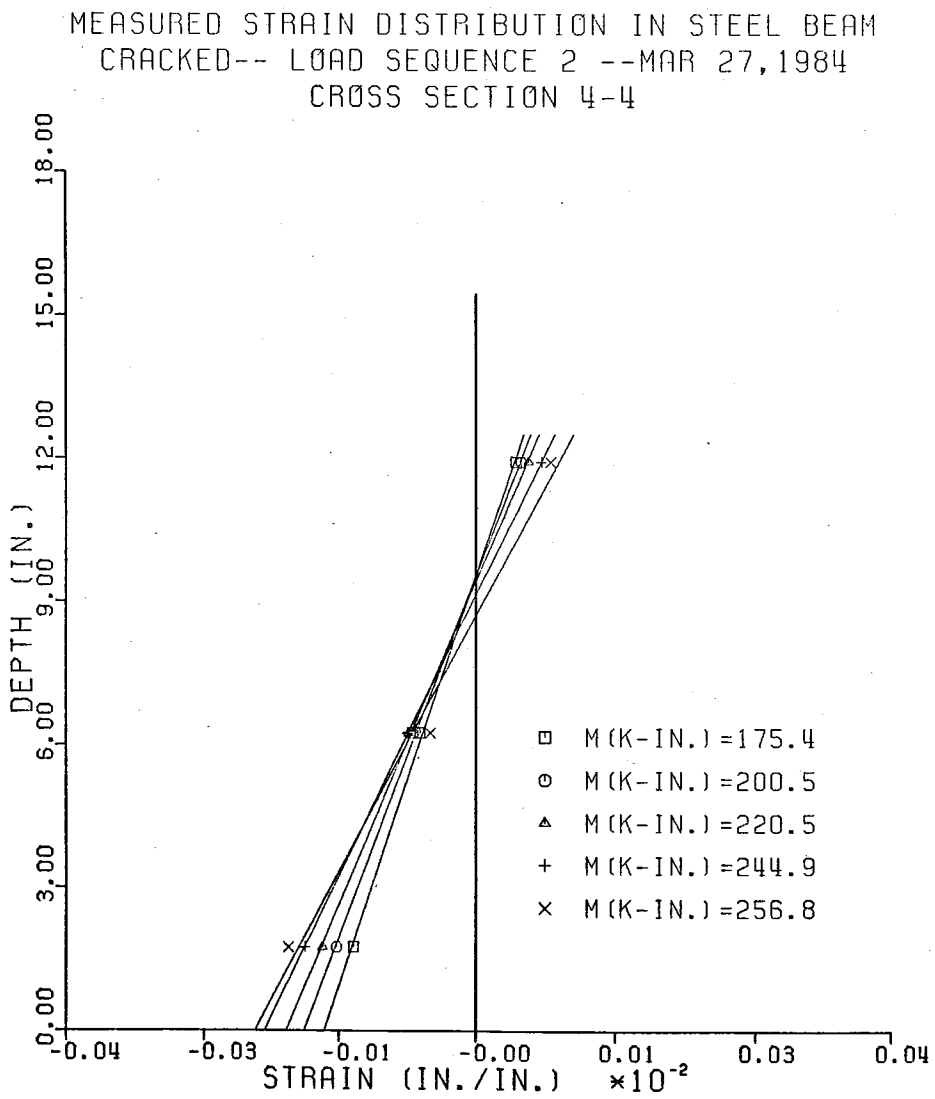

FIG. B29. Measured Strain Distribution in Stringer 1 for the Cracked Load Sequence 2 at Monitored Section 4 for Loads 6-10

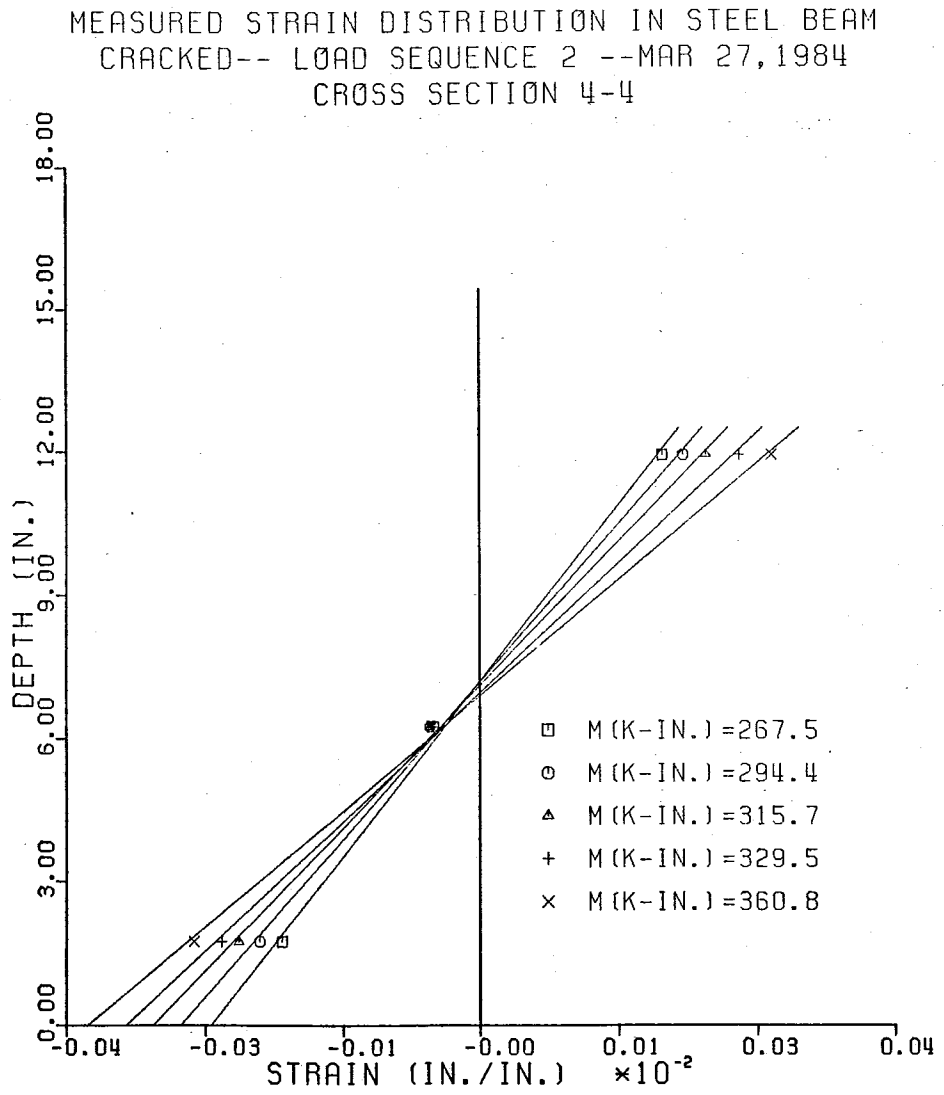

FIG. B30. Measured Strain Distribution in Stringer 1 for the Cracked Load Sequence 2 at Monitored Section 4 for Loads 11-15

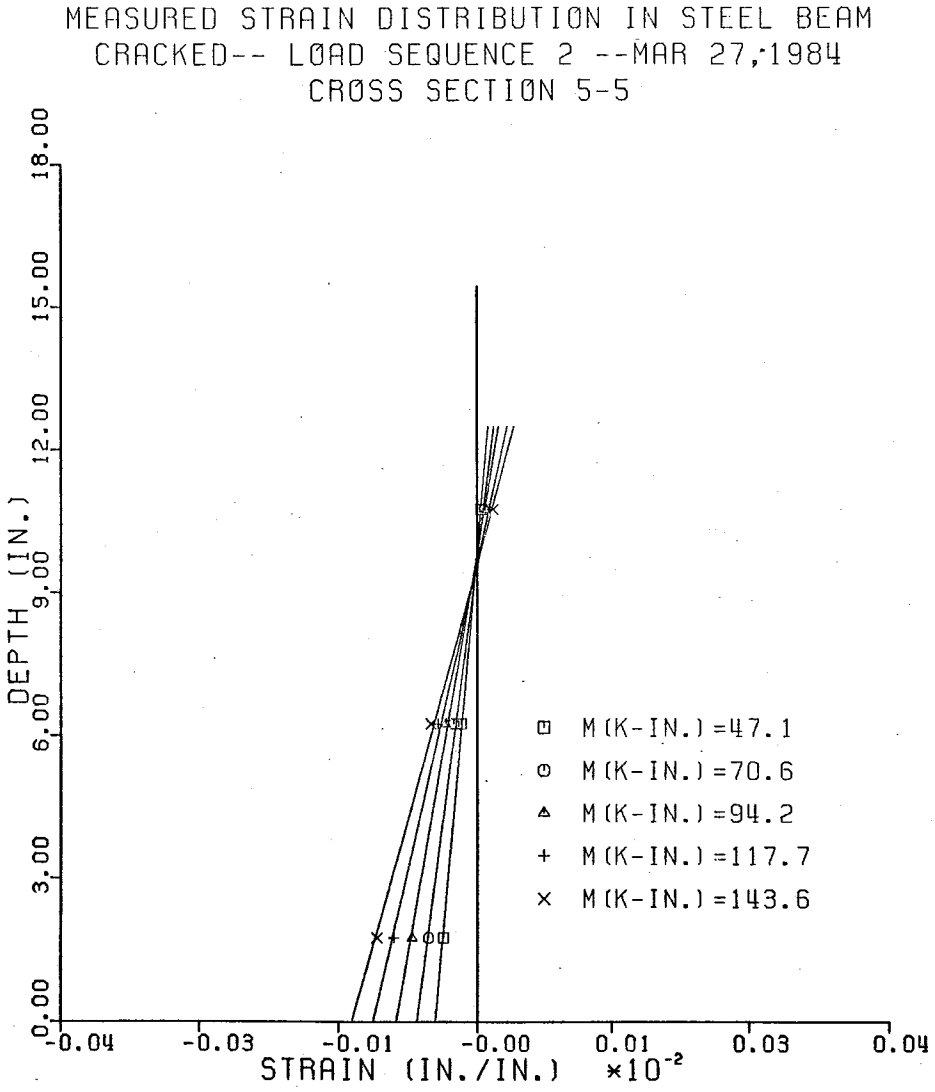

FIG. B31. Measured Strain Distribution in Stringer 1 for the Cracked Load Sequence 2 at Monitored Section 5 for Loads 1-5

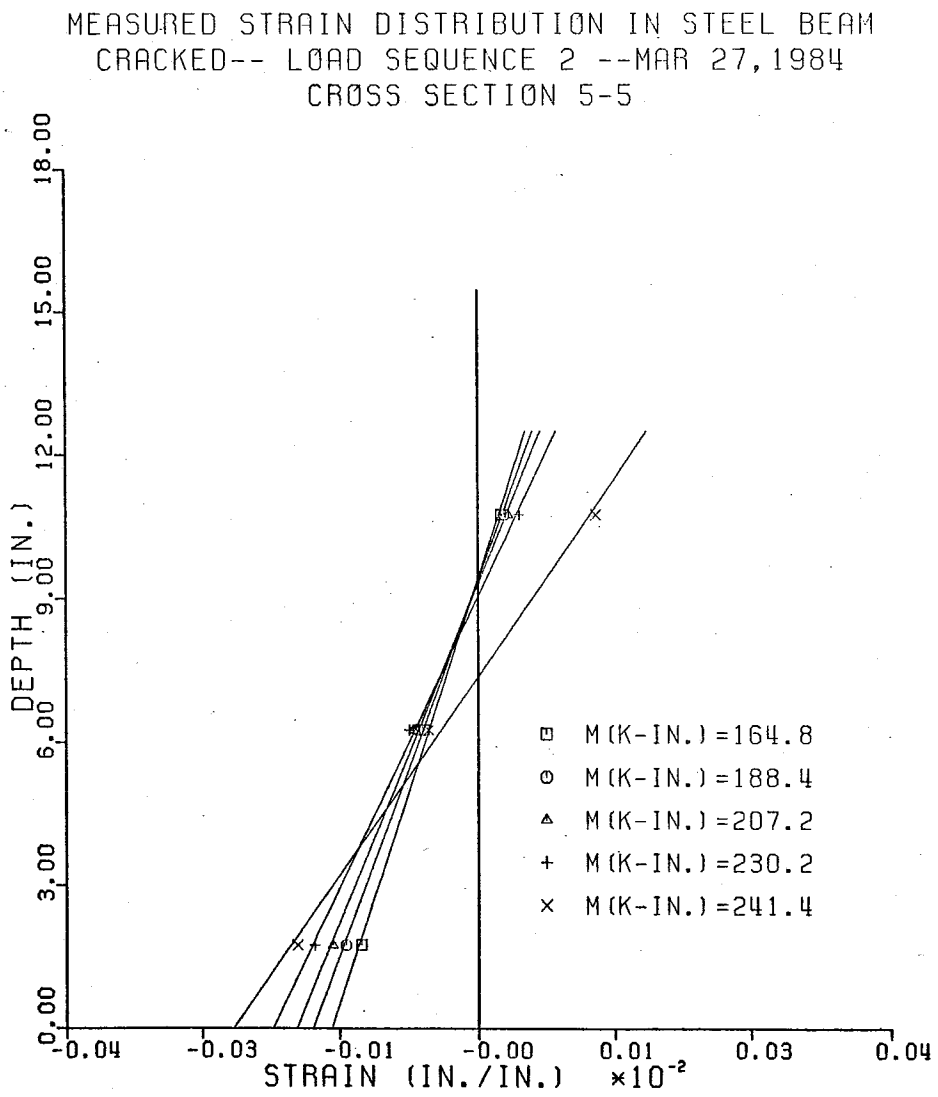

FIG. B32. Measured Strain Distribution in Stringer 1 for the Cracked Load Sequence 2 at Monitored Section 5 for Loads 6-10.

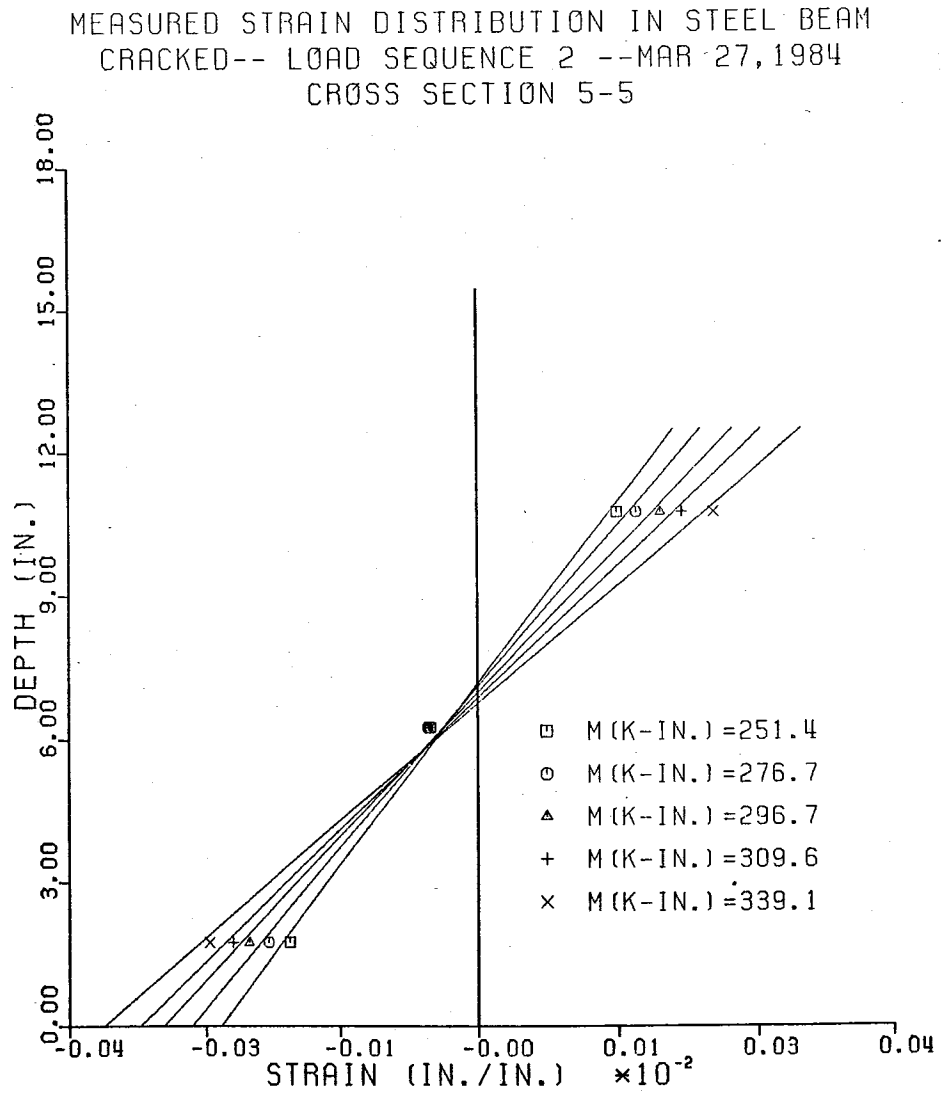

FIG. B33. Measured Strain Distribution in Stringer 1 for the Cracked Load Sequence 2 at Monitored Section 5 for Loads 11-15.

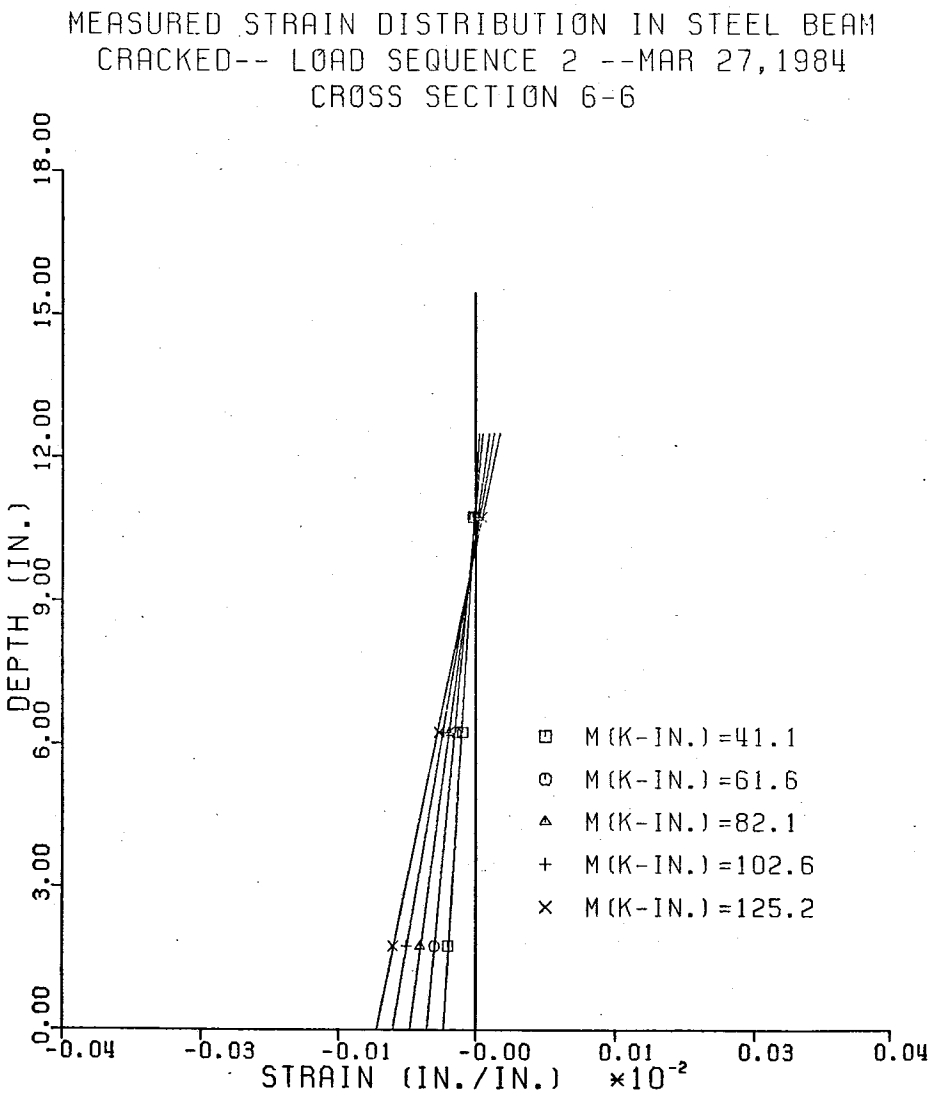

FIG. B34. Measured Strain Distribution in Stringer 1 for the Cracked Load Sequence 2 at Monitored Section 6 for Loads 1-5.

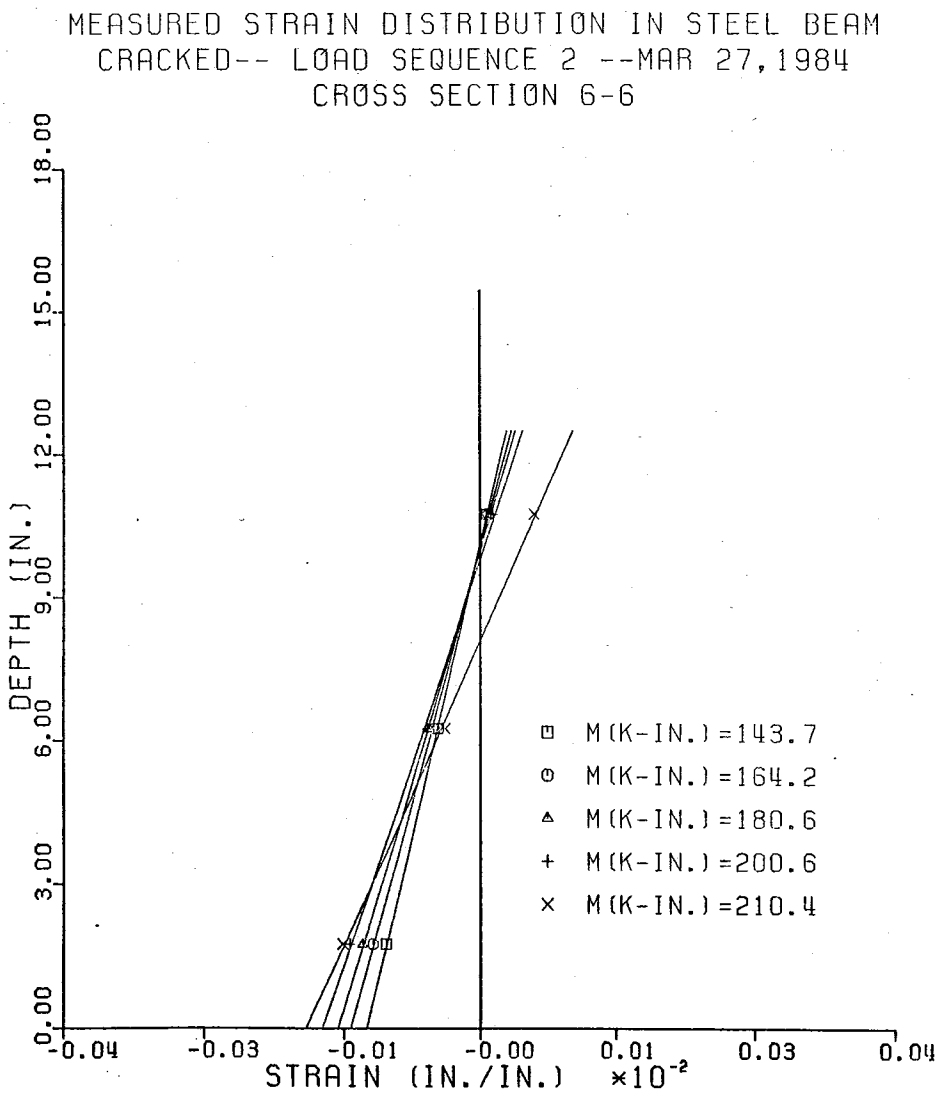

FIG. B35. Measured Strain Distribution in Stringer 1 for the Cracked Load Sequence 2 at Monitored Section 6 for Loads 6-10

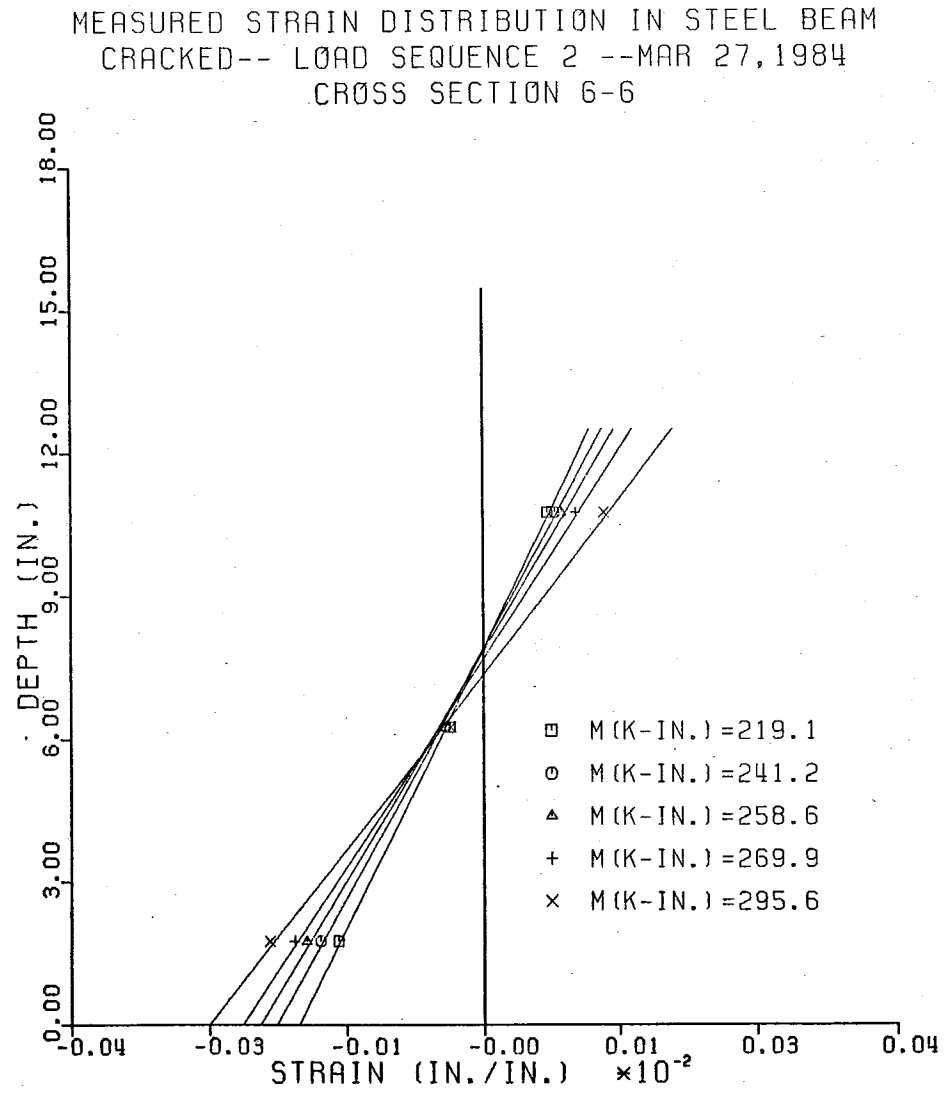

FIG. B36. Measured Strain Distribution in Stringer 1 for the Cracked Load Sequence 2 at Monitored Section 6 for Loads 11-15.

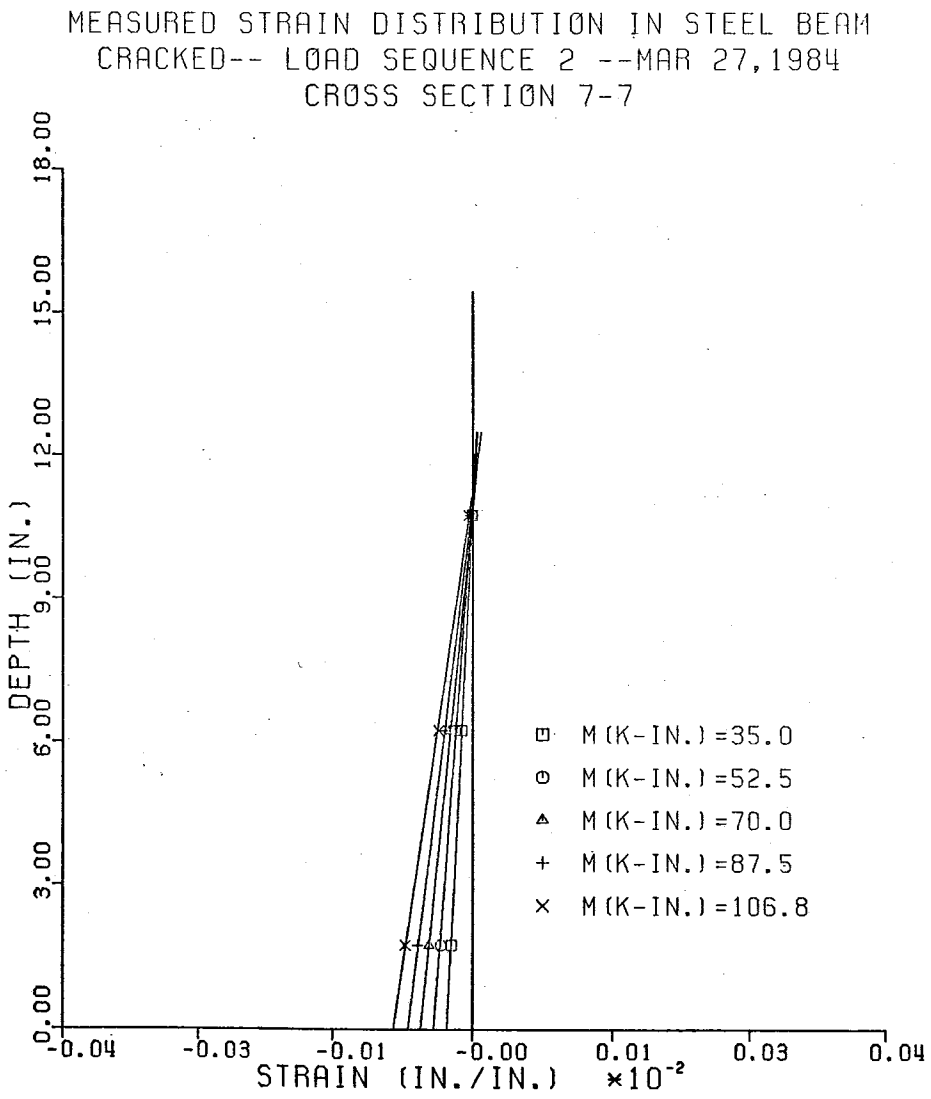

FIG. B37. Measured Strain Distribution in Stringer 1 for the Cracked Load Sequence 2 at Monitored Section 7 for Loads 1-5

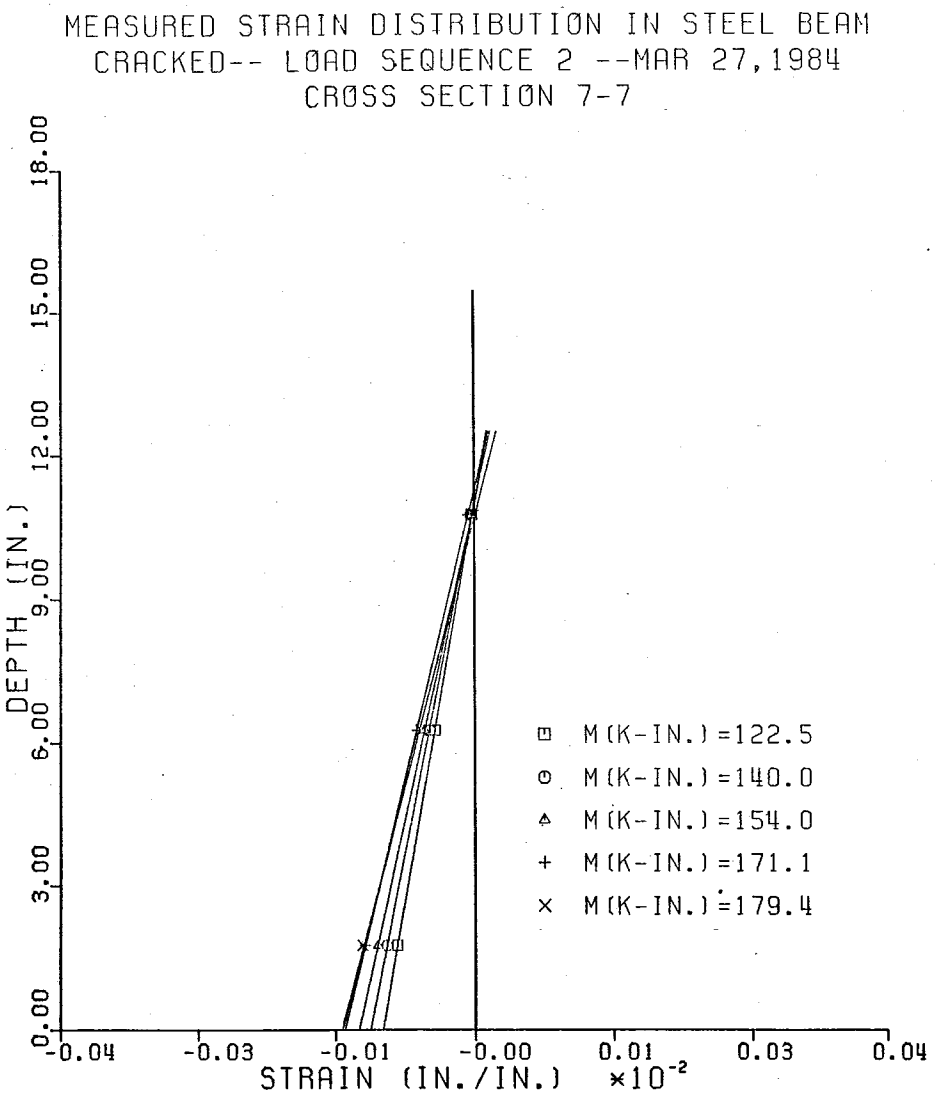

FIG. B38. Measured Strain Distribution in Stringer 1 for the Cracked Load Sequence 2 at Monitored Section 7 for Loads 6-10

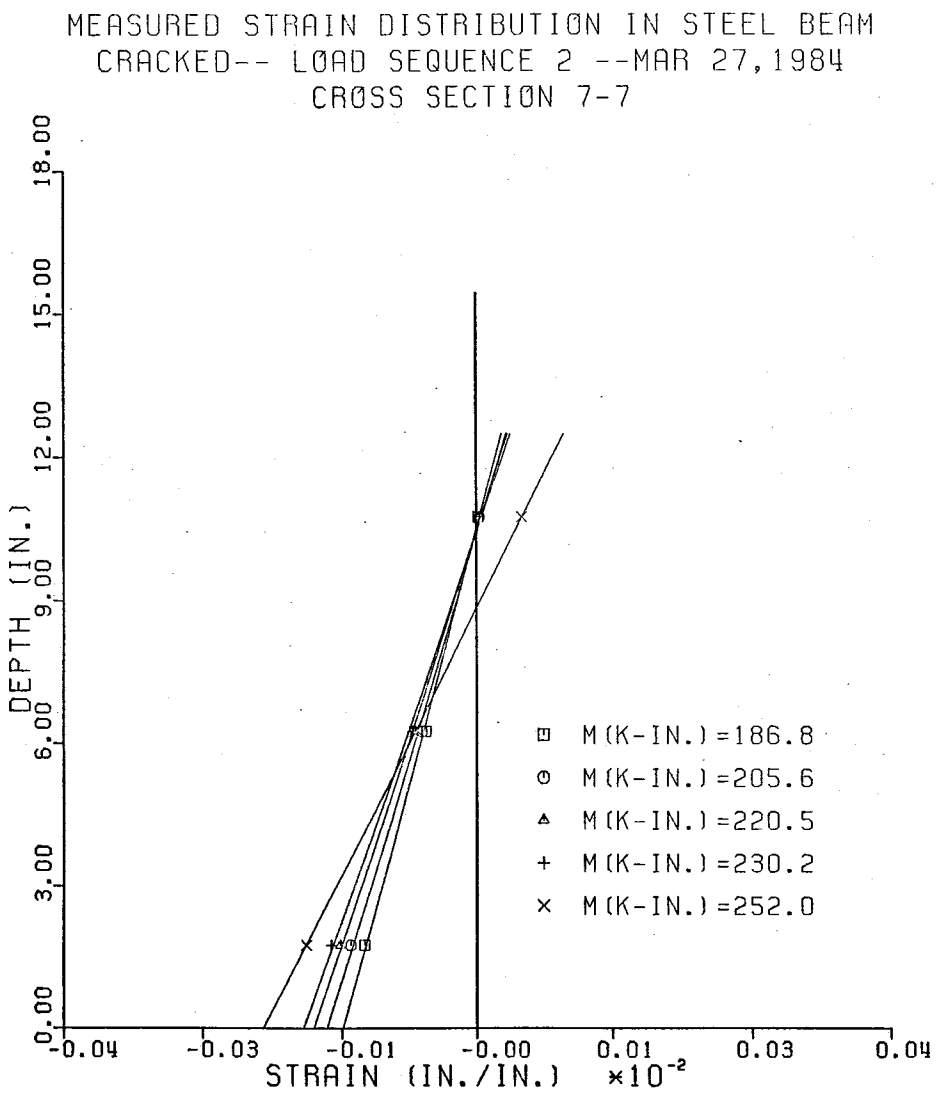

FIG. B39. Measured Strain Distribution in Stringer 1 for the Cracked Load Sequence 2 at Monitored Section 7 for Loads 11-15.

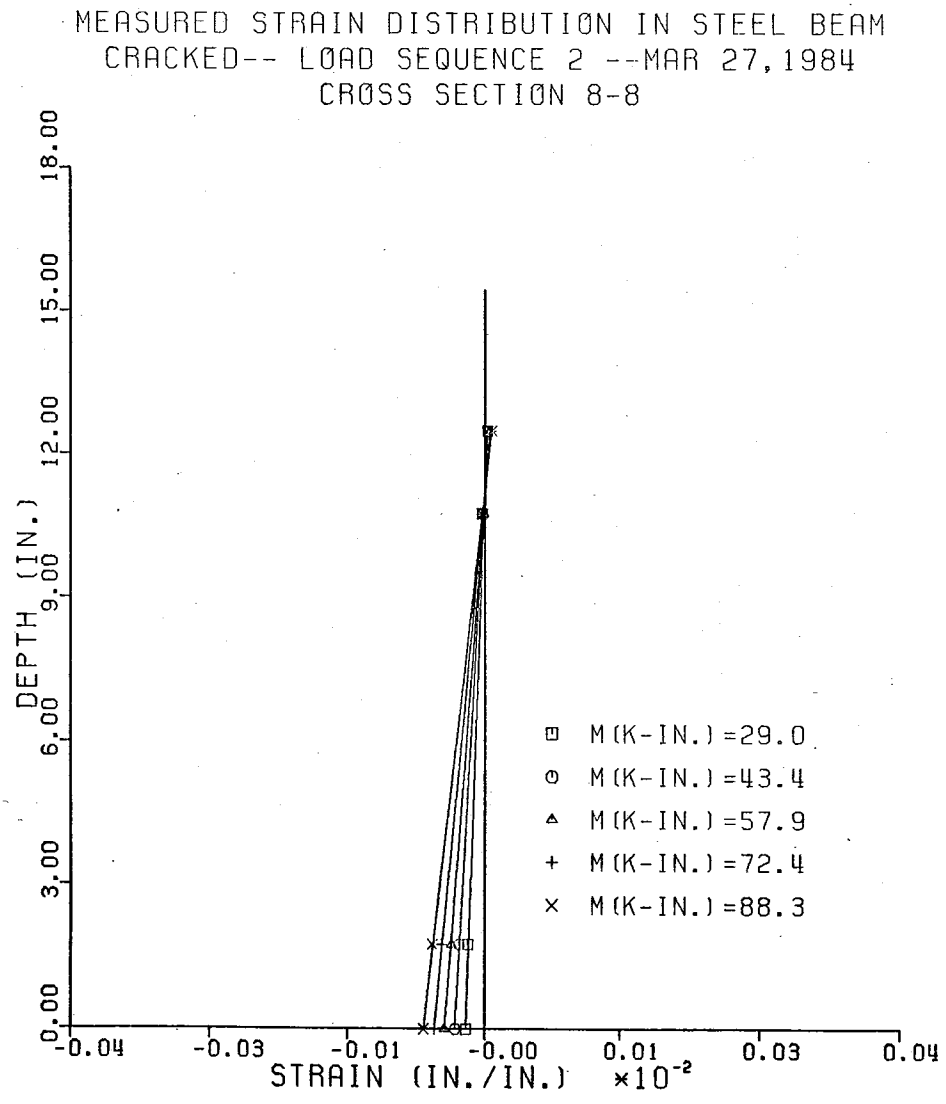

FIG. B40. Measured Strain Distribution in Stringer 1 for tne Cracked Load Sequence 2 at Monitored Section 8 for Loads 1-5.

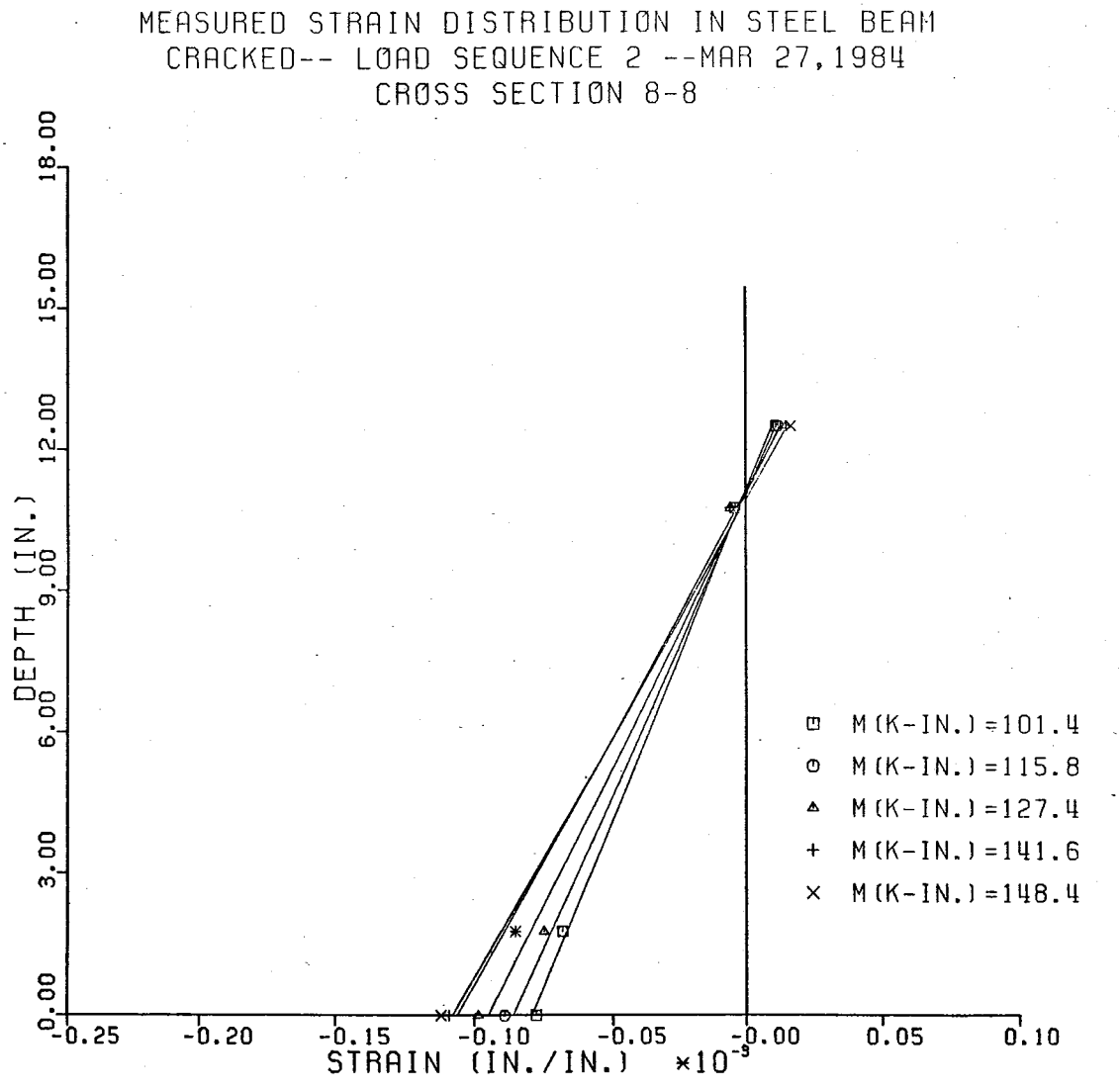

FIG. B41. Measured Strain Distribution in Stringer 1 for the Cracked Load Sequence 2 at Monitored Section 8 for Loads 6-10.

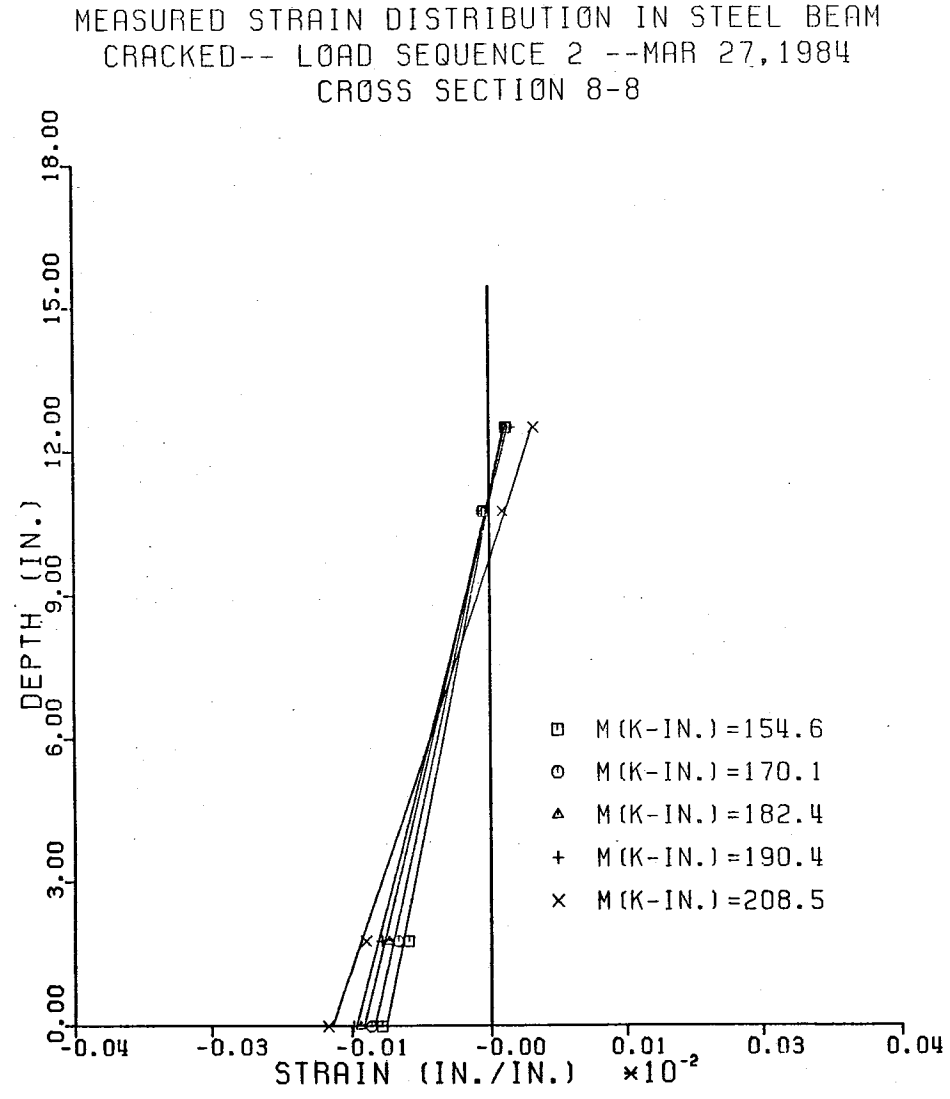

FIG. B42. Measured Strain Distribution in Stringer 1 for the Cracked Load Sequence 2 at Monitored Section 8 for Loads 11-15

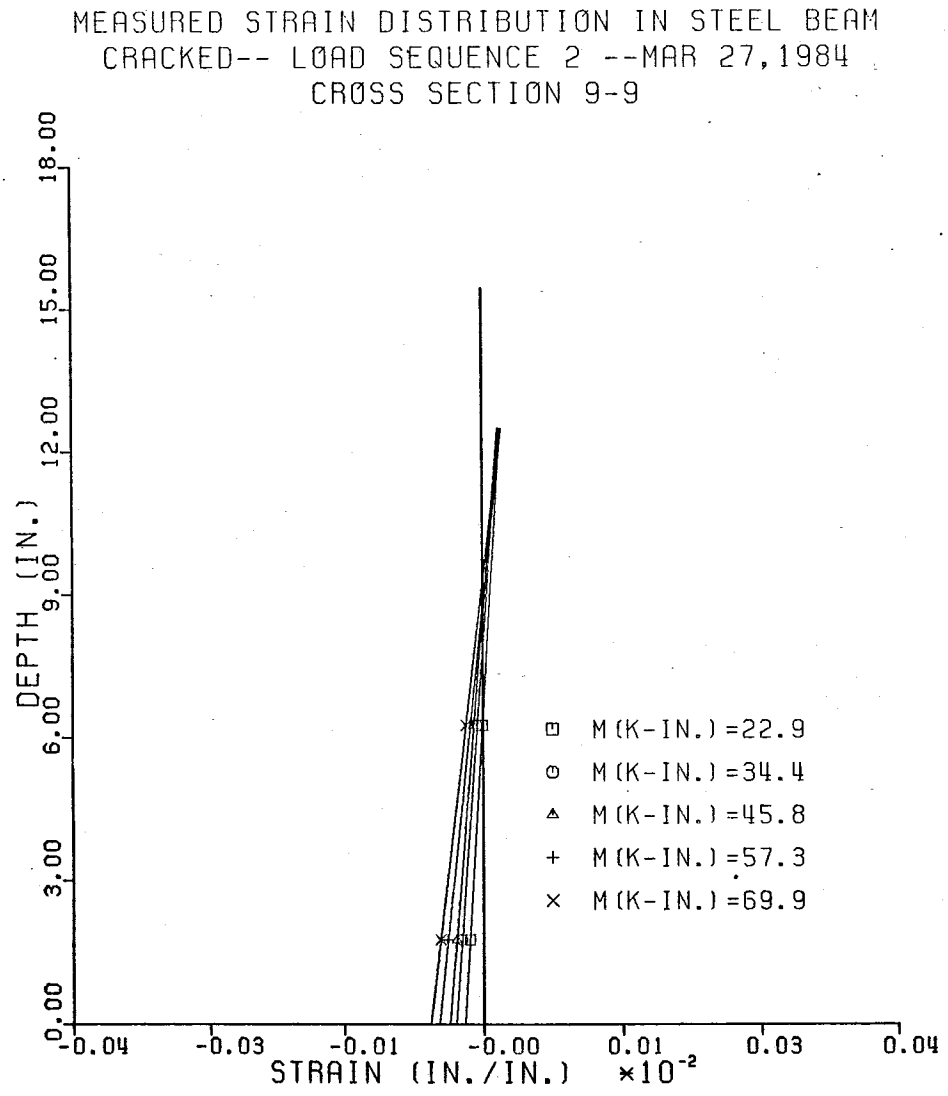

FIG. B43. Measured Strain Distribution in Stringer 1 for the Cracked Load Sequence 2 at Monitored Section 9 for Loads 1-5

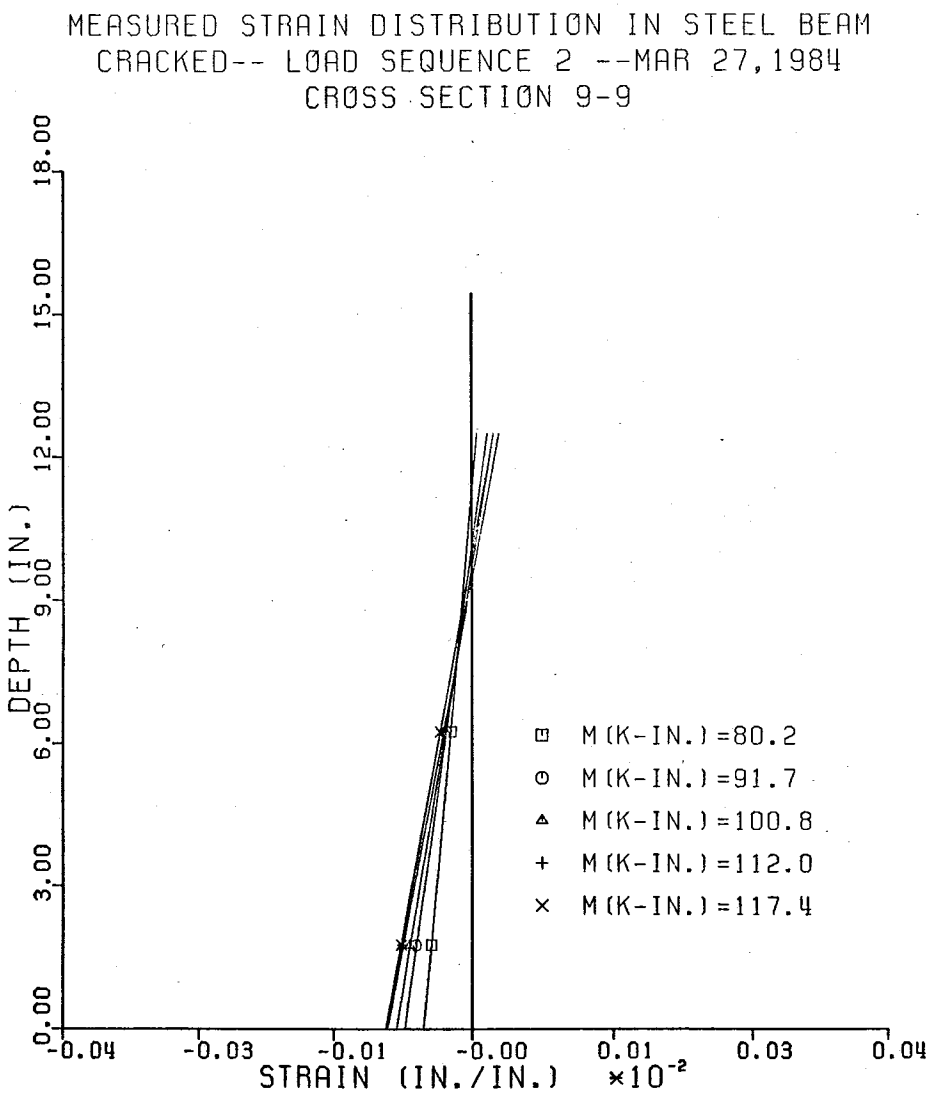

FIG. B44. Measured Strain Distribution in Stringer 1 for the Cracked Load Sequence 2 at Monitored Section 9 for Loads 6-10

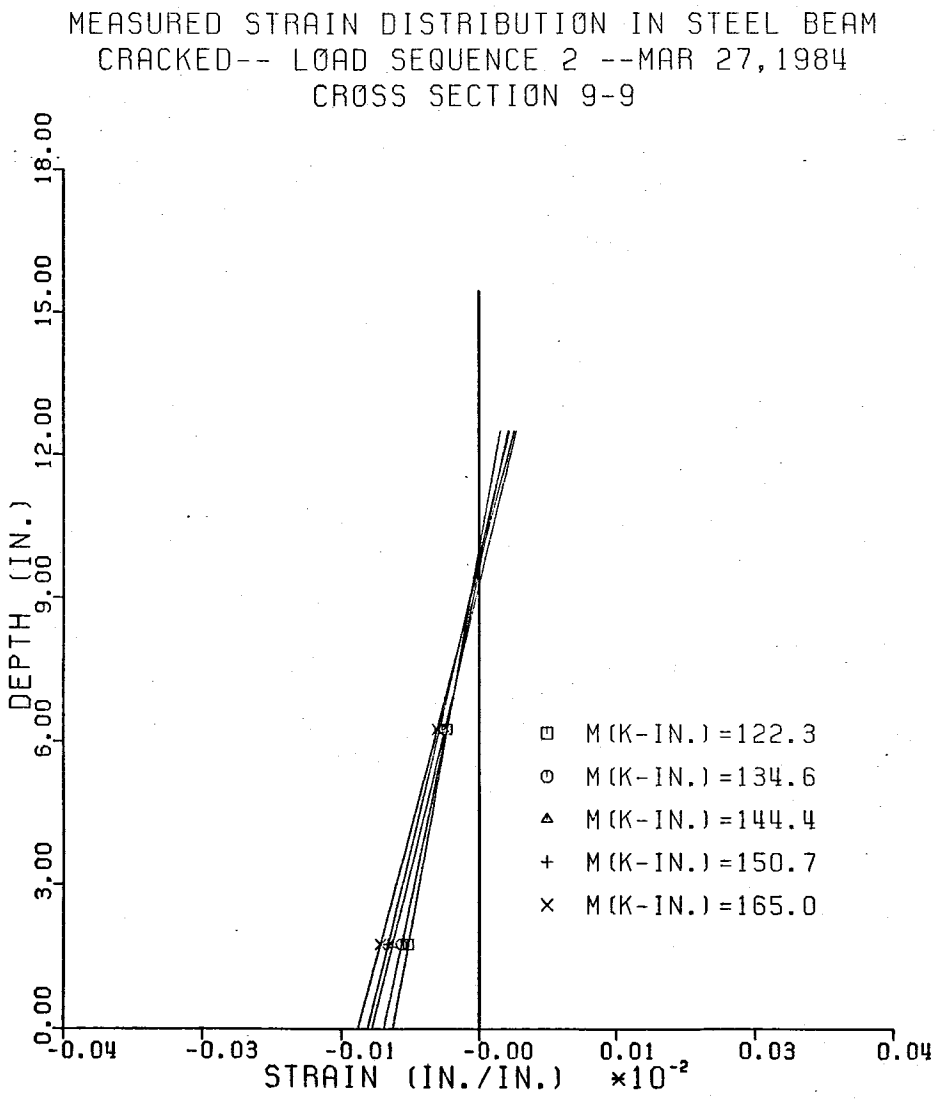

FIG. B45. Measured Strain Distribution in Stringer 1 for the Cracked Load Sequence 2 at Monitored Section 9 for Loads 11-15

APPENDIX C

CALCULATIONS OF TRANSFORMED AREA SECTION PROPERTIES

During the analysis of the structure the section properties of the model were calculated using two different theories, transformed area and partial interaction, from which two analytical models were derived.

The first model was based on the assumption that concrete has the same modulus of elasticity in compression as in tension. Since the structure was not instrumented in the end regions, the section properties at these areas were obtained by multiplying a ratio of the end to midspan transformed area inertia properties and the inertia properties derived from the first analytical model. The second analytical model was derived using the transformed area theory with the assumption that the modulus of elasticity of concrete in tension was only 67 per cent of the compressive modulus.

Computation of Section Properties for First Model

Midspan Regions

The midspan region of the model consisted of two A36 W12X19 steel stringers with 3/16 in. cover plates welded to the top and bottom flanges and a 2.70 in. thick concrete slab. A cross section of this region is shown in Fig. C1. Table C1 shows the calculations necessary to find the inertia properties.

Computing the location of neutral axis from the bottom of the stringer, gives

$$d_b = d_s + d_{ss} = \frac{\Sigma Ay}{\Sigma A} + 6.25 \text{ in.} = 11.32 \text{ in.}$$

Computing the composite moment of inertia of each stringer, yields

$$I = \Sigma Ay^2 + \Sigma I_o - \Sigma A\, d_s^2$$

$$I = 734.37 \text{ in.}^4 + 171.39 \text{ in.}^4 - (18.45 \text{ in.}^2)\ (5.071 \text{ in.})^2$$

Finally, computing the composite bottom section modulus of each stringer gives the results

$$S_{bot} = I / d_b = (431.35 \text{ in.}^4) / (11.32 \text{ in.})$$
$$S_{bot} = 38.10 \text{ in.}^3$$

End Regions

The end region of the model consisted of two modified A36 W12X19 steel stringers. Two 3/8 in. wide strips were removed from each flange of the stringers at both ends. The thickness of the slab was 2.70 in. Details of the cross section of the model at the end regions and the respective dimensions are shown in Fig. C2. The calculation of the inertia properties at these regions is shown in Table C2.

Computing the location of neutral axis from the bottom of the stringer, yields

$$d_b = d_s + d_{ss} = \frac{\Sigma Ay}{\Sigma A} + 6.06 \text{ in.} = 11.45 \text{ in.}$$

Computing the composite moment of inertia of each stringer, gives

$$I = \Sigma Ay^2 + \Sigma I_o - \Sigma A\, d_s^2$$
$$I = 699.71 \text{ in.}^4 + 114.79 \text{ in.}^4 - (16.96 \text{ in.}^2)\,(5.384 \text{ in.})^2$$
$$I = 322.90 \text{ in.}^4$$

Therefore, the composite bottom section modulus of each stringer is

$$S_{bot} = I / d_b = (322.90 \text{ in.}^4) / (11.45 \text{ in.})$$
$$S_{bot} = 28.21 \text{ in.}^3$$

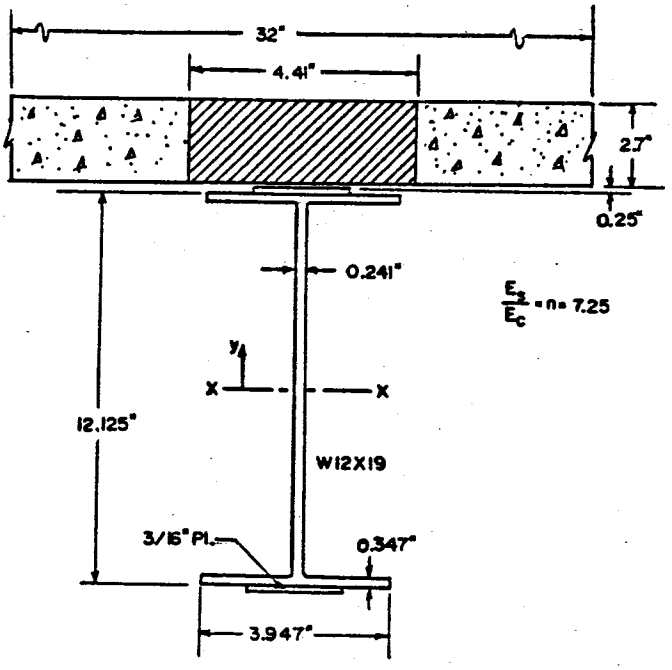

FIG. C1. First Analytical Model, Midspan Region

TABLE C1. Midspan Inertia Calculations for the First Analytical Model

SECTION	A $in.^2$	y in.	Ay $in.^3$	Ay^2 $in.^4$	I_o $in.^4$
Stringer	6.53	0.	0.	0.	164.15
Deck	11.92	7.85	93.55	734.37	7.24
Total	18.45	7.85	93.55	734.37	171.39

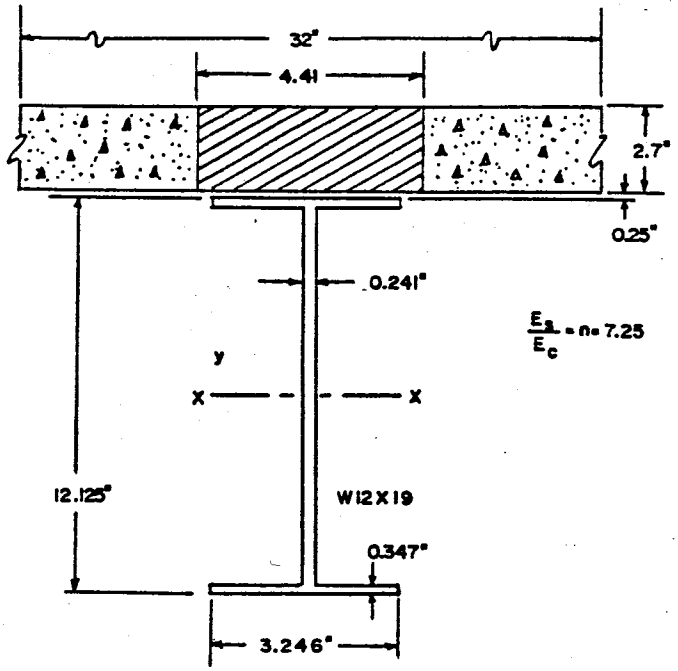

FIG. C2. First Analytical Model, End Region

TABLE C2. End Inertia Calculations for the First Analytical Model

SECTION	A $in.^2$	y in.	Ay $in.^3$	Ay^2 $in.^4$	I_o $in.^4$
Girder	5.05	0.	0.	0.	107.55
Deck	11.92	7.66	91.32	699.71	7.24
Total	16.96	7.66	91.32	699.71	114.79

Computation of Section Properties for Second Model

Both the dimensions of the steel stringer cross sections and the dimensions of the concrete deck in the midspand and end regions are the same for the first and second analytical model. However, since the modulus of elasticity of concrete in the second model is only 67 per cent of that used in the first model, the transformed area of the deck for the former model is smaller than for the latter model.

Midspan Region

Based on the dimensions shown in Fig. C3 and the calculations shown in Table C3, the location of the neutral axis with respect to the bottom of the stringer can be computed.

$$d_b = d_s + d_{ss} = \frac{\Sigma Ay}{\Sigma A} + 6.25 \text{ in.} = 10.56 \text{ in.}$$

Computing the composite moment of inertia of each stringer, gives

$$I = \Sigma Ay^2 + \Sigma I_o - \Sigma A\, d_s^2$$
$$I = 489.58 \text{ in.}^4 + 168.98 \text{ in.}^4 - (14.47 \text{ in.}^2)\,(4.309 \text{ in.})^2$$
$$I = 389.85 \text{ in.}^4$$

Finally, the composite bottom section modulus of each stringer becomes

$$S_{bot} = I / d_b = (389.85 \text{ in.}^4) / (10.56 \text{ in.})$$
$$S_{bot} = 36.92 \text{ in.}^3$$

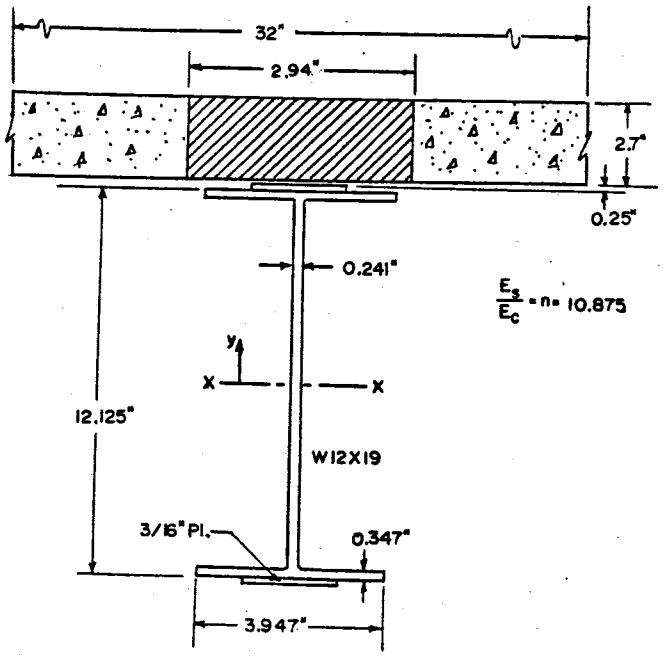

FIG. C3. Second Analytical Model, Midspan Region

TABLE C3. Midspan Inertia Calculations for the Second Analytical Model

SECTION	A $in.^2$	y in.	Ay $in.^3$	Ay^2 $in.^4$	I_o $in.^4$
Stringer	6.52	0.	0.	0.	164.15
Deck	7.94	7.85	62.37	489.58	4.83
Total	14.46	7.85	62.37	489.58	168.98

End Regions

Based on the dimensions of the cross section shown in Fig. C4 and the calculations shown in Table C4, the position of the neutral axis of the composite section at the end section with respect to the bottom flange can be calculated as follows:

$$d_b = d_s + d_{ss} = \frac{\Sigma Ay}{\Sigma A} + 6.06 \text{ in.} = 10.75 \text{ in.}$$

Computing the composite moment of inertia of each stringer gives

$$I = \Sigma Ay^2 + \Sigma I_o - \Sigma A\, d_s^2$$

$$I = 466.47 \text{ in.}^4 + 112.38 \text{ in.}^4 - (12.99 \text{ in.}^2)\,(4.69 \text{ in.})^2$$

$$I = 293.81 \text{ in.}^4$$

Therefore, the composite bottom section modulus of each stringer becomes

$$S_{bot} = I / d_b = (293.81 \text{ in.}^3) / (10.75 \text{ in.})$$

$$S_{bot} = 27.33 \text{ in.}^3$$

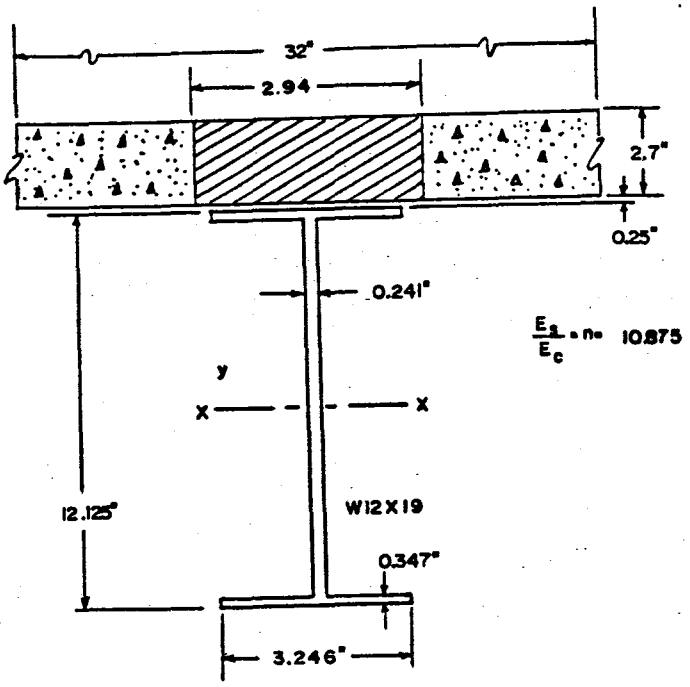

FIG. C4. Second Analytical Model, End Region

TABLE C4. End Inertia Calculations for the Second Analytical Model

SECTION	A $in.^2$	y in.	Ay $in.^3$	Ay^2 $in.^4$	I_o $in.^4$
Stringer	5.05	0.	0.	0.	107.55
Deck	7.94	7.66	60.88	466.47	4.83
Total	12.99	7.66	60.88	466.47	112.38